Role and regulation of alveolar protein clearance in influenza virus-induced lung injury

Inaugural Dissertation

in partial fulfillment of the requirements for the Doctor in Human Biology-Degree

of the Faculty of Medicine

of the Justus Liebig University Giessen

by

Andrés Alberro-Brage

of

Montevideo, Uruguay

Giessen, 2022

From the Department of Internal Medicine II
Director / Chairman: Prof. Dr. Werner Seeger
of the Faculty of Medicine of the Justus Liebig University Giessen

First Supervisor and Committee Member: Prof. Dr. Werner Seeger
Committee Members:
Prof. Dr. Ana Pardo Saganta

Date of Doctoral Defense: 2 December 2022.

I hereby declare that I have completed this work independently and without inadmissible assistance or the use of other than the resources quoted. All texts that have been quoted verbatim or by analogy from published and non-published writings and all details based on verbal information have been identified as such. In the analyses that I have conducted and to which I refer in this thesis, I have followed the principles of good scientific practice, as stated in the Statute of Justus Liebig University Giessen for Ensuring Good Scientific Practice, as well as ethical principles and those governing data protection and animal welfare. I give my assurance that third parties have not received from me, either directly or indirectly, any financial remuneration for work in connection with the content of this doctoral thesis and that the work presented has not been submitted in the same or a similar form to another assessment authority in Germany or elsewhere for the purpose of being awarded a doctorate or another assessment procedure. All material taken from other sources and other persons and used in this thesis or to which direct reference is made has been identified as such. In particular, all those who took part directly and indirectly in the production of this study have been named. I agree to my thesis being subjected to scrutiny by plagiarism detection software or by an internet-based software program.

_____ _____

Place, date Signature

Contents

List of abbreviations

AF	Alexa Fluor dye
ALI	Acute lung injury
ARDS	Acute respiratory distress syndrome
AF488	Alexa Fluor 488
AF647	Alexa Fluor 647
AEC	Alveolar epithelial cells
ANOVA	Analysis of variance
AT1	Alveolar epithelial type 1 cell
AT2	Alveolar epithelial type 2 cell
ATPase	Adenosine triphosphate hydrolase
BAL	Broncho-alveolar lavage
BMM	Bone marrow-derived macrophages
BSA	Bovine serum albumin
cDNA	Complementary DNA
CPAP	Continuous positive airway pressure
CT	Computerized tomography
Da	Dalton
DMEM	Dulbecco's Modified Eagle Medium
DPBS-G	Dulbecco's phosphate-buffered saline with glucose
ECM	Extracellular matrix
EDTA	Ethylenediaminetetraacetic acid
EGF	Epidermal growth factor
ELISA	Enzyme-linked immunosorbent assay
EpCAM	Epithelial Cell Adhesion Molecule
FC	Flow cytometry
FiO_2	Fraction of inspired oxygen
FITC	Fluorescein isothiocyanate
FMO	Fluorescence minus one control
Gal	Galactose
GSK3β	Glycogen Synthase Kinase beta
HA	Hemagglutinin
HEPES	4-(2-hydroxyethyl)-1-piperazineethanesulfonic acid
hMPV	Human metapneumovirus
Ig G	Immunoglobulin G
IL	Interleukin
IV	Influenza virus
LAP	Latency-associated peptide
LDL	Low density lipoprotein
LRP	Low-density lipoprotein receptor-related protein
LTGF-β	Latent TGF-β1
M1	Matrix protein 1
M2	Ion channel matrix protein 2
MCTF	Membrane-associated carboxyl-terminal fragment
MDCK	Madin-Darby Canine Kidney

MIF	Macrophage inhibitory factor
MLE-12	Mouse lung epithelial – 12
MMP	Matrix metalloproteinase
MFI	Median of the fluorescence intensity
MLI	Mean linear intercept
mRNA	Messenger RNA
MT-MMP	Membrane tethered MMP
MW	Molecular weight
MOI	Multiplicity of infection
NA	Neuraminidase
PAF	Platelet activator factor
PaO_2	Partial pressure of arterial oxygen
PB	Pacific blue dye
PB1	Polymerase basic protein 1
PB2	Polymerase basic protein 2
PBS	Phosphate-buffered saline
PCLS	Precision cut lung slices
PEEP	Positive end-expiratory pressure
PFA	Paraformaldehyde
Pfu	Plaque forming units
PIV	Parainfluenzavirus
PMN	Polymorphonuclear leukocytes
PP1	Protein phosphatase 1
qRT-PCR	Quantitative real time – polymerase chain reaction
RAGE	Receptor for advanced glycation end products
rAM	Resident alveolar macrophages
RIP	Regulated intramembrane proteolysis
RSV	respiratory syncytial virus
RLE-6TN	Rat lung epithelial-T-antigen negative
RNA	Ribonucleic acid
RT	Room temperature
SA	Sialic acid
SDS-PAGE	Sodium dodecyl sulphate–polyacrylamide gel electrophoresis
siRNA	Small interference RNA
SP	Surfactant protein
SV40	Simian virus 40
TIMPs	Tissue inhibitors of metalloproteinases
TNF- α	Tumor necrosis factor α
TGF-β1	Transforming Growth Factor beta 1
TPCK	Tosyl phenylalanyl chloromethyl ketone
TR	Texas red
Tris	Tris(hydroxymethyl)aminomethane
T-TBS	Tris-buffered saline -Tween 20
WB	Western Blot

1. Introduction

Lung structure and the alveolar function

The human lungs consist of a series of tubes, first starting in the cartilaginous trachea before branching into the bronchi and bronchioles- forming the airways- and ultimately ending in the alveoli. The airways and alveoli are overlaid with a continuous epithelium and form the interfaces between the external environment and the lungs. Gas exchange occurs in the alveoli, or terminal respiratory units (figure 1.1), located within the respiratory bronchioles, alveolar ducts, and alveolar sacs. The alveolar region of the lung comprises approximately 90% of its total volume, with the remaining 10% consisting of conducting airways and larger blood vessels. The walls of the alveoli, or septa, consist of the pulmonary capillaries, the interstitium, and the alveolar epithelium. The capillaries, formed by the vascular endothelium, may comprise more than 75% of the total volume and are the main component of the wall. The alveolar epithelium and the vascular endothelium are in close apposition, facilitating an efficient exchange of gases while forming an alveolar-capillary barrier which obstructs the free movement of liquid and proteins from the interstitial and vascular spaces (Tomashefski and Farver 2008; Albertine 2016). The epithelial component of this barrier is the main responsible for limiting the amounts of fluid inside the alveolar lumen, which is critical for effective gas exchange (Gorin and Stewart 1979).

In mammals and other air-breathing species, such as reptiles or amphibians, the alveolar epithelium is composed of two types of alveolar epithelial cells (AEC), namely, cuboidal alveolar type 2 (AT2) cells and squamous alveolar type 1 (AT1) cells (Albertine 2016). In mammals, AT2 cells make up approximately 15% of the lung parenchymal tissue (Crapo et al. 1982; Haies, Gil, and Weibel 1981). They are small cells with short microvilli, and are responsible for the production of pulmonary surfactant; the lining fluid which reduces surface tension and stabilizes the alveolar structure, thus facilitating gas exchange by enabling the alveoli to remain open (Veldhuizen and Haagsman 2000; Goerke 1998). The AT2 cells present characteristic secretory lysosomes (lamellar bodies) containing surfactant phospholipids, surfactant proteins (SP-A, SP-B, SP-C), enzymes, transporters, and other molecules (de Vries et al. 1985). AT2 cells not only secrete, but also internalize

and recycle surfactant lipids and proteins from the alveolar space (Hallman, Epstein, and Gluck 1981; Kalina and Socher 1990; Agassandian and Mallampalli 2013). These endocytosis processes involve clathrin-mediated endocytosis and macropinocytosis, and ensure the optimal function of the surfactant layer while playing an important role in alveolar protein clearance after lung injury (Yumoto et al. 2006; Tagawa et al. 2008; Buchäckert et al. 2012; Grzesik et al. 2013). AT2 cells also function as stem cells in the alveoli, since they can differentiate into AT1 cells in vivo, a vital feature that helps repair the alveolar epithelium in the case of damage (M. J. Evans et al. 1973; Barkauskas et al. 2013). Transdifferentiation of AT2 cells into AT1 (-like) cells is also observed under in-vitro conditions in primary AT2 cell cultures (Kinnard et al. 1994; Demling et al. 2006).

AT1 cells account for approximately 8% of the total alveolar cells, however, they cover 90 to 95% of the alveolar surface area of the peripheral lung (Crapo et al. 1982; Haies, Gil, and Weibel 1981). These cells have a flattened and extensive cytoplasm which forms a large surface area and are in close apposition with the capillaries for gas exchange. Such a large surface area represents a problem for the transport of newly synthesized proteins and substances within the cell and may play a role in the fragility shown by AT1 cells (Albertine 2016; Weibel 2015). These cells have been described as containing non-clathrin coated vesicles- or caveolae- which are distributed either on the alveolar lumen, on the interstitium, or as free vesicles in the cytoplasm. These vesicles contain caveolin-1 as a scaffolding protein and play a role in the regulation of intracellular concentrations of cholesterol, as well as sequestration of receptors and signal molecules to regulate their functionality (Gil, Silage, and McNiff 1981; Kasper et al. 1997; Newman et al. 1999; Dahlin et al. 2004). Additionally, it has recently been suggested that caveolae in AT1 cells may function as mechanosensors within alveoli, regulating stretch-induced surfactant secretion from AT2 cells (Diem et al. 2020). One of the main roles of AT1 cells is regulating alveolar fluid homeostasis. They express aquaporins, which gives these cells a high permeability to water (Leland G. Dobbs et al. 1998). They also express Na^+ channels and Na^+/K^+ ATPase pumps on their membranes, allowing them to control the sodium transport across the alveolo-capillary barrier. The flux of water through aquaporins follows then passively in response to the osmotic gradients (Hollenhorst, Richter, and Fronius 2011). For this reason, the polarized epithelial cells from the alveolar

epithelium have the capacity to absorb fluid from the alveolar space via vectorial ion transport, a vital feature in the recovery of the gas exchange function after lung edema conditions. In recent years it has been also shown that AT1 cells also have the ability to proliferate and give rise to AT2 cells in order to repair the alveolar epithelium in the case of damage (Jain et al. 2015; Y. Wang et al. 2018).

As mentioned earlier, the walls in the alveolar epithelium are in close apposition with the vascular endothelium. In the body, vascular endothelial cells are responsible for the maintenance of blood fluidity through the expression of coagulation-inhibiting factors (Arnout, Hoylaerts, and Lijnen 2006), the regulation of blood flow (Palmer, Ferrige, and Moncada 1987; Busse and Fleming 2006), the maintaining of leukocytes in a quiescent state (Ley and Reutershan 2006), and through controlling capillary-wall permeability (Bazzoni and Dejana 2004). The pulmonary vasculature is lined with a homogenous layer of squamous endothelial cells and is recognized as a dynamic and metabolically active organ. It can modulate several functions, such as the regulation of leukocyte diapedesis, coagulation, vasomotor tone, and barrier permeability. The integrity of this barrier depends on homophilic interactions between neighboring cells via tight junctions (composed of claudins, occludins, and junctional adhesion molecules) and adherens junctions (composed of E-cadherin). These junctions regulate the paracellular gating function which controls the transport of leukocytes, proteins and other solutes between the blood and the interstitium. Hence, they are key regulators of paracellular permeability and edema formation (reviewed in Millar et al. 2016). Additionally, endothelial cells control the passage of proteins from the luminal to the abluminal side of the endothelial cell monolayer via caveolae-mediated transcytosis. It has been shown that lung microvascular endothelial cells are caveola rich cells and that the transcytosis process is macropinocytosis and receptor-mediated, with the involvement of the scavenger receptors gp18, gp30, and gp60 (Pober and Sessa 2007; Predescu, Predescu, and Malik 2007; Raheel et al. 2019).

Acute respiratory distress syndrome

Acute Respiratory Distress Syndrome (ARDS) is a non-cardiogenic pulmonary edema occurring due to increased alveolar-capillary barrier permeability secondary to cellular damage, inflammatory cascades, and/or over-inflation by mechanical lung

ventilation. ARDS is a life-threatening condition first observed and described in the 1960s as the clinical presentation in ill adults and children of acute hypoxemia due to pulmonary gas exchange failure (Ashbaugh et al. 1967). Over the years, the need to unify the concept and definition of ARDS led to an American/European consensus on the criteria for its diagnosis (Bernard et al. 1994). The definition was updated in 2012, known as the Berlin definition (Ranieri et al. 2012) (table 1), and further revised in 2016 in the Kigali modification (Riviello et al. 2016).

Table 1.1 The Berlin Definition of Acute Respiratory Distress Syndrome

Acute Respiratory Distress Syndrome	
Timing	Within 1 week of a known clinical insult or new or worsening respiratory symptoms.
Chest imaging[1]	Bilateral opacities – not fully explained by effusions, lobar/lung collapse, or nodules.
Origin of edema	Respiratory failure not fully explained by cardiac failure or fluid overload. Need objective assessment (e.g., echocardiography) to exclude hydrostatic edema if no risk factor is present.
Oxygenation[2]	
Mild	200 mmHg < PaO_2/FiO_2 ≤ 300 mmHg with PEEP or CPAP ≥ 5 cm H_2O[3]
Moderate	100 mmHg < PaO_2/FiO_2 ≤ 300 mmHg with PEEP ≥ 5 cm H_2O
Severe	PaO_2/FiO_2 ≤ 300 mmHg with PEEP ≥ 5 cm H_2O

Abbreviations: CPAP, continuous positive airway pressure; FiO_2, fraction of inspired oxygen; PaO_2, partial pressure of arterial oxygen; PEEP, positive end-expiratory pressure.

[1] Chest radiograph or computed tomography scan.

[2] If altitude is higher than 1000 m, the correction factor should be calculated as follows: PaO_2/FiO_2 x (barometric pressure/760).

[3] This may be delivered noninvasively in the mild acute respiratory distress syndrome group. Adapted from (Ranieri et al. 2012)

The current definition describes ARDS as a condition fulfilling the following criteria: respiratory failure within one week of a known insult or new and/or worsening respiratory symptoms, pulmonary edema of non-cardiogenic origin, bilateral opacities on chest radiograph or CT, and acute onset of hypoxemia. ARDS develops mostly in the context of viral or bacterial pneumonia, non-pulmonary sepsis, gastric or oral content aspiration, and major physical trauma (Cochi et al. 2016; Bellani et al. 2016).

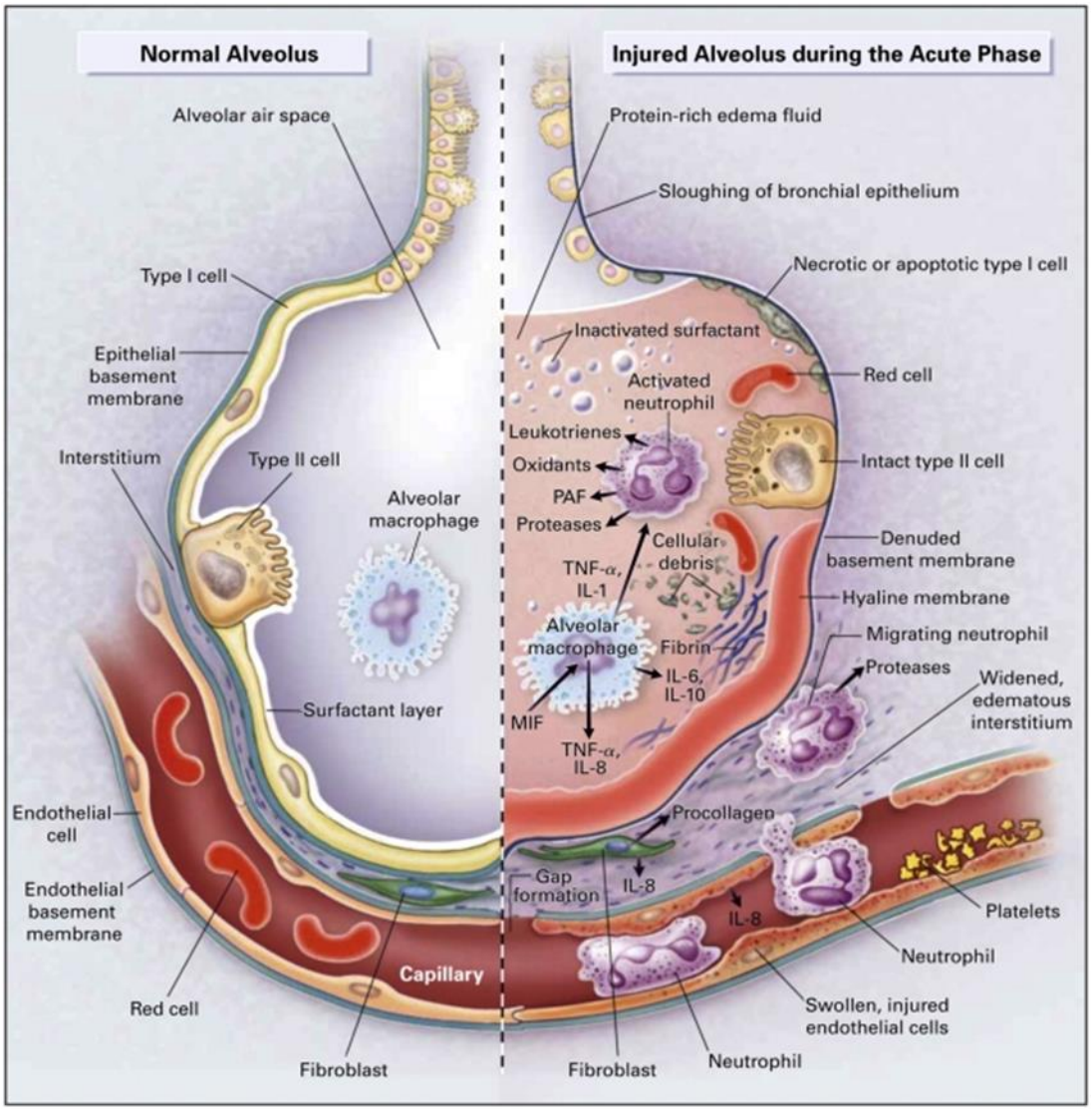

Figure 1.1: Schematic representation of a healthy (normal) and injured alveolus during the acute phase of ARDS. Right-hand side: multiple cellular responses and mediators contribute to alveolar-capillary membrane injury during the acute phase of the syndrome. There is sloughing of bronchial and epithelial cells, with the formation of protein-rich hyaline membranes on the denuded basement membrane. In the capillary can be seen neutrophils during the diapedesis process in their way to the alveolar space, filled with protein-rich edema fluid. An alveolar macrophage can be seen in the alveolar space, secreting cytokines (interleukin-1, 6, 8 and10) and tumor necrosis factor α (TNF-α), which act to stimulate chemotaxis and the activation of neutrophils. Cytokines can also stimulate fibroblast to produce extracellular matrix. Activated neutrophils release proteases, oxidants, leukotrienes, platelet activator factor (PAF) and other pro-inflammatory molecules. In the alveolus can also be found anti-inflammatory mediators such as interleukin-1 receptor antagonist, tumor necrosis factor receptor, antibodies against interleukin-8 and cytokines. The surfactant has been inactivated due to the protein rich fluid. MIF: macrophage inhibitory factor. Reproduced with permission from (Ware and Matthay, 2000), Copyright Massachusetts Medical Society.

Though less common, it can also be associated with several other settings such as pancreatitis, frozen plasma/red cells/platelets transfusion, drug overdose, inhalation of fresh or saltwater, hemorrhagic shock, reperfusion damage after a surgical

procedure, or the inhalation of smoke. Other causes for pulmonary edema which can be associated with ARDS are high altitude edema, primary dysfunction after lung transplantation, central nervous system damage and neurogenic edema, and drug-induced pulmonary damage (Michael A. Matthay et al. 2019).

ARDS is a complex syndrome, currently not diagnosable through laboratory tests, imaging, or any other “gold standard” techniques. Current treatments are based only on supportive care and mechanical ventilation. More than 10% of all ICU admissions in the world are due to ARDS cases and the mortality rate in hospitalized patients is around 40% (Michael A. Matthay et al. 2019). Patients who die with ARDS or its milder form, acute lung injury (ALI), have large quantities of insoluble protein in their air spaces. Non-survivors of ARDS exhibit threefold higher levels of precipitated protein in their edema fluid than survivors of the disease (Bachofen and Weibel 1977; Clark et al. 1995). Therefore, clearance of protein from the alveolar space is both a physiologically and clinically important process (Randolph H Hastings, Folkesson, and Matthay 2004; Michael A. Matthay et al. 2019).

Numerous clinical trials have been performed, where several compounds including neuromuscular blockade drugs (Moss et al. 2019), surfactant (Willson et al. 2015), beta-agonists (Michael A. Matthay et al. 2011), and steroids (Steinberg et al. 2006) were tested. Nevertheless, these studies yielded mixed results, and potential patient prognosis-improving pharmacological therapies have yet to be successfully developed (Bellani et al. 2016; Peck and Hibbert 2019).

Viral pneumonia and pulmonary edema

Infections of the lower respiratory tract are one of the main causes of mortality in humans, having these been responsible in 2015 for 3.2 million deaths worldwide (Mathers et al. 2017; Lozano et al. 2012). Pneumonia is a form of acute respiratory infection affecting the lungs which can be caused by pathogens such as respiratory viruses, bacteria, fungi, or combinations of these (Bosch et al. 2013; Bellinghausen et al. 2016; Zhou et al. 2018; Van Asten et al. 2018) and is one of the clinical risks that most frequently trigger ARDS. Previous to the new Covid-19 pandemic, data from epidemiologic studies of adults admitted to the intensive care unit (ICU) with respiratory failure suggest that respiratory viruses account for from 26 to 37% of severe pneumonia cases (Shah and Wunderink 2017). The reports differ in the most

commonly detected viruses, most likely due to differences in seasons and locations where the studies were performed. The viruses most often identified in patients with lower respiratory tract infections include influenza virus (IV), rhinovirus, coronavirus, respiratory syncytial virus (RSV), human metapneumovirus (hMPV), parainfluenzavirus (PIV), and adenovirus (Nguyen et al. 2016).

Influenza viruses are members of the Orthomyxoviridae family whose members are enveloped viruses containing a genome consisting of segmented negative-sense single-stranded RNA segments. There are four genera in this family: types A, B, C, and Thogotovirus. From these, only A and B are clinically relevant for humans (Blümel et al. 2009). The genome of IV consists of a negative sense, single-stranded RNA. For this reason, the virus requires its own viral RNA-dependent RNA polymerase for the transcription of at least 16 different viral proteins (Rossman and Lamb 2011; Dubois, Terrier, and Rosa-Calatrava 2014). One mature virion contains eight segments of RNA that together with the RNA polymerase form RNA-protein complexes called ribonucleoproteins (Figure 1.2). IV has an envelope derived from portions of the host cell membrane containing the antigenic determinants hemagglutinin (HA) and neuraminidase (NA), and the ion channel matrix protein 2 (M2). The HA glycoprotein binds to sialic acid (SA) residues linked to galactose bound to receptor proteins expressed on the respiratory epithelium, which then triggers the endocytosis of the virion. As the endosome matures, its acidification leads to the fusion of the viral HA with the endosomal membrane. The M2 ion channel is also activated, and the low pH dissociates the ribonucleoprotein complex which is later imported to the nucleus where the viral replication takes place. After the replication of its genome and the synthesis of new viral proteins, the assembly, budding, and release of new virions are coordinated at lipid rafts on the plasma membrane of the host cell. Once it leaves the cell, the HA protein from the new virion is bound to the sialic acid residues on membrane receptor proteins. These bonds are cleaved by NA, which then leads to the release of the new viral progeny which is then free to infect other cells (Subbarao and Joseph 2007; Herold et al. 2015).

Influenza A viruses are classified into subcategories, according to their HA and NA subtypes. So far, 16 different subtypes of HA and 9 different subtypes of NA have been identified. The nomenclature of the different strains includes the HA and NA

subtype following the pattern H(x)N(y), adding the host of origin, geographical location, strain number, and year of isolation (Blümel et al. 2009).

Influenza viruses bind through HA to SA residues bound to galactose through α2,6 (SAα2,6Gal) and α2,3 (SAα2,3Gal) linkages on the host cells (Rogers and Paulson 1983). It has been shown that the epithelium which lines the upper respiratory tract

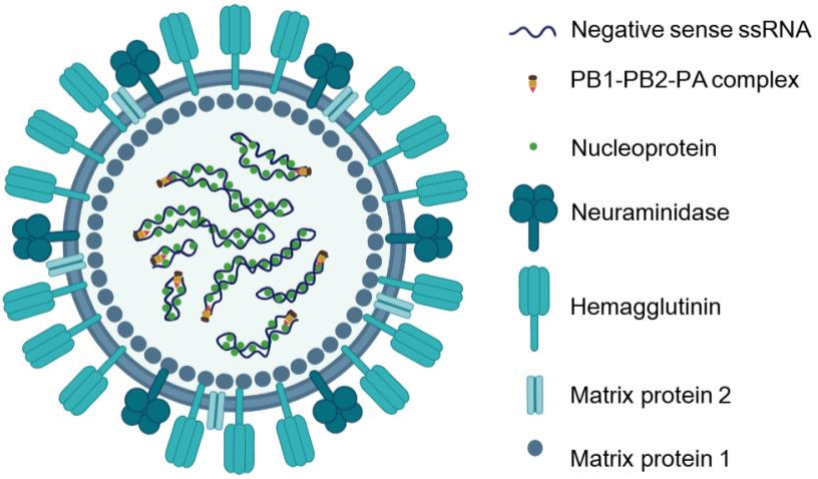

Figure 1.2: Schematic representation of an influenza virus particle. Influenza A virus (IAV) has an envelope (lipidic membrane) derived from portions of the host cell membrane, that contains the proteins hemagglutinin (HA), neuraminidase (NA) and the ion channel matrix protein 2 (M2). The main surface glycoproteins in IAV are HA and NA, which have an abundance ratio that ranges from 4:1 to 5:1. Matrix protein 1 (M1), the most abundant protein in the virion, is a structural protein that lies beneath the envelope and is also associated to the ribonucleoprotein (RNP) complex. The RNP is comprised of a negative sense, single-stranded RNA encapsidated with nucleoprotein (NP) and associated with three viral RNA polymerase proteins: polymerase basic proteins 1 and 2 (PB1, PB2), and polymerase acidic protein (PA). The virus genome encodes also a non-structural protein (NS) and a nuclear export protein (NEP). Image created with Biorender.com. Adapted from Subbarao and Joseph 2007.

(nasal and pharyngeal) and the upper part of the lower respiratory tract (tracheal and bronchiolar) expresses mainly SAα2,6Gal, whereas the dominant receptor in the lower respiratory tract (bronchiolar non-ciliated cuboidal cells and alveolar) is SAα2,3Gal (Shinya et al. 2006; Van Riel et al. 2006, 2007). HA from different strains of IV show different preferences for SA receptors. Avian IV strains contain an HA with a preference for binding to SA linked to the rest of the sugar via an α2,3 linkage. In contrast, HAs from human IV strains show enhanced binding to α2,6–linked sialic acids (Shinya et al. 2006; Van Riel et al. 2006, 2007; García-Sastre 2010). One of the main parameters in determining the level of disease is how much the lower respiratory tract is invaded by the virus (Sanders et al. 2013). Infection of AEC, in particular, seems to lead to a more severe outcome development since it provokes

the destruction of these cells and impairs gas exchange. IV strains with a preference for SAα2,3Gal linkages would then comprise a higher risk of severe outcome in humans.

Clathrin-mediated endocytosis has for long been identified and studied as the major route of IV cell entry (Patterson, Oxford, and Dourmashkin 1979; Matlin et al. 1981). However, it has been reported that macropinocytosis, the main route for the non-selective uptake of extracellular fluid by cells, also functions as an alternative viral entry route (de Vries et al. 2011).

AT1 cells have increased susceptibility to environmental insults, potentially explaining why they show a quick demise during IV infection. It has been shown that when 10% or more of alveolar type I cells are lost, the maintenance of an adequate respiratory function is compromised (Sanders et al. 2013; Kalil and Thomas 2019). Early epithelial injury is followed rapidly by AT2 cell proliferation and since they are precursors of AT1 cells, the infection and loss of AT2 cells could impair the repairing of the alveolar epithelium. Injured AEC have been shown to drive the release of pro-coagulant factors and intra-alveolar fibrin deposition, which are also deposited next to endothelial cells in the injured alveoli and can lead to the development of fibrosis in the alveoli and interstitium (Sanders et al. 2013; Michael A. Matthay et al. 2019).

During ARDS, the destruction of AEC exposes the associated endothelium to cytokines and to the pathogenic antigens, leading to the activation of resting endothelial cells which in turn acquire new capacities. Endothelial cell activation can be divided into rapid responses (type 1 activation) and slower responses (type 2 activation) which are independent and dependent on new gene expression, respectively (Pober and Cotran 1990). This activation can amplify the inflammation response as endothelial cells are capable of secreting pro-inflammatory cytokines, being the main contributors to what is known as “cytokines storm”, an excessive or uncontrolled release of these compounds (figure 1.3). Higher levels of pro-inflammatory cytokines in the circulation have been associated with higher morbidity and mortality during viral respiratory infections (Bradley-Stewart et al. 2013). This response will then dictate the level of the innate and adaptive immune reactions as well as the severity of the disease (Teijaro et al. 2011; Short, Kuiken, and Van Riel 2019; Kalil and Thomas 2019).

Within hours, increased blood flow, leukocyte adhesion and extravasation occur, as well as an increased leakage of plasma-protein-rich fluid to the inflammation site, creating a provisional matrix to support leukocyte entry into the tissue (Pober and Cotran 1990; Pober and Sessa 2007). This increased permeability to liquid and protein across the lung endothelium leads to edema within the lung interstitium, resulting in the edematous fluid translocating to the alveoli facilitated by injury to the tight barrier properties of the alveolar epithelium. This leads to an alveolar flooding that impairs alveolar gas exchange, and results in alveolar hypoxia and systemic hypoxemia which have additional deleterious effects on the alveolar epithelial function and further impairs fluid balance of the lung (Vadász and Sznajder 2006).

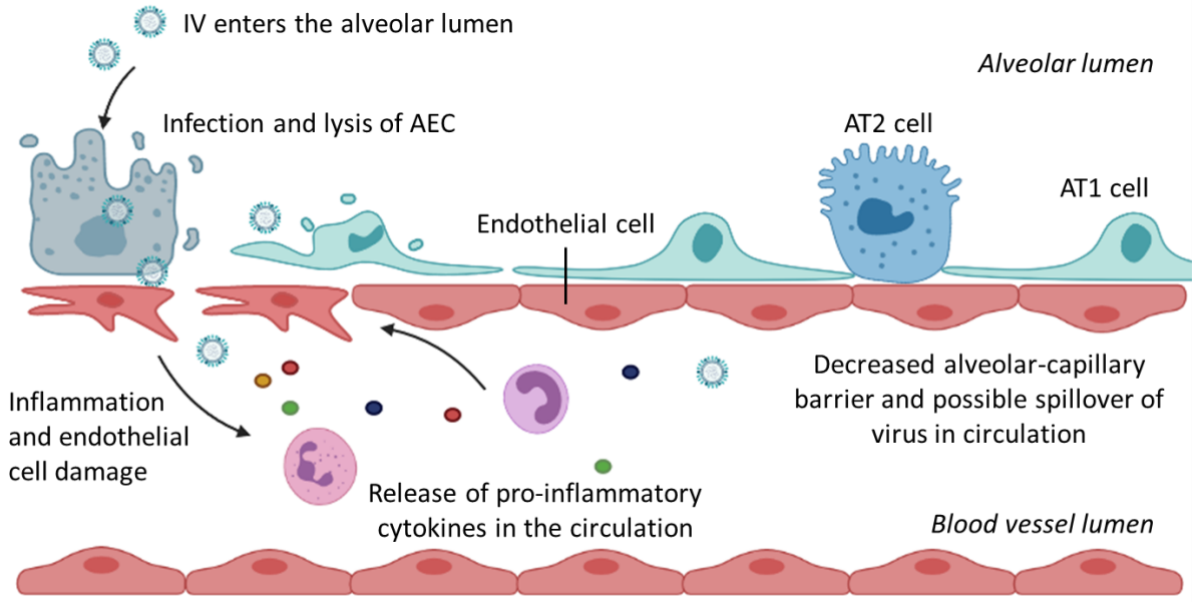

Figure 1.3 Schematic representation of the role of mammalian endothelial cells in influenza virus pathogenesis. IV, influenza A virus; AEC: alveolar epithelial cells; AT1: alveolar type 1; AT2: alveolar type 2. Figure created with BioRender.com. Adapted from Short et al. 2019

The duration of the increased lung endothelial permeability in clinical ARDS is unknown, however, studies suggest that it could last from many hours to weeks and that its persistence is associated with lung injury and slow recovery (Gotts, Abbott, and Matthay 2014). Studies have also shown that alveolar barrier permeability restoration is temporally correlated to AT2 to AT1 cell transdifferentiation (Jansing et al. 2017). Altogether, a more precise understanding of the timing of this barrier disruption could influence the timing and administration of potential therapeutic treatments (Michael A. Matthay et al. 2019).

Protein clearance in the alveolar epithelium

Human albumin is a relatively small protein (66 kDa) that constitutes nearly 50% of plasma proteins in normal, healthy individuals. It functions as a plasma carrier of a diversity of molecules including hormones, fatty acids, sterols, vitamins, and drugs. Being the main component found in blood and having a strong net negative charge, albumin is responsible for approximately 70% of the oncotic pressure of plasma, interstitial fluid, and lymph, therefore playing a critical role in modulating the distribution of fluid between compartments (T. W. Evans 2002). Albumin concentration in plasma is near 40 mg/mL and is tightly regulated in order to maintain the osmotic homeostasis. In the alveolar lining fluid, albumin concentration under normal conditions is no more than 10% of that in the plasma (less than 4 mg/mL) (Takano et al. 2015). During ARDS, the increased lung endothelial permeability leads to the formation of a protein-rich alveolar edema. Protein leakage from plasma can increase the protein concentration in the alveoli to 75-95% of the levels found in plasma and therefore impair the edema resolution (Randolph H Hastings, Folkesson, and Matthay 2004). Also, an excess of protein in the alveolar space may contribute to the formation of a conglomerate of plasma proteins, fibrin strands, cell debris, and macrophages, known as the hyaline membrane, and induce fibrogenesis (Tomashefski and Farver 2008). Moreover, protein degradation products, such as amino acids and peptides, may affect the epithelial barrier and enforce edema formation (Kim and Malik 2003). Thus, the removal of excess protein from the alveolar space is essential for a positive resolution in ARDS.

Several mechanisms have been proposed for the removal of protein from the alveoli, including clearance by the mucociliary escalator, phagocytosis by macrophages, intra-alveolar catabolism, passive diffusion between cells in the epithelial barrier, and transcytosis (endocytic transport across the epithelial cells in vesicles) (reviewed by Hastings, Folkesson, and Matthay 2004; Folkesson et al. 1996). Evidence was found indicating that the mucociliary escalator is an insignificant route for the escape of protein from the lung (M. A. Matthay, Berthiaume, and Staub 1985; M. A. Matthay, Landolt, and Staub 1982). On the other hand, only small amounts of alveolar tracer protein are found in macrophages, and most alveolar protein reaches the blood-stream without alteration within days after the instillation of protein solutions in the air spaces (Berthiaume et al. 1989; Goodale, Goetzman, and Visscher 1970; M. A.

Matthay, Berthiaume, and Staub 1985), suggesting minimal impact for the first three mechanisms in acute alveolar protein clearance(Randolph H Hastings, Folkesson, and Matthay 2004; Folkesson et al. 1996; Patton 1996). Hence, the main protein clearance mechanisms recognized in the lung are passive diffusion and transcytosis.

Several FITC-albumin uptake studies were performed in alveolar cell culture models; either AT2 type cell lines (RLE-6TN, A549) or primary AT2 and AT1-like cells. The findings indicated that albumin is taken up mainly by clathrin-mediated endocytosis and that the rate of albumin uptake in AT2 cells is higher than in AT1 cells. In both cells, FITC-albumin uptake was inhibited by clathrin-mediated endocytosis inhibitors, but not caveolae-mediated endocytosis inhibitors (Ikehata et al. 2008; Yumoto et al. 2006; Tagawa et al. 2008; Yumoto et al. 2012; Kawami et al. 2018).

Alveolar epithelial monolayers are a convenient model for studying transcellular transport as they are readily available and can be easily analyzed. However, they comprise only one of the 40 or more cell types present in the distal lung, and they model only the AT2 cells of the alveolar epithelial barrier, lacking other components of the lung stroma. Consequently, data from monolayer studies may not represent a complete picture of transport mechanisms active in the lung in vivo (Randolph H Hastings, Folkesson, and Matthay 2004).

In the works of Buchäckert et al. and Rummel et al. where rabbit whole-lung models were employed, it was suggested that the transport of albumin from the alveoli into the vascular compartment is unidirectional, receptor-mediated, and facilitated by active transcytosis across the alveolar epithelium (Buchäckert et al. 2012; Rummel 2007). Several other studies of alveolar protein clearance in whole-animal or whole-lung models under normal conditions showed evidence for endocytosis across the alveolar epithelium, as well as evidence for paracellular diffusion. At low albumin concentrations (<5 mg/mL), the transport of protein shows saturable properties, is dependent on the temperature, and is sensitive to pharmacological agents which either stimulate or inhibit endocytosis. In higher concentrations of protein (>5 mg/mL), the rate of clearance is not affected by pharmacological agents, doesn't show saturation kinetics, and is proportional to the concentration (John et al. 2001; R. H. Hastings et al. 1994, 1995; Randolph H Hastings, Folkesson, and Matthay 2004; Rummel 2007; Buchäckert et al. 2012).

Megalin, a key alveolar protein clearance mediator

Protein uptake in the alveolar epithelium is a receptor-mediated, active process. Our group has previously identified the endocytic receptor megalin as the main player in the clearance of albumin from the alveolar space (Buchäckert et al. 2012; Grzesik et al. 2013; Vohwinkel et al. 2017; Mazzocchi et al. 2017).

Megalin was first identified in 1982 as the major pathogenic antigen in Heymann nephritis, a rat model of membranous glomerulonephritis (Kerjaschki and Farquhar 1982). It is a 600 kDa protein member of the low-density lipoprotein (LDL) receptor-related protein (LRP) gene family and encoded by the LRP2 gene. It has a large extracellular domain containing four clusters of ligand-binding, cysteine-rich complement-type repeats (figure 1.4). The clusters contain 7 to 11 complement-type repeats, with approximately 40 amino acids each. These binding clusters are separated by YWTD and EGF domain repeats that participate in ligand release within the acidic environment of the lysosomes and the subsequent recycling of the receptor. Megalin also has a single transmembrane domain that is comprised of 23 amino acids and has 209 amino acids in its cytoplasmic c-terminal tail, where several consensus phosphorylation sites for different protein kinases are located (NPXY, PPPSP). These modules regulate megalin trafficking and endocytosis (Willnow, Nykjaer, and Herz 1999; Christensen et al. 2012; Willnow, Hammes, and Eaton 2007).

Megalin acts as a multi-ligand clearance receptor. It has been reported to bind and mediate the endocytosis of more than fifty ligands, playing an important role in different tissues at various stages of development. It is expressed on the apical surfaces of embryonic and adult polarized epithelial cells, including the neuroepithelium, kidney, lung, intestine, eye, oviduct, uterus, and male reproductive tract (Willnow et al. 1996; Christ, Marczenke, and Willnow 2020; Spuch, Ortolano, and Navarro 2012; Zheng et al. 1994). In the lung, megalin is found in the apical section of AT2 cells (Zheng et al. 1994). Under some specific ligand-triggered conditions, megalin undergoes transcytosis migrating from the apical side to the opposite cell surface. This transcytosis has been reported in several epithelial cell types and plays a role in the transport of internalized ligands like thyroglobulin, leptin, sonic hedgehog, and albumin to the opposite plasma membrane, thus releasing them

to the extracellular environment without degradation (reviewed by (Marzolo and Farfán 2011)).

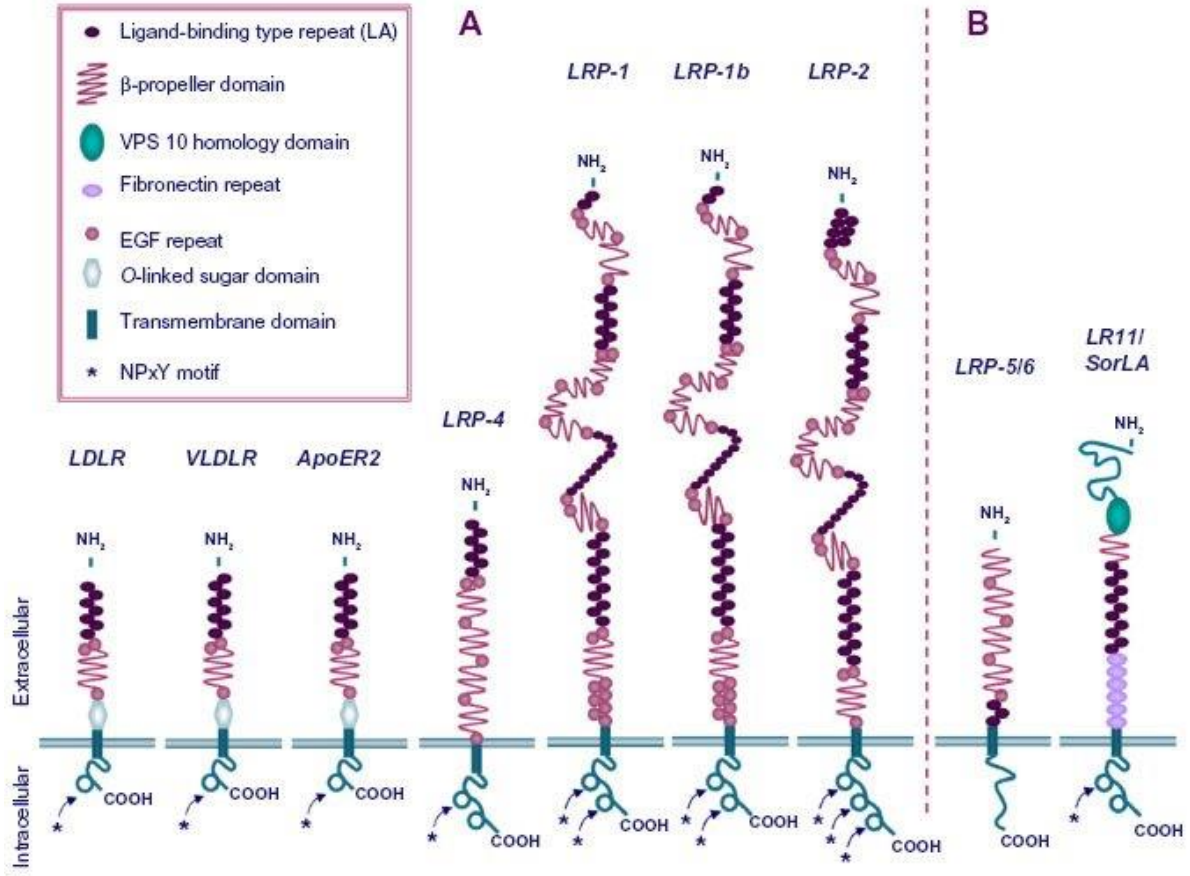

Figure 1.4. Schematic representation of the LDL receptor family. Megalin shares common structural motifs with other members of the LDL receptor family. The clusters of ligand-binding complement type repeats in their extracellular domain, the epidermal growth factor-type (EGF) repeats, β-propeller domains which are essential for the pH-dependent release of ligands in endosomes, a single transmembrane domain and a short cytoplasmic domain containing conserved NPXY endocytic motifs. While the ectodomains share significant sequence similarity, the cytoplasmic domains are unique, which indicates that the ligands internalized by each receptor will have distinct cellular fates. Receptors on the left are considered to be core members of the protein family since their extracellular domains are built from a unifying module that can exist in single (LDLR) or multiple (e.g. LRP2) copies in the receptors. Receptors on the right are more distantly related, as the module is inverted (LRP5/6) or combined with motifs that are not seen in the other receptors (e.g. SORLA). APOER2, apolipoprotein E receptor 2; Ce, C. elegans; LDLR, low-density lipoprotein receptor; LRP, LDL receptor-related protein; MEGF7, multiple epidermal growth factor-type repeat containing protein 7; RME-2, receptor-mediated endocytosis-2; SORLA, sortilin-related receptor with A-type repeats; VLDLR, very low-density lipoprotein receptor. Adapted from Emonard and Marbaix 2015.

Regulation of megalin expression and receptor activity in the lung

TGF-β and ARDS

Transforming growth factor β (TGF-β) is a family of small polypeptide factors whose functions influence cellular processes playing an important physiological and immunological role. TGF-β is a bifunctional regulator that either inhibits or stimulates cell proliferation. In the immune system, it regulates the initiation, development, and resolution of immune responses. It can function as both an immunosuppressive and as a potent pro-inflammatory agent due to its ability to regulate inflammatory molecules, induce cytokine secretion, and stimulate T-cell differentiation. (Massagué 1992; Morikawa, Derynck, and Miyazono 2016).

TGF-β is secreted as a biologically inactive protein termed latent TGF-β (LTGF-β), composed of an amino-terminal latency-associated peptide (LAP) that remains non-covalently associated with the carboxy-terminal mature TGF-β molecule. Although TGF-β synthesis and expression of its receptors are widespread, activation is localized to sites where TGF-β is released from LAP (Massagué 1992; Shi et al. 2011). The activation mechanisms that result in the release of active TGF-β protein have been mostly studied in the case of TGF-β1. LTGF-β1 contains an integrin recognition motif and binds to integrins. Biochemical and structural studies revealed that contractile force is necessary for the release of mature TGF-β1 after complex formation between the integrin and LTGF-β1 (reviewed by Morikawa, Derynck, and Miyazono 2016). Proteases such as plasmin, thrombin, MMP-2, and MMP-9, and reactive oxygen species-mediated conformational changes in LAP, can also release TGF-β1 from the LAP. Bacterial and viral sialidases can desialylate TGF-β1, leading to the release of active mature TGF-β1 (Karhadkar, Meek, and Gomer 2021). In the specific case of IV infection, *in vitro* studies showed that the viral NA is able to directly activate latent TGF-β through cleavage of the sialic acid residues on the LAP (Schultz-Cherry and Hinshaw 1996; Carlson et al. 2010). Proinflammatory factors, including TGF-β, are elevated in BAL fluid from ARDS patients (Morty, Eickelberg, and Seeger 2007) and TGF-β-inducible genes are upregulated in the lungs of ARDS patients (Fahy et al. 2003). Moreover, during ARDS TGF-β has an impact on epithelial and endothelial permeability through action on protease-activated receptor-1 and regulating ion and fluid transport in the lung to promote alveolar flooding and fibrosis, making this cytokine a key mediator in ARDS pathology (Jenkins et al. 2006; Peters et al. 2014; Budinger et al. 2005).

TGF-β1/GSK3β/megalin axis

Previous work from our group showed that megalin plays a central role in alveolar protein clearance (Buchäckert et al. 2012; Vohwinkel et al. 2017) in cell lines, primary cultured cells and megalin heterozygous knockout mice models (megalin homozygous knockout mice show neural deficiencies and die perinatally due to respiratory failure (Willnow et al. 1996)). Transforming Growth Factor β1 (TGF-β1), a key mediator cytokine in ARDS (Dhainaut, Charpentier, and Chiche 2003), reduces protein transport by promoting the de-phosphorylation and consequent activation of Glycogen Synthase Kinase 3β (GSK3β) through the activity of protein phosphatase 1 (PP1). Active GSK3β phosphorylates the PPPSP motif located on megalin's cytoplasmic domain leading to a continuous internalization of the receptor, hence negatively regulating megalin recycling and cell surface availability, and as a result leading to an impaired protein uptake (fig. 1.5) (Vohwinkel et al. 2017). Further studies of this pathway found that expression of GSK3β could be regulated by the RNA-binding protein ELAVL-1/HuR (Embryonic Lethal, Abnormal Vision, Drosophila-Like) in A549 cells (Hoffman et al. 2017), highlighting that protein uptake in the alveolar space is a multi-level regulated process.

Regulated intramembrane proteolysis of megalin

There is increasing evidence that megalin undergoes regulated intramembrane proteolysis (RIP) in response to ligand binding in a Notch-like signaling pathway (Zou et al. 2004; Mazzocchi et al. 2017). RIP is a conserved process that connects a receptor function with intracellular signaling. (Schroeter, Kisslinger, and Kopan 1998; Kühnle, Dederer, and Lemberg 2019). This process involves the shedding of megalin's ectodomain by a matrix metalloprotease (MMP), which produces a characteristic membrane-associated carboxyl-terminal fragment (MCTF). Subsequently, the activity of γ-secretase mediates the intramembrane proteolysis of MCTF, producing a soluble COOH-terminal cytosolic domain that translocates into the nucleus where it regulates genetic expression (fig. 1.6) (Zou et al. 2004; Biemesderfer 2006; Y. Li, Cong, and Biemesderfer 2008; Mazzocchi et al. 2017).

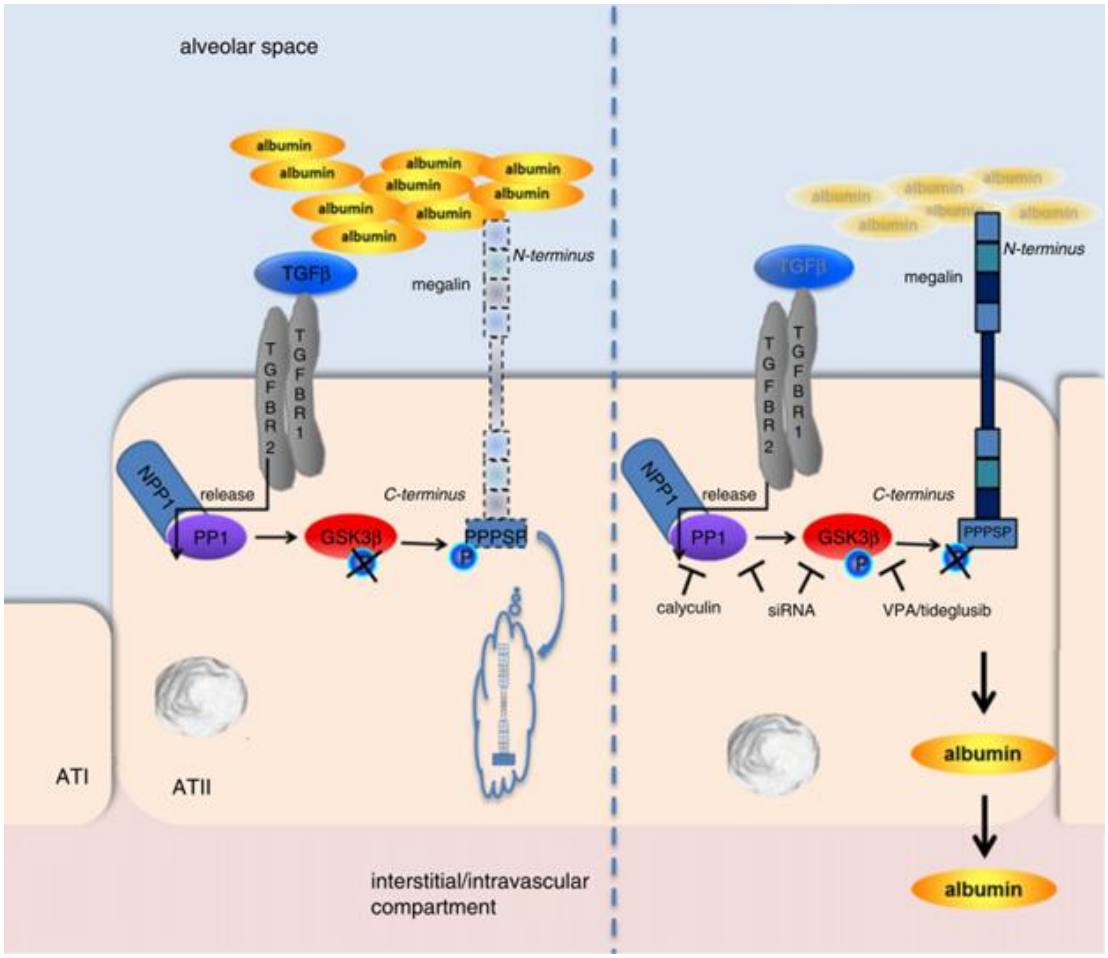

Figure 1.5. Schematic representation of the mechanisms of impaired alveolar protein clearance in ARDS and potential means of rescue. In acute lung injury (ALI) and acute respiratory distress syndrome, enhanced alveolar concentrations of TGF-β1 impair megalin-mediated alveolar albumin clearance, resulting in persistence of the protein-rich alveolar edema. The underlying signaling cascade includes the release of nuclear inhibitor of PP1 (NIPP1) from PP1, thereby activating the phosphatase, which dephosphorylates glycogen synthase kinase 3β (GSK3β) at Ser-9, leading to its activation. Active GSK3β phosphorylates the albumin receptor, megalin, at the C-terminal PPPSP domain and promotes its internalization, and thus loss of albumin clearance. In contrast, interference with PP1 (siRNA or calyculin) or GSK3β (siRNA or the clinically relevant pharmacological agents valproic acid (VPA) or tideglusib) prevents megalin phosphorylation and re-establishes alveolar transepithelial protein clearance, thus promoting ALI resolution. ATI, alveolar epithelial type 1 cell; ATII, alveolar epithelial type 2 cell. Adapted from Vohwinkel et al. 2017.

Matrix metalloproteinases (MMPs) comprise a family of zinc-dependent extracellular proteases with a variety of substrates like cell-surface receptors, matrix macromolecules, and hormones, which can act while attached to the plasma membrane (MT-MMPs) or secreted into the extracellular space (Page-McCaw, Ewald, and Werb 2007). MMPs are produced by a variety of stromal, epithelial and inflammatory cells and together are capable of degrading all known components of the extracellular matrix (ECM).

It has also been demonstrated that MMPs act on several non-ECM substrates such as pro-tumor necrosis factor α (TNF-α), pro-interleukin 1β (IL-1β), pro-TGF-β, chemokines, antiproteases and pro-proteases (Davey, McAuley, and O'Kane 2011). They are important in normal physiological processes such as embryogenesis, proliferation, angiogenesis, cell motility, wound healing, and degradation of the extracellular matrix (Quintero-Fabián et al. 2019; Rojas-Quintero et al. 2018; Caley, Martins, and O'Toole 2015; Cui, Hu, and Khalil 2017). During ALI/ARDS, MMPs play an important role in the degradation of protein components in the alveolo-capillary barrier, including intercellular junction proteins, the basal membrane and the proteins anchoring cells to it, all of which are considered central in the pathogenesis of the disease.

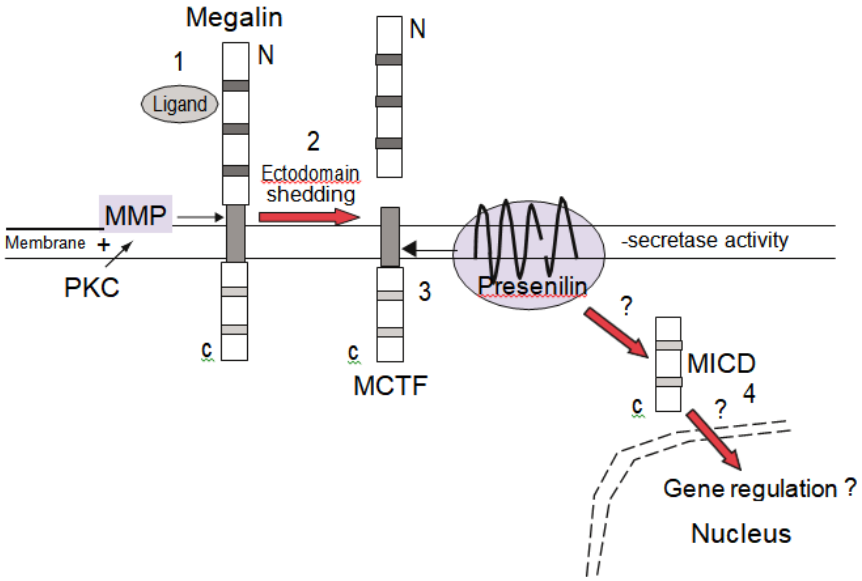

Figure 1.6. Regulated intramembrane proteolysis of megalin. This scheme shows known and postulated (?) events in a proposed megalin signaling pathway. Metalloprotease (MMP) activity, activated by ligand binding (1) and regulated by protein kinase C, results in ectodomain shedding (2) of megalin. Ectodomain shedding produces an MCTF, which in turn becomes the substrate for γ-secretase activity acting in the membrane and releasing the 'free' C-terminal intracellular domain (megalin intracellular domain) into the cytosol (3). The megalin intracellular domain translocates (4) to the nucleus where it may act as a transcriptional regulator. Presenilin is the active component of the γ-secretase protein complex. Reprinted from Biemesderfer 2006, with permission from Elsevier.

MMPs are commonly classified using a combination of domain organisation, sequence homology and substrate specificity, as "collagenases" (MMP-1, -8 and -13), "gelatinases" (MMP-2 and -9), "stromelysins" (MMP-3 and -10), "matrilysins" (MMP-7 and -26), "membrane-bound" (MMP-14, -15, -16, -17, -24 and -25) and others (MMP-11, -12, -19, -20, -21, -22, -23, -27 and -28) (Davey, McAuley, and

O'Kane 2011). They all share common mechanisms of activity regulation, including the activating cleavage of the latent proenzyme form and the inhibition of the active enzyme by tissue inhibitors of metalloproteinases (TIMPs)(Visse and Nagase 2003). Extracellular levels of certain MMPs are also regulated by selective internalization and intracellular degradation, and studies have shown that cell-surface receptors such as megalin may interact with secreted MMPs to mediate their re-endocytosis and regulate pericelular proteolysis (Johanns et al. 2017; Murphy and Nagase 2011; Emonard and Marbaix 2015).

In the lung, MMPs have been reported to be upregulated in the BAL of patients with ARDS and to play a critical role in the remodeling of the ECM and the reparation of the alveolar-capillary barrier (Torii et al. 1997; Corbel, Boichot, and Lagente 2000). In the previous work from our group by Mazzocchi et al., 2017, it was shown that TGF-β1 treatment led to increased shedding and RIP of megalin at the cell surface. Subsequently, there was an increase in the abundance of the intracellular megalin COOH-terminal fragment and a transcriptional downregulation of the receptor was observed. The activities of protein kinase C enzymes and γ-secretase were required for the TGF-β1-induced megalin downregulation, which further supports a Notch-like processing mechanism. Additionally, TGF-β1-induced shedding of megalin was mediated by MMPs-2, -9, and -14, since silencing MMP-2, -9, or -14 prevented TGF-β1 induced reduction of megalin cell surface abundance and restored albumin binding and uptake in RLE-6TN cells (Mazzocchi et al. 2017).

Hypothesis

Based on the evidence that:

a) IV is one of the leading causes of acute lung injury and ARDS
b) TGF-β1 is activated in the presence of IV
c) TGF-β1 acts as a regulator of the ARDS pathogenesis
d) There is evidence that the axis TGF-β1/GSK3β induces downregulation of megalin in the lung
e) Megalin has been shown to play a key role in protein uptake in the alveoli

We hypothesize that:

IV induces megalin downregulation in alveolar epithelial type 2 cells, through activation of the TGF-β1/GSK3β axis, impairing alveolar protein clearance and promoting inflammation and alveolar edema.

Aims of the study

In this study, we aimed to:

- Characterize the albumin uptake process in cultured and PCLS derived AEC.
- Study the effect of IV infection on the TGF-β1 expression, GSK3β activation, and megalin cell surface expression.
- Study the effect of IV infection on the protein uptake process within the alveolar epithelium.

2. Materials and methods

In vitro experiments

Cell culture

MLE-12 cells, an SV40 transformed alveolar epithelial cell line (ATCC CRL-2110), were incubated at 37°C in air containing 5% carbon dioxide and 80-90% humidity. Cell cultures were kept in a Heracell 150i CO_2 Incubator (ThermoFisher Scientific, Waltham MA, USA). Nutrients were provided in DMEM/F-12, GlutaMAX culture medium containing 2% FBS Solution, and 1% penicillin/streptomycin antibiotics (conditioned medium). The culture medium was replaced every two days for cell culture maintenance. For subculturing, cells were rinsed once with sterile phosphate saline buffer (PBS) and incubated for 5 minutes with 0,25% trypsin-EDTA for cellular detachment. Digestion was stopped by adding conditioned medium into the plates, and cells were resuspended through pipetting and plated as needed in appropriate Petri dishes, six-well plates, or microscopy slides. All media, supplements, and reactants were purchased from Gibco, ThermoFisher Scientific, Waltham, MA, USA.

Mouse strains

Precision-cut lung slices (PCLS) were obtained from Wildtype C57BL/6 and SftpcCre$^{ERT2/+}$; tdTomato$^{flox/flox}$ mice kindly provided by Dr. Christos Samakovlis, Justus Liebig University, Giessen. Wildtype C57BL/6 mice for animal experiments were kindly provided by Dr. Susanne Herold, Justus Liebig University, Giessen.

Precision-cut lung slices (PCLS) and in vitro culture

The methodology involved in preparing and culturing PCLS has been described elsewhere (Sanderson 2011; Wu et al. 2019). Briefly, adult mice aged six to eight months were euthanized in a CO_2 chamber followed by cervical dislocation, and they were placed on a Styrofoam bed in the supine position. After disinfection of the skin and hair with ethanol 70%, the abdominal cavity was opened through a long incision on the medial line of the abdomen up to the xiphoid process of the sternum. By gently lifting the xiphoid process, a small incision was made on the diaphragm, which was cut along the inner surface of the costae to the spine in the back. Then, the thoracic cavity was opened by cutting along the sternum until the jugular notch was

reached. The ribs were pulled aside and fixed aside, revealing the heart and lungs. The lungs were flushed with cold PBS in order to remove the remaining blood in the tissue. After tracheostomy, the lungs were inflated with a solution of 1% ultra-low melting agarose (A2576, Sigma-Aldrich, Darmstadt, Germany) in PBS at 37 °C until the tip of the accessory lobe was completely inflated (approximately 1-1.5 mL of agarose). The lungs were removed and placed in ice-cold, sterile PBS for 10 minutes to allow the agarose to solidify. The lobes were then separated and embedded into 5% Agarose NEEO ultra-quality (2267.4, Carl Roth, Karlsruhe, Germany) blocks for vibratome sectioning. 200 µm thick sections were obtained using a Leica VT 1200 S vibratome (Leica, Wetzlar, Germany) with an amplitude of 1.5 mm and a speed of 0.5 mm/s. The lung slices were transferred immediately after sectioning to conditioned culture medium. During experiments, each slice was cultured in 400 µl of culture medium with daily medium changes. When PCLS were obtained from SftpcCre$^{ERT2/+}$; tdTomato$^{flox/flox}$ mice, on day 0, slices were treated with either (Z)-4-Hydroxytamoxifen (H7904, Sigma-Aldrich, Darmstadt, Germany) 2,5 µM or vehicle for 24 hours, which was removed on day 1 with three washes with medium before starting treatments.

Conditioned culture medium composition: DMEM/F12 (Gibco, 11320-074) with 10% FBS (Gibco, 10270-106), 1% penicillin/streptomycin (Gibco, 15070-063), 0,1% Amphotericin B (Gibco, 15290018)

PCLS tissue dissociation

After treatment, PCLS were dissociated following a modified protocol for AEC isolation from lung tissue (Finkelstein and Shapiro 1982). Briefly, five PCLS per condition were pooled together and digested for 20 minutes at 37°C with 500 µL of a solution containing elastase 250 ng/mL (EC134, Elastin Products Co. Inc., Owensville, MO, USA) Trypsin/EDTA 0.5% (Gibco, 15400054) in FCS free DMEM:F12 medium (Gibco, 31331093,) with gentle shaking. Cells were then washed in MACS buffer pelleted at 300 x g for 10 min at 37°C, resuspended in PBS+/+ and kept on ice for further analysis.

Virus strain

In all viral infection experiments, the influenza virus (IV) strain used was A/Puerto Rico/8/1934 H1N1 seasonal, mouse-adapted originated at Stephan Pleschka,

Medicinal Virology department, Justus Liebig University Gießen and propagated on MDCK II cells.

Infection with Influenza A virus

Frozen vials containing IV (stock) were thawed on ice and then diluted in DMEM:F12 (Gibco) 0.1% BSA (A0281, Sigma-Aldrich, Darmstadt, Germany) 0,01% TPCK-treated trypsin (LS003740, Worthington Biochemical, Lakewood, NJ, USA) to prepare the incubation medium. PCLS were washed with PBS and incubated in 48 wells plates, one slice per well with 400 µL of incubation medium containing $1x10^6$ plaque-forming units (pfu) of IV per piece for 2 h. Then the medium was removed, washed once with PBS, and incubated in DMEM:F12 0.1% BSA 0,01% trypsin at 37°C in 5% CO_2 for the incubation times of each experiment.

For IV infection in cell culture cells were inoculated as previously described (Högner et al. 2013). IV was added in DMEM:F12 0.1% BSA to MLE-12 cells in multiplicities of infection (MOI) of 0.1 or 1 depending on the experiment. Cells were incubated at 37°C in 5% CO_2 for one hour and then washed once with PBS and incubated with fresh DMEM:F12 0.1% BSA for the required time until the experiment was performed. TPCK-treated trypsin was not added into cell cultures as it exhibited toxicity and increased cell death in timepoints longer than one hour.

Albumin binding and uptake assay

Measurements of cellular binding and uptake of FITC-labeled albumin were made following an adaptation of previously described protocols (Buchäckert et al. 2012; Grzesik et al. 2013; Vohwinkel et al. 2017; Mazzocchi et al. 2017). After treatment, MLE-12 cells were washed with pre-warmed PBS and incubated in a 50 µg/mL solution of FITC-albumin (A9771, SigmaAldrich, Darmstadt, Germany) dissolved in Dulbecco's PBS containing 5 mM glucose and 0.1 mM $CaCl_2$, 0.5 mM $MgCl_2$ for 1 hour. Cells were rinsed three times with ice-cold PBS without Ca^{2+} and Mg^{2+} (PBS) and incubated for 10 minutes with ice-cold Solution-X (DPBS-G, 0.5 mg/mL trypsin, 0.5 mg/mL proteinase K, 0.5 mM EDTA) in amounts of 0.5 mL of solution per p35 Petri dish, in order to detach the cells from the culture dish and cleave proteins on the cell surface. Cells were recovered and centrifuged at 10000 x g for 10 min. The supernatant was then removed and stored on ice to assess the bound fraction (binding of FITC-albumin to the cell surface). The pellet was solubilized in 0.5 mL of

0.1% Triton-X-100 to detect taken-up FITC-albumin. Fluorescence in the bound and solubilized fractions was detected using a plate fluorescence spectrophotometer reader (Infinite 200, Tecan Group) at an excitation wavelength of 500 nm and an emission wavelength of 520 nm.

DPBS-G: 0.1 mM $CaCl_2$, 0.5 mM $MgCl_s$, 5 mM Glucose in PBS.

Inhibition experiments

For inhibition studies, the following compounds were used: MT1-MMP Inhibitor, NSC405020 (444295 Sigma-Aldrich, Darmstadt, Germany) in 0.1% DMEM, Chlorpromazine hydrochloride (C8138 Sigma-Aldrich, Darmstadt, Germany), Dynasore - CAS 304448-55-3 - Calbiochem (324410 Sigma-Aldrich, Darmstadt, Germany), Tideglusib SML0339 (Sigma-Aldrich, Darmstadt, Germany). In all cases, compounds were dissolved in DMSO. MLE-12 cells or PCLS were incubated in the presence of the inhibitor or vehicle only in the case of controls.

In vivo experiments

All animal studies were performed according to protocols approved by the Animal 120 Ethics Committee of the Regierungspraesidium Giessen (permit numbers: G71/2018 and GI 20/10 No. 21/2017 No.838-GP).

Eight-week-old wildtype C57BL/6 mice (wt) mice were obtained from Charles River Laboratories. Two groups of 5 individuals were created: control and infected. Previous to intratracheal instillation, mice were premedicated with Atropine (application 0.05 mg/kg; diluted in 0.9% sterile NaCl 1:100 and applied subcutaneously at 0.2 mL per 20 g bodyweight, pre-warmed to body temperature). Mice were anesthetized by isoflurane gas inhalation (4% during initial anesthesia in isoflurane chamber, adjusted to 3% via face mask inhalation during fluid application) and kept on heating pads to maintain body temperature. Anesthetic depth was assessed by pinching the webbed area between the toes. Mice were then fixed by the upper teeth in the supine position on an intubation stand. An orotracheal tube (27G) was inserted into the mouth, through the vocal cords, and into the trachea. Using a Hamilton syringe, mice were inoculated with $0.35x10^3$ pfu of PR8 IAV diluted in 70 µL of sterile PBS-/- (IV infected group) or 70 µL of sterile PBS -/- alone (control group). Mice were then transferred to individually ventilated cages

and monitored 1-3 times a day for 5 days. Mice were sacrificed 5 days after infection via exsanguination during anesthesia with Xylazine (Rompun, Bayer Healthcare LLC, Tarrytown, NY, USA) (16mg/kg), Ketamin (Ketaset, Zoetis Manufacturing and Research, S.L., Girona, Spain) (100 mg/kg) diluted in 0.9% sterile NaCl given at 0.2 mL/20g bodyweight via intraperitoneal injection (29G). Anesthetic depth was assessed by pinching the webbed area between the toes and the last third of the tail, the abdominal cavity was opened, and the vena cava incised for exsanguination.

Tissue sampling and AEC isolation

After anesthetic depth was assessed, the chest cavity was opened, and the lungs were perfused with sterile PBS -/- via the right ventricle. A small incision was made into the trachea to insert a shortened 21-gauge cannula. To obtain the broncho-alveolar lavage (BAL), 300 µL of PBS-EDTA was added through the cannula (first fraction). The procedure was then repeated twice with 400 µL and 500 µL, respectively, and all fractions were kept on ice until further processing. The superior lobe was tied by the bronchus, excised, and stored in paraformaldehyde (PFA) 4% for 24h at 4°C. Through the cannula, 1.5 mL of sterile dispase followed by 500 µl of pre-warmed low-melting agarose (1% in PBS) was administered into the lungs to allow enzymatic separation of distal but not proximal epithelial cells. After agarose jellied at room temperature (RT), the lungs and trachea were removed, washed in PBS, and placed in dispase for 40min at RT. Next, the heart, trachea, and large airways were removed, and the remaining lung tissue was dissected in DMEM/2,5% HEPES plus 0.01% DNase in C tubes using the gentleMACS Dissociator (Miltenyi Biotec, Bergisch Gladbach, Germany). Cells were filtered through 70, 40, and 20 µm cell filters, washed, resuspended in DMEM/2,5% HEPES, and counted. Then cells were incubated with biotinylated anti-mouse CD31, CD16/32, and CD45 antibodies for 30 min at 37°C to remove remaining endothelial and lymphoid cells. After incubation, cells were washed, and streptavidin-linked magnetic beads (150 µl per $1x10^6$ cells) were added for 30 min at RT with gentle rocking. After incubation, magnetic separation was performed for 15 min. The remaining cells were washed, resuspended in PBS, and kept on ice for mRNA and protein expression analysis.

Flow cytometry analysis of immune cell populations in the bronchioalveolar fluid (BAL)

Multicolor flow cytometric analysis was performed with an LSR Fortessa using DIVA software (BD Biosciences). In summary, BAL was obtained from control and influenza-infected mice as described in the previous section. BAL samples were centrifuged at 1600rpm, 8min, 4°C and resuspended in FACS buffer (PBS, 7.4% EDTA, 0.5% FCS pH 7,2, 0,01% NaAz) containing immune globulin blocking solution [10% Gamunex-C (Grifols, ES)/1% BSA/0.02% NaAz]. Cells were incubated in an antibody mixture for 20min at 4°C, washed, resuspended in 400µl FACS buffer, then routinely stained for 7min with 7-AAD (BioLegend, USA) for dead cell exclusion. The list of antibodies used can be seen in table 2.0. Gating strategy and antibody concentrations were set with the help of corresponding isotype antibodies which served as negative controls. Data analysis was performed with FlowJo™ v10.7 software (BD Biosciences, USA).

Staining protocol for immune cell populations:

Table 2.0 Antibodies for analysis of immune cell populations in the bronchioalveolar fluid

	Antibody	**Dilution**
Leukocytes	CD45 APC/Cy7, Biolegend, 103116	1:100
Neutrophils	Ly6G APC, Biolegend, 127614	1:50
Resident alveolar macrophages /eosinophils	SiglecF BV421, BD Biosciences, 565934	1:50
Resident cells	CD11c PE/Cy7, Biolegend, 117318	1:20
Cell adhesion marker	CD11b FITC, Biolegend, 101205	1:50
Dead cell staining	7AAD, Biolegend, 420403	3.5µl/sample

Analysis of protein expression

Total protein extraction and quantification

For MLE-12 experiments, cells were washed twice with PBS, and mRIPA buffer (50 mM Tris-HCl, pH 8, 150 mM NaCl, 1% NP-40 (Sigma-Aldrich, Darmstadt, Germany), 1% sodium deoxycholate (Sigma-Aldrich, Darmstadt, Germany), cOmplete Protease Inhibitor Cocktail (Roche) was added to the cell cultures and incubated on ice for 10min. Then, cells were disrupted with a cell scraper and centrifuged at 4°C for 10 min at 10,000 x g. In the case of PCLS, after treatment, five PCLS were pooled together and incubated in mRIPA buffer for 10 min on ice. Next, the PCLS were mechanically disrupted using a tissue homogenizer (Polytron 1200E, Kinematica AG,

Malters, Switzerland) three times, 30 seconds each, on ice, and then centrifuged at 4°C for 10 min at 10,000 x g.

The protein concentrations of the supernatants of disrupted cells, PCLS, or BAL were measured by Bradford assay (BioRad, Hercules, CA, USA) according to manufacturer recommendations. Samples were diluted from 1:10 to 1:20 in 1 mL of Bradford reagent and incubated for 20 minutes at room temperature, protected from light. Measurements of absorbance were performed in a spectrophotometer (Mo. 6131, Eppendorf).

SDS PAGE and Western Blotting

Regular TRIS/Glycine SDS-PAGE systems allow the separation of proteins with a molecular weight (MW) of up to approximately 200 kDa. In our case, we aimed for the detection of megalin, a protein with a MW approx. 600 kDa. In order to achieve a better resolution of a wide range of molecular proteins, a TRIS/Acetate SDS-PAGE system (Cubillos-Rojas et al. 2010) was optimized to analyze protein expression. After protein quantification, samples were denaturalized with LDS sample buffer (NuPage, NP0007, Invitrogen, ThermoFisher Scientific, Darmstadt, Germany) for 10 min at 70°C. Gradient gels from 3 to 10 % of poly-acrylamide (Carl Roth, Karlsruhe, Germany) were prepared, and equal amounts of protein were loaded for each sample. After separation, the proteins were transferred to PVDF membranes (Amersham Hybond P 0.45 µm, GE Healthcare Life Sciences) for 1,5 hours at a fixed intensity of 200 mA in transfer buffer (1% methanol, 0,01% SDS, 25 mM Bicine, 25 mM Bis-Tris, 1 mM EDTA, 1,3 mM sodium bisulfite pH 7.2, Carl Roth, Karlsruhe, Germany) and blocked for 1 hour in 5% nonfat-dried bovine milk (M7409 Sigma-Aldrich, Darmstadt, Germany) T-TBS buffer. Membranes were then incubated overnight with specific antibodies at 4°C. Primary antibodies were washed in T-TBS for 15 minutes and incubated for 1 hour at RT with secondary antibodies conjugated to horseradish peroxidase (HRP). The list of antibodies used can be seen in table 2.1. Then membranes were washed as before and developed with SuperSignal West Pico or Femto Chemiluminescent Substrate detection kit (Thermo Scientific, Waltham, MA, USA), as recommended by the manufacturer, in a CP 1000 automatic film processor (AGFA, Mortsel, Belgium). Densitometric quantification of bands was made using ImageJ software (National Institutes of Health, Bethesda, Maryland, USA).

Table 2.1 List of antibodies used for Western Blotting

Primary antibodies	**Species**	**Dilution**	**MW (kDa)**	**Company**
Megalin	Rabbit	1/1000	600	Proteintech
Phospho-GSK-3α/β(Ser21/9)	Rabbit	1/1000	46β, 51α	Cell Signaling
GSK-3β	Rabbit	1/1000	46β, 51α	Cell Signaling
Phospho-SMAD2 (Ser465/Ser467)	Rabbit	1/1000	60	Cell Signaling
Smad-2	Rabbit	1/1000	60	Cell Signaling
Influenza A NP	Mouse	1/200	56	Santa Cruz Bio.
β-Actin Antibody	Mouse	1/200	43	Santa Cruz Bio.
MMP-14	Rabbit	1/1000	66	ThermoFisher
MMP-2	Rabbit	1/200	63-72	Santa Cruz Bio.
MMP-9	Rabbit	1/200	92-120	Santa Cruz Bio.
MMP-19	Rabbit	1/1000	57	Novus Bio.
Transferrin receptor	Mouse	1/1000	95	Invitrogen
Secondary antibodies	**Species**	**Dilution**		**Company**
Anti-rabbit IgG HRP-linked	Goat	1:10000		Cell Signaling
Anti-mouse IgG HRP-linked	Rabbit	1/10000		Thermo Fisher

Surface proteins biotinylation

MLE cells were plated in 30 mm Petri dishes 24h prior to the viral infection or mock treatment. Immediately before treatment, cells were rinsed 3 times with PBS with Ca^{2+}/Mg^{2+} (PBS+/+) on ice and pre-labeled with a solution of EZ-link NHS-LC-biotin (ThermoFisher Scientific, 21336) 1 mg/mL in PBS+/+ for 20 minutes at 37°C. After the incubation, the cells were washed 3 times for 10 minutes with 100 mM glycine in PBS+/+ (in order to neutralize the linking reaction) and once with PBS +/+. After this pre-labeling of total cell-surface proteins, the cells were lysed with mRIPA buffer and centrifuged at 10.000g for 10 minutes at 4°C. Whole-cell homogenates were kept at 4°C during the entire experiment and quantified by Bradford. 100 to 200 ug of total proteins were prepared for streptavidin pulldown with 60 to 80 µL of streptavidin beads. Samples were rotated at 14 revolutions per minute (RPM) overnight at 4°C and washed one time with buffer A (150 mM NaCl, 50 mM Tris pH7,4, 5 mM EDTA pH 8), two times with buffer B (500 mM NaCl, 50 mM Tris pH7,4, 5 mM EDTA pH 8), and three times with buffer C (500 mM NaCl, 20mM Tris pH7,4, 0,2% BSA), in this

order before one last wash with a solution 10 mM of Tris pH 7,4. Pulled down proteins were denaturalized with NuPAGE LDS Sample Buffer (4X) (Invitrogen, NP0007) for 10 min at 70°C and separated by SDS-PAGE in 3 to 10% gradient gels in a Tris/Acetate system, blotted into a membrane, and then specific antibodies were used for detection.

Enzyme-Linked Immunosorbent Assay (ELISA)

Mouse TGF-β1 ELISA Kit (Colorimetric, NBP1-92671 Novus Biologicals, Wiesbaden, Germany) was used according to the manufacturer's instructions to determine concentrations of active and total TGF-β1 released from samples into the culture media or bronchoalveolar lavages. Samples stored at -80°C were thawed on ice and used either undiluted or in a 1:2 dilution for ELISA. Samples and standards were transferred to an antibody-coated, 96-well plate and incubated for a specific antibody-epitope reaction. Next, wells were washed, incubated, and stained with a soluble, TGF-β1-specific primary and secondary antibody. The cytokine abundance was then quantified by adding a luminescent substrate and colorimetric detection at the given wavelength in a microplate reader (Infinite 200, Tecan Group, Männedorf Switzerland). TGF-β1 concentrations were calculated based on samples of known concentrations in a standard curve. For the analysis of BAL at different time points (day 0 to day 9), samples were kindly provided by Dr. Christina Malainou.

Flow cytometric analysis of albumin uptake

For flow cytometry analysis of labeled albumin uptake, MLE-12 cells or PCLS were treated according to the experimental design, washed with pre-warmed PBS and incubated at 37°C or 4°C with a solution 50 µg/mL (MLE-12 cells) or 100 µg/mL (PCLS) of albumin from bovine serum (BSA) conjugated with AlexaFluor 488 (AF488-albumin, Invitrogen, A13100), transferrin from human serum conjugated with AlexaFluor 647 (AF647-transferrin, Invitrogen, T23366) or dextran conjugated with TexasRed (TR-dextran, MW 70,000 Dalton, D1830, Invitrogen) in DPBS-G.

After incubation, MLE-12 cells were washed with PBS and treated with ice-cold Solution X for 10 min, recovered in microcentrifuge tubes pelleted at 300 x g for 10 min at 4°C, washed in PBS+/+ and stained for 15 min at RT with Zombie Violet Fixable Viability Kit (which has an excitation/emission spectrum similar to PacificBlue

dye) (423114, BioLegend, San Diego, CA, USA), 1/500 dilution before being analyzed by flow cytometry.

Cells obtained from PCLS tissue dissociation were washed with MACS buffer, pelleted at 300 x g, 10 min at 4°C, and stained for 15 min at RT with Zombie Violet Fixable Viability Kit. Next, the cells were pelleted and resuspended in a mix of the antibody solution and a pooled immunoglobulin G (IgG) antibody preparation (Sandoglobulin, CSL Behring, King of Prussia, PA, USA) for 15 min. at 4°C in MACS buffer (PBS, 7.4% EDTA, 0.5% FCS pH 7.2). The cells were stained with Anti-Influenza A Virus antibody (ab20841, Abcam), APC.Cy7 rat anti-mouse EpCAM (118218, Biolegend), rabbit anti Megalin AF647 (bs-3909R-A647, Bioss, Woburn, MA, USA) or APC rat anti-mouse Podoplanin (127410, Biolegend), BV605 rat anti-mouse CD31 (740356, BD Horizon), BV605 rat anti-mouse CD45 (563053, BD Horizon) for 15 min at 4°C. Cells were then washed once with MACS buffer, pelleted, and resuspended in secondary staining (Donkey anti-Goat AF546, A-11056 Invitrogen) and incubated for 15 min at 4°C. Cells were then rewashed with MACS buffer, pelleted, and resuspended in 200 µL of MACS buffer before being filtered into a FACS tube for cell analysis. Multicolor flow cytometry was performed on a BD FACS Fortessa III cytometer using DIVA software (BD Bioscience, Heidelberg, Germany). For each fluorochrome, automatic compensation and fluorescence minus one (FMO) controls were used to ensure no fluorescence spill from other channels was present.

The staining protocol for analysis of albumin uptake and cell-surface megalin expression by FC in PCLS derived cells is summarized in table 2.2:

Table 2.2 Staining protocol for FC analysis of albumin uptake.

Staining step	Antibody	Dilution
1	Zombie Violet Fixable Viability Kit	1:500
2	Goat anti-Influenza A Virus	1:75
	Rat anti-mouse EpCAM APC.Cy7	1:50
	Rat anti-Mouse CD31 BV605	1:50
	Rat anti-Mouse CD45 BV605	1:50
	Rabbit anti-mouse Megalin AF647	1:50
	Rat anti-mouse Podoplanin APC	1:40
3	Donkey anti-goat Alexa Fluor 546	1:500

Microscopy stainings

PCLS: For microscopy analysis, samples were fixed in 4% PFA (28908, ThermoFisher Scientific) for 24h, then permeabilized with Triton-X 0,5% for 30 min and blocked with 5% BSA for 1h at 4°C. After washing with T-TBS buffer (Tris-buffered saline: 20 mM Tris, pH 7,4, 0,9% NaCl, 0,4% Tween-20), samples were incubated with the primary antibodies diluted in T-TBS/5% BSA overnight at 4°C (RAGE Rat anti-Mouse/Rat, MAB1179, R&D Systems Minneapolis, MN, USA; Influenza A NP FITC, ab20921, Abcam Cambridge, UK; SFTPC rabbit anti-mouse, ab211326Abcam). If secondary staining was required, the antibodies (Goat anti-rat IgG AF568, A11077, Invitrogen; Goat anti-rabbit AF594, Invitrogen, A11037) were used for 1 h at RT. Then were stained with Hoechst 33342 in a 1/1000 dilution for 30 min at RT temperature. Lastly, in the required cases, Phalloidin DyLight 594 (21836 ThermoFisher Scientific) was incubated for 30 min in the dark at RT.

MLE-12 cells: Cells were plated in 8 wells micro slides (80826, ibidi GmbH Gräfelfing, Germany). After treatment, they were incubated with 50-250 µg/mL of AF488-albumin, AF647-transferrin, or lysine-fixable TexasRed-dextran (MW 70,000 Dalton, D1864, Invitrogen), then washed three times with PBS and fixed in 4% Formaldehyde (28908, Thermo Scientific, Waltham, MA, USA) for 10 min. In the required experiments, they were incubated with primary antibody solutions in PBS/0.2% BSA overnight at 4°C and washed 5 times for 5 min at RT with PBS/0.2% BSA. When necessary, a secondary fluorescent-labeled antibody (Goat anti-rabbit AF594 (A11012, Invitrogen), Goat anti-rat IgG AF568 (A11077, Invitrogen) was

diluted in PBS/0.2% BSA and the samples incubated for 1h at RT in the dark. In order to counterstain nuclei, an aqueous solution of DAPI (D1306, Invitrogen) 300nM was added for 5 min, then washed three times with PBS. In experiments where visualization of the actin cytoskeleton was needed, phalloidin conjugated to DyLight 594 (21836, Invitrogen) was added as the last step in a concentration of 2,5 units/mL in PBS and incubated at RT for 10 min, then washed three times with PBS.

Reactants and dilutions for PCLS and MLE-12 staining for laser scanning microscopy are summarized in table 2.3.

Table 2.3. Staining protocol for laser scanning Microscopy

Antibody	**Dilution**
RAGE Rat anti-Mouse/Rat	1:100
Goat anti-rat IgG AF568	1:300
Influenza A NP FITC	1:20
SFTPC rabbit anti-mouse	1:100
Goat anti-rabbit AF594	1:300
Phalloidin DyLight 594	2,5 u/mL
DAPI	300 nM

Histology and H&E stainings

Lung samples were fixed in formaldehyde 4% at 4°C for 24h, then washed with PBS, embedded in paraffin, sectioned at 10 µm thickness in a microtome (Leica Biosystems, Wetzlar, Germany), and fixed in glass slides. Samples were incubated for 1h at 58° in a dry incubator. Next, they were immersed in Xylol 3 times, 10min, 2 times in ethanol 99,6%, 5 min, one time in ethanol 96%, 5min and one time in ethanol 70%, 5 min, and 2 times in distilled water for 5 min. Next, samples were put in a water bath at 100°C in 10% Rodent Decloaker (pH 6.0, Biocare Medical, Pacheco, CA, USA.) for 20min. After cooling, they were rinsed in distilled water for 5 min and incubated in a solution of 3,3% H_2O_2 in methanol for 20min. After rinsing for 5 min in distilled water (dH_2O), samples were incubated with Novocastra Enzyme Proteinase K (IHC), (RE7160-K, Leica Biosystems, Buffalo Grove, IL, USA) for 5 min, rinsed again in dH_2O, and washed in PBS for 5 min. Next, blocked with 10% BSA for 1h and washed twice with PBS. Next, they were incubated for 20min in Rodent Block M (Biocare Medical) and washed 4 times with PBS, 5 min. The rabbit anti-mouse megalin primary antibody (19700-1-AP, Proteintech, Rosemont, IL, USA) was then

incubated overnight in a 1/200 dilution and rinsed with PBS for 2h. Next, secondary antibody HRP-linked was added (ZytoChem Plus HRP Polymer System Rabbit, Zytomed Systems GmbH, Berlin, Germany) for 30 min, washed with PBS, and HRP substrate was added for one minute (NovaRED Substrate Kit, SK-4800, Vector Laboratories, Burlingame, CA, USA). After washing for 5 min with dH_2O, Hematoxylin/Eosin, staining was performed according to standard procedures.

Fluorescence Microscopy

Fluorescence microscopy was performed using a Carl Zeiss Axio Observer Z1 microscope (Carl Zeiss, Wetzlar, Germany). Confocal fluorescent laser-scanning microscopy was performed using a Leica TCS SP5 confocal microscope (Leica Microsystems GmbH, Wetzlar, Germany) with 63x or 40x ocular. Z-Stacks were acquired using a 0.3-1 µm distance between stacks. Acquired pictures were analyzed using LAS AF software.

Fixation and Preparation of Lung Tissue for Histology

For histological staining of mouse lung tissue, lung lobes were fixed for 24 h in 4% PFA. Subsequently, they were embedded in paraffin, cut into 3-5 µm thick sections with a microtome (Leica Biosystems) and stained with hematoxylin and eosin in the following procedure: Xylene 5 min (twice), 100% ethanol 30 sec (twice), 96% ethanol 30 sec, 96% ethanol 30 sec, 70% ethanol 30 sec, 70% ethanol 30 sec, hematoxylin 3min, 0.1% HCl 2 sec, H_2O 5min, Eosin G solution 3 min, H_2O 30 sec, 70% ethanol 30 sec, 90% ethanol 30 sec, 100% ethanol 30 sec (twice), xylene 5 min (twice).

Image acquisition and analysis

For mean linear intercept (MLI) calculations, hematoxylin-eosin-stained paraffin sections were imaged with a bright field Axioimager microscope (Zeiss, Oberkochen Germany) at 40X magnification. Measurements of average wall thickness, airspace percentage, and mean linear intercept were made with Leica Qwin Image Processing and Analysis Software.

Analysis of gene expression

RNA extraction

Treated MLE-12 cells, as well as primary AECs-enriched samples and the BAL cells, were processed for RNA extraction using the RNeasy Mini Kit (Qiagen, Hilden, Germany) according to the manufacturer's instructions. Cells were washed with PBS and disrupted in Buffer RLT, which causes cell lysis and RNase inactivation. Ethanol was then added to the lysates, and the samples were then applied to the RNeasy Mini spin column for RNA to selectively bind to the membrane. The contaminants were washed away, and the RNA was eluted in RNAse-free water. All bind, wash, and elution steps were performed by centrifugation in a microcentrifuge at RT. The extraction was followed by on-column DNAse digestion (RNase-Free DNase Set, Qiagen) in order to avoid contamination by genomic DNA.

Bulk mRNA analysis

RNA integrity was verified by Bioanalyzer RNA 6000 Nano assays (Agilent Technologies). Library preparation and sequencing were performed in the Deep Sequencing Platform of the Max Planck Institute for Heart and Lung Research, (Bad Nauheim, Germany) by Dr. Stefan Günther. Library preparation integrity was verified with LabChip Gx Touch 24 (Perkin Elmer). For BAL, 10ng of total RNA was used as input for SMARTer® Stranded Total RNA-Seq Kit - Pico Input Mammalian (Takara Bio). For AECs, 100ng of total RNA was used as input for SMARTer Stranded Total RNA Sample Prep Kit - HI Mammalian (Takara Bio). Sequencing was performed on the NextSeq500 instrument (Illumina) using v2 chemistry, resulting in an average of 35M reads (BAL) or 27M reads (AECs) per library, with a 1x75bp single end setup. The resulting raw reads were assessed for quality, adapter content and duplication rates with FastQC (Andrews S., FastQC: a quality control tool for high throughput sequence data. Avail. at http://www.bioinformatics.babraham.ac.uk/projects/fastqc). Trimmomatic version 0.39 was employed to trim reads after a quality drop below a mean of Q20 in a window of 10 nucleotides (Bolger et al., Trimmomatic: a flexible trimmer for Illumina sequence data). Only reads between 30 and 150 nucleotides were cleared for further analyses. Trimmed and filtered reads were aligned versus the Ensembl mouse genome version mm10 (GRCm38) using STAR 2.6.1d with the parameter "--outFilterMismatchNoverLmax 0.1" to increase the maximum ratio of mismatches to mapped length to 10% (Dobin et al., STAR: ultrafast universal RNA-seq aligner). The number of reads aligning to genes were counted using the featureCounts 1.6.5 tool from the Subread package (Liao, Smyth, and Shi 2014).

Only reads mapping at least partially inside exons were admitted and aggregated per gene. Reads that were overlapping multiple genes or aligning to multiple regions were excluded. Differentially expressed genes were identified using DESeq2 version 1.18.1 (Love, Huber, and Anders 2014). Only genes with a minimum fold change of +- 1.5 (log2 +-0.59), a maximum Benjamini-Hochberg corrected p-value of 0.05, and a minimum combined mean of 5 reads were deemed to be significantly differentially expressed. The Ensemble annotation was enriched with UniProt data (release 06.06.2014) based on Ensembl gene identifiers (Apweiler et al. 2014). Transcripts per million (TPM) were calculated as described by Wagner et al. (Wagner, Kin, and Lynch 2012).

cDNA synthesis

RNA extracted from the treated MLE12 cell cultures was used as a template for cDNA synthesis. iScript cDNA synthesis kit (Bio-Rad) was used, which contains a reverse transcriptase, an RNase inhibitor, and a blend of oligo(dT) and random hexamer primers. For each sample, 1 µg of RNA was added in a tube with the reaction mix and the following reaction protocol was programmed in a thermal cycler (Bio-Rad): Priming 5 min at 25°C, reverse transcription 20 min at 46°C, RT inactivation 1 min at 95°C.

Quantitative Real-Time Polymerase Chain Reaction (qRT-PCR)

qRT-PCR technique was used to quantify the levels of expression of mRNA in the samples. The kit iTaq Universal SYBR Green Supermix (BioRad) was used according to the manufacturer's protocol and the mouse-specific primers combinations used were:

LRP2 FW: 5' AGG CCA CCA GTT CAC TTG CT 3'
LRP2 RV. 5' AGG ACA CGC CCA TTC TCT TG 3'
TGF-β1 FW: 5' TGG AGC AAC ATG TGG AAC TC 3'
TGF-β1 RV: 5' GTC AGC AGC CGG TTA CCA 3'
18S FW: 5' AGT CCC TGC CCT TTG TAC ACA 3'
18S RV. 5' GAT CCG AGG GCC TCA CTA AAC 3'

Ribosomal 18S served as a normalization control. Data are presented as ΔCt ($Ct_{target\ gene} - Ct_{reference\ gene}$). Primer specificity was validated by analyzing the melt curve of the qRT-PCR product.

Specific mRNA knockdown (siRNA)

To evaluate the specificity of megalin antibodies in Western Blot, microscope imaging and FC, specific megalin knockdown was performed with small interference RNA technology (Lipofectamine RNAiMAX, ThermoFisher Scientific) in OptiMEM medium (Gibco). For microscopy analysis, 10,000 cells per well were plated 24 hours before transfection in 8 wells micro-slides to reach approximately 70 % confluency on the day of the experiment. Transfection complexes were formed at room temperature according to table 2.4.

Table 2.4 Transfection complexes for siRNA

	Reagents	Volume (µL)
Tube 1	OptiMEM	15
	Lipofectamine RNAiMAX	0,9
Tube 2	OptiMEM	15
	siRNA (10 uM stock)	0,8

After five minutes of incubation, the contents of tubes 1 and 2 were mixed and incubated at room temperature for 30 minutes. Meanwhile, culture medium from cells was replaced for fresh conditioned DMEM:F12. Once incubation time was over, lipofectamine-siRNA complexes were placed on the cells and incubated for another 6 hours at 37°C. Then, the culture medium was removed and replaced with fresh conditioned DMEM:F12. Transfected cells were incubated at 37°C for 48 hours. For western blot analysis, the cells were plated in p35 plates, with the transfection complexes quantities scaled up accordingly.

Statistical analysis

All data is given as median ± standard deviation. Statistical significance between two groups was analyzed by unpaired Student's t-test, while differences between three or more groups were analyzed using randomized-block-experiments, one-way ANOVA and Dunnett's multiple comparisons test (GraphPad Prism v.5 and v.8). Differences were considered significant when p-values were inferior to 0.05. *p<0.05; **p<0.01; ***p<0.005; ****p<0,001.

3. Results

Albumin uptake characterization in MLE-12 cells

First, we set out to characterize the albumin uptake in AECs (fig. 3.1 A). The top view images show the AF488 signal is inside the boundaries of the MLE-12 cells cytoskeleton, and the 3D reconstruction side view shows how albumin is distributed as well on the vertical axis, suggesting it was taken up by the cells.

Transferrin endocytosis mechanism has been widely studied, presents a specific receptor-mediated endocytosis mechanism (Huebers and Finch 1987) and can therefore be used as a positive control for cellular uptake. Dextran is widely used as a probe for micropinocytosis and can be used as a negative control for endocytosis (L. Li et al. 2015), so we incubated the cells with a dextran polymer of the same molecular weight as albumin (70,000 Da), as a negative control. We stimulated MLE-12 cells with a solution of 200 µg/mL of AF488-albumin, fixable TexasRed-dextran, and AF594-transferrin for 60 min (fig. 3.1 B). Compared to dextran, albumin and transferrin showed a higher fluorochrome signal intensity, indicating a higher intake into the cells.

To quantify the cellular uptake of the fluorescent compounds, we analyzed the cells by flow cytometry (FC) (fig. 3.1 C-E). MLE-12 cells were incubated for 10, 30, and 60 min at 37°C, as well as for 60 min at 4°C, in the presence of AF488-albumin, TexasRed-dextran, and AF647-transferrin. Also, they were treated with a solution containing trypsin and proteinase K, to ensure no probe remains bound to the cellular membrane. The percentage of cells that showed a positive signal for albumin increased over time and was the highest at 60 min with an average of 92,4% of cells positive, while for transferrin, almost 100% of the cells were positive as soon as after 10 min of incubation. At 4°C, both compounds showed a significantly decreased uptake level. These results are consistent with a receptor-mediated endocytosis mechanism (Yumoto et al. 2006).

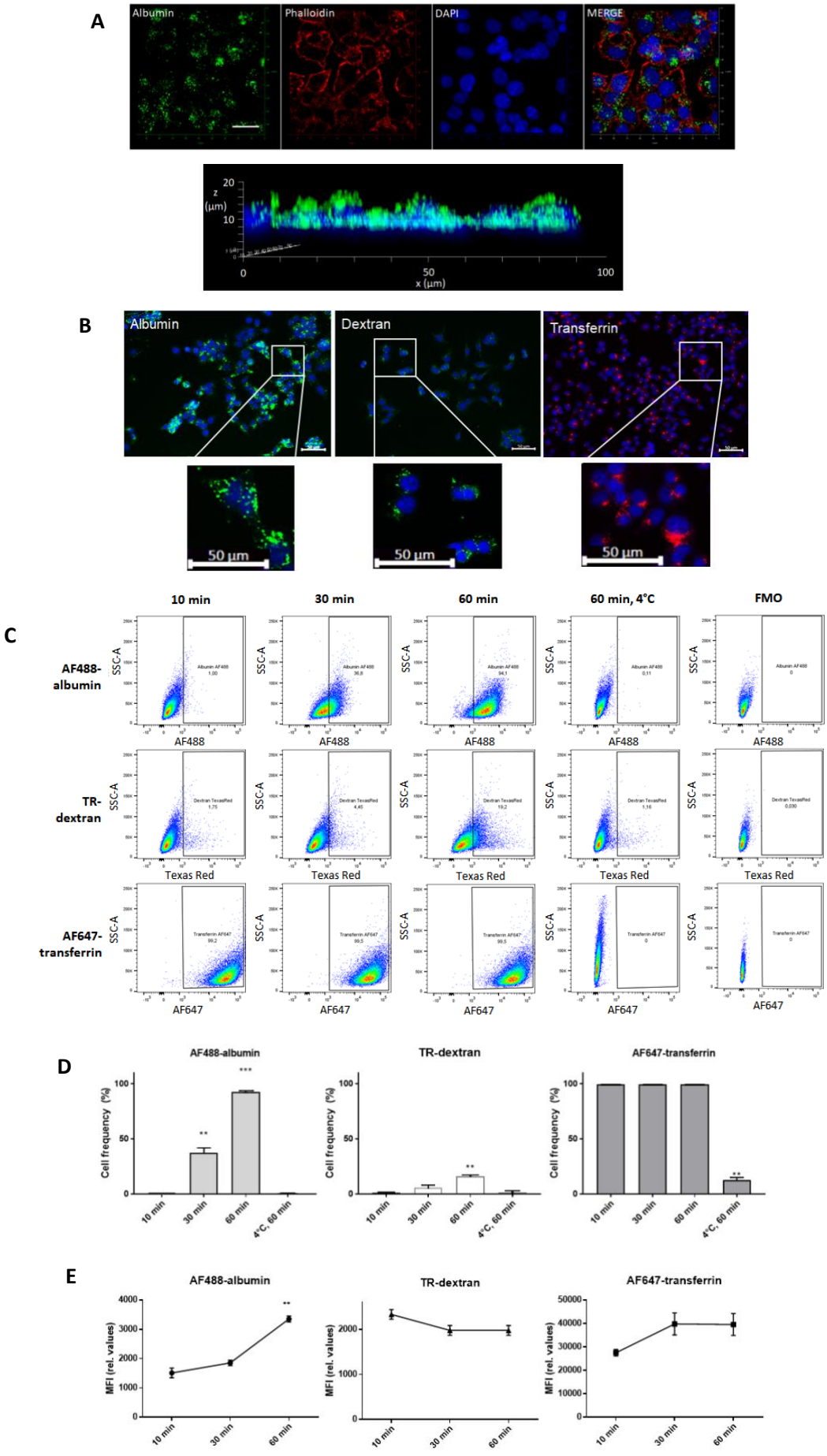
A
Albumin
Phalloidin
DAPI
MERGE
z (µm)
x (µm)
B
Albumin
Dextran
Transferrin
50 µm
C
10 min
30 min
60 min
60 min, 4°C
FMO
AF488-albumin
TR-dextran
AF647-transferrin
SSC-A
AF488
Texas Red
AF647
D
AF488-albumin
TR-dextran
AF647-transferrin
Cell frequency (%)
10 min
30 min
60 min
4°C, 60 min
E
AF488-albumin
TR-dextran
AF647-transferrin
MFI (rel. values)

Figure 3.1. *Characterization of albumin uptake in MLE-12 cells.* **A:** Upper panel: Confocal microscopy images of MLE-12 cells incubated in a solution containing AF488-albumin 250 µg/mL for 1h. Cells were fixed and stained with Phalloidin and DAPI. Scale bar 20µm. Zoom 63X. Lower panel: 3D reconstruction side view. **B:** MLE-12 cells were incubated in solutions containing 250 µg/mL of AF488-albumin, TexasRed-dextran or AF594-transferrin for 60 min fixed with 4% PFA and stained with DAPI. Fuorescence microscopy images are displayed. Scale bar 50µm. Zoom 40X and 63X. **C:** Representative gating strategy of flow cytometry analysis of MLE-12 cells treated with a solution of AF488-albumin, TexasRed-dextran and AF647-transferrin 50 µg/mL each, for 10, 30 and 60 minutes. After treatment with solution X, cells were incubated with a dead cell staining, washed with PBS and analyzed. FMO = fluorescence minus one control. **D:** Frequency of positive cells for each fluorochrome, as a percentage of total live cells. **E:** Relative median fluorescence intensities (MFI) for each fluorochrome and time point. N=3. All bar graphs show mean ±SD. Statistic comparisons are relative to mock controls.

The frequency of cells taking up dextran also increased with the incubation time. However, its maximum was 16,2% at 60 min time point, showing a marked reduction compared to the frequency of cells that took-up albumin and transferrin.

Fluorescence intensity data in FC is directly correlated to the amount of fluorochrome taken up by the cells (Gratama et al. 1998), hence providing a quantifiable measure of the levels of fluorescently labeled-probes uptake per cell. We analyzed the relative median fluorescence intensity (MFI) of the fluorochromes to quantify the level of uptake of each compound at different time points (fig 3.1 E). AF488-albumin MFI increased over time and was the highest after 60 min incubation. TexasRed-dextran and AF647-transferrin MFI did not vary significantly during the experimental timeframe, indicating that the level of uptake for both compounds reached a plateau at least after 10 min of incubation.

Assessment of IV infection in MLE-12 cells

Next, we set out to analyze the infective capabilities of the strain PR8 mouse-adapted influenza A virus in MLE-12 cells. In order to quantify the infection level and the cell death rates, we analyzed infected MLE-12 cells by FC (fig. 3.2 A, B, C). To detect the presence of the virus, we used an antibody against influenza A H1N1, that allows the detection of the viral protein HA once it is expressed by the cells. We were able to detect HA on the cell surface, confirming that the percentage of infected cells correlates with the MOI and the incubation time, as also does cellular death rate (fig. 3.2 B) which demonstrates that the virus can infect MLE-12 cells in culture. We also infected MLE-12 cells at MOIs 0.1 and 1, and after 24h of infection, the cells were lysed and analyzed by Western Blot against influenza nucleoprotein (NP) (fig. 3.2 D).

The NP signal intensity correlates with the MOI, being stronger at MOI 1 when compared with MOI 0.1.

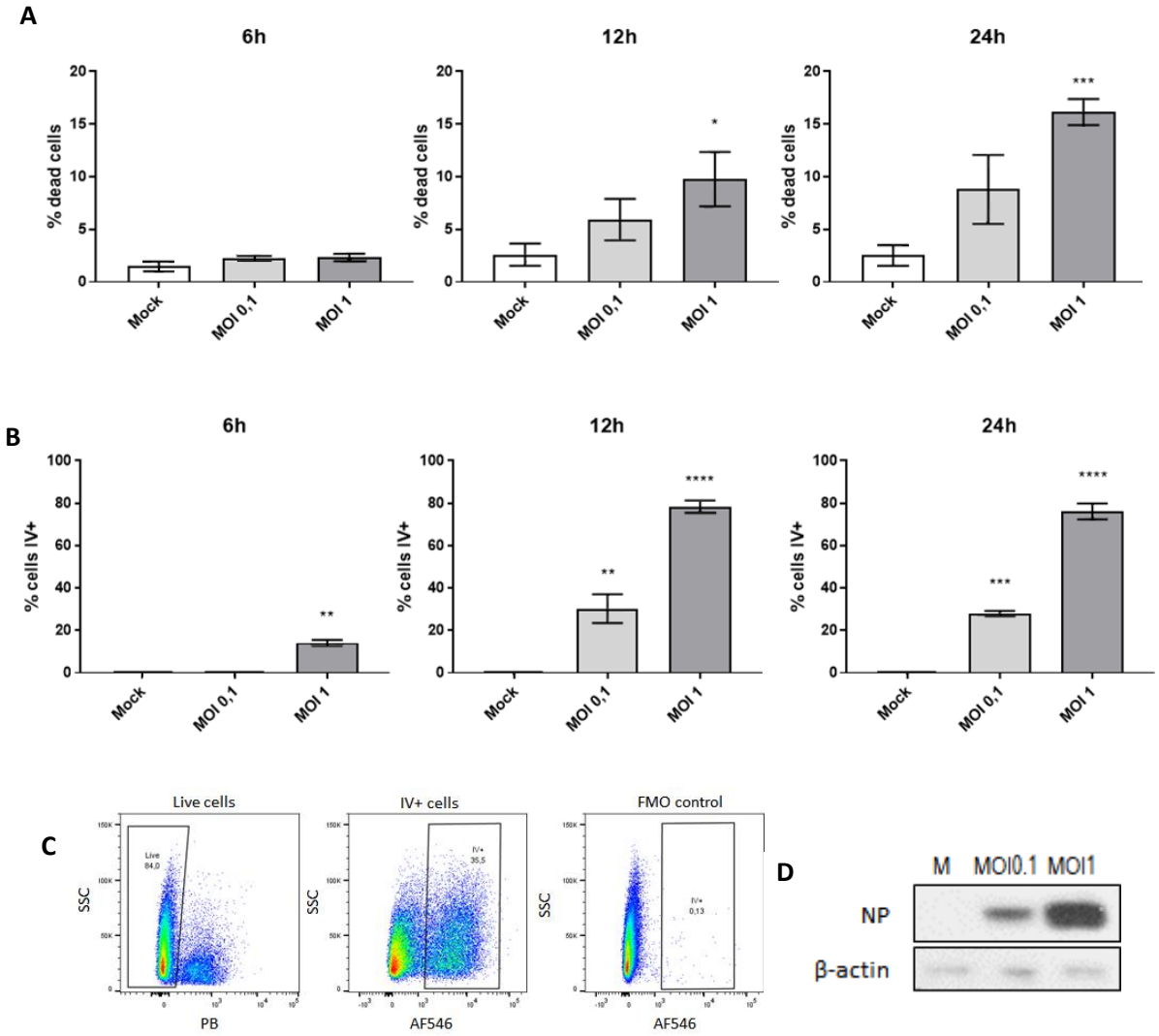

Figure 3.2. *Characterization of influenza A PR8-mouse-adapted infection in MLE-12 cells.* ***A-C.*** MLE-12 cells were inoculated with PR8 at MOI 0,1 and 1 and analyzed at 6h, 12h and 24h. **A:** Flow cytometric analysis showing cell death percentages for each time point and MOI. **B:** Live cells were stained with a specific IAV antibody and Infection levels assessed (as a percentage of live cells). **C:** Gating strategy showing representative dot plots for live cells (PB^{neg}), IV infected cells ($AF546^{pos}$) and a representative FMO control for AF546 (HA antibody). **D:** MLE-12 cells were infected with IV MOI 0.1 and MOI 1 for 24h and Western Blot analysis of Influenza nucleoprotein was performed. All bar graphs show mean ±SD. Statistic comparisons are relative to mock controls.

Albumin uptake in infected MLE-12 cells

In order to study the effect of IV infection on albumin uptake in MLE-12 cells, we inoculated the cultured cells with IV at MOIs of 0,1, 1 or mock, and incubated them in a medium containing 0.1% BSA for 1, 6, 12, or 24h and then an albumin binding-and-uptake assay was performed (fig. 3.3 A). Although the albumin uptake levels showed

a decreasing tendency at 12 and 24h, either surface-bound or taken-up levels did not show statistically significant differences at all time points.

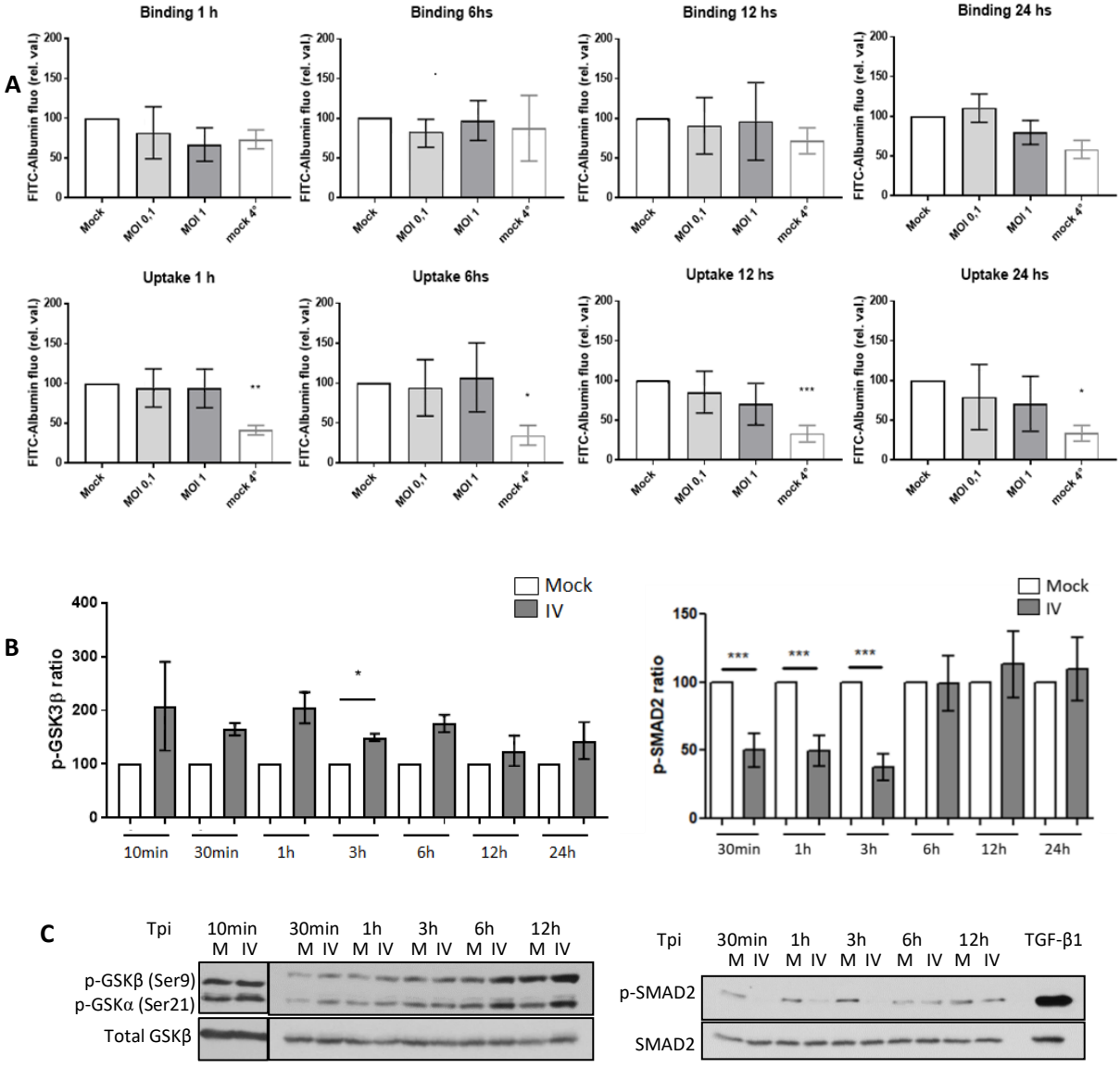

Figure 3.3. *Influenza virus infection did not increase GSK3β ser9 phosphorylation and activation in MLE-12 cells up to 24h post influenza infection.* **A:** Albumin binding and uptake in IV infected MLE-12 cells. Cells were infected with influenza virus at MOIs of 0,1 and 1 for 1, 6, 12 and 24h and then incubated with a 50µg/mL FITC-albumin solution for 1h and the binding and uptake assay was performed. All FITC-albumin fluorescence values for each timepoint are shown as relative to mock. Mock 4°C: control at 4°C degrees. **B:** Densitometry quantification of western blot analysis of (left) phospho-GSK3β and (right) phosphor-SMAD2 in relation to total protein in MLE-12 cell lysates inoculated with IV at MOI1 (IV) and analyzed at different time points. The antibody used to detect phosphorylation levels in GSK3 is able to bind to GSK3α as well and hence it shows two distinct bands. **C:** Representative blots. Tpi = time post infection. TGFβ-1: positive control for SMAD2 phosphorilation, 20 ng/mL, 30 min. All bar graphs show mean ±SD of 3 to 7 independent experiments. Statistic comparisons are relative to mock controls.

In order to test our hypothesis that IV impairs albumin uptake by TGF-β1-mediated activation of GSK3β, we analyzed the levels of phosphorylation of GSK3β and

SMAD2, a downstream target of the TGF-β1 canonical pathway, in IV treated MLE-12 cells (fig. 3.3 B and C). MLE-12 cells were inoculated with the virus at MOI 1, incubated for different times, and total protein lysates were analyzed by Western Blot. The densitometry analysis from the western blot bands indicates that the phosphorylation of GSK3β remains and even increases during the experimental time frame (10min to 24h) indicating that there's no activation of the kinase. Phosphorylation levels of SMAD2 were significantly decreased during the first 3 hours and remained not significantly different from the mock control at 6, 12, and 24 hours indicating that there's no TGF-β1 activity during the experimental time frame.

Our group has described that megalin is the main player mediating albumin endocytosis in the alveolar epithelium (Buchäckert et al. 2012; Vohwinkel et al. 2017), so we set out to analyze the expression of megalin on infected AEC in vitro. We inoculated MLE-12 cells with IV at MOI1 and incubated them for 30min, 1h, 3h, 6h, 12h, and 24h and studied the expression of megalin by western blot (fig. 3.4 A). The results revealed a significant decrease in the total megalin expression at 24h, down an average of 70%. In order to see if this decrease is reflected in the levels of the endocytic receptor located on the cell surface (as opposed to intracellular compartments), we performed a cell-surface protein biotinylation assay on the inoculated cells after 24h of incubation (fig. 3.4 B). Densitometric quantification showed an average reduction of the receptor on the plasma membrane of 63% compared to the control. Specificity of the megalin antibody was validated by small interfering RNA knockout of megalin in MLE-12 cells (fig. 3.4 C).

Next, we aimed to identify if megalin expression was downregulated at a transcriptional level. We isolated RNA from control or IV-treated cells at 1, 6, 12, and 24h after inoculation and measured the levels of LRP2 by qPCR (fig. 3.4 D). We found a decreasing tendency in LRP2 transcription levels already at the 6h time point and a significant downregulation at 24h p.i.

Since one of the megalin regulation pathways involves TGF-β1 receptor activation by its ligand, we aimed to study TGF-β1 transcription levels in MLE-12 cells (fig. 3.4 E). Contrary to what was expected, our findings show no increase but a decreasing tendency in its transcription levels, with a significant difference at 24h. We then measured the amounts of active TGF-β1 peptide in the culture media 24h post-infection at two different MOIs, 0,1 and 1 (fig. 3.4 F). Our results showed no

significant differences in active TGF-β1 concentration between control and infected samples culture media.

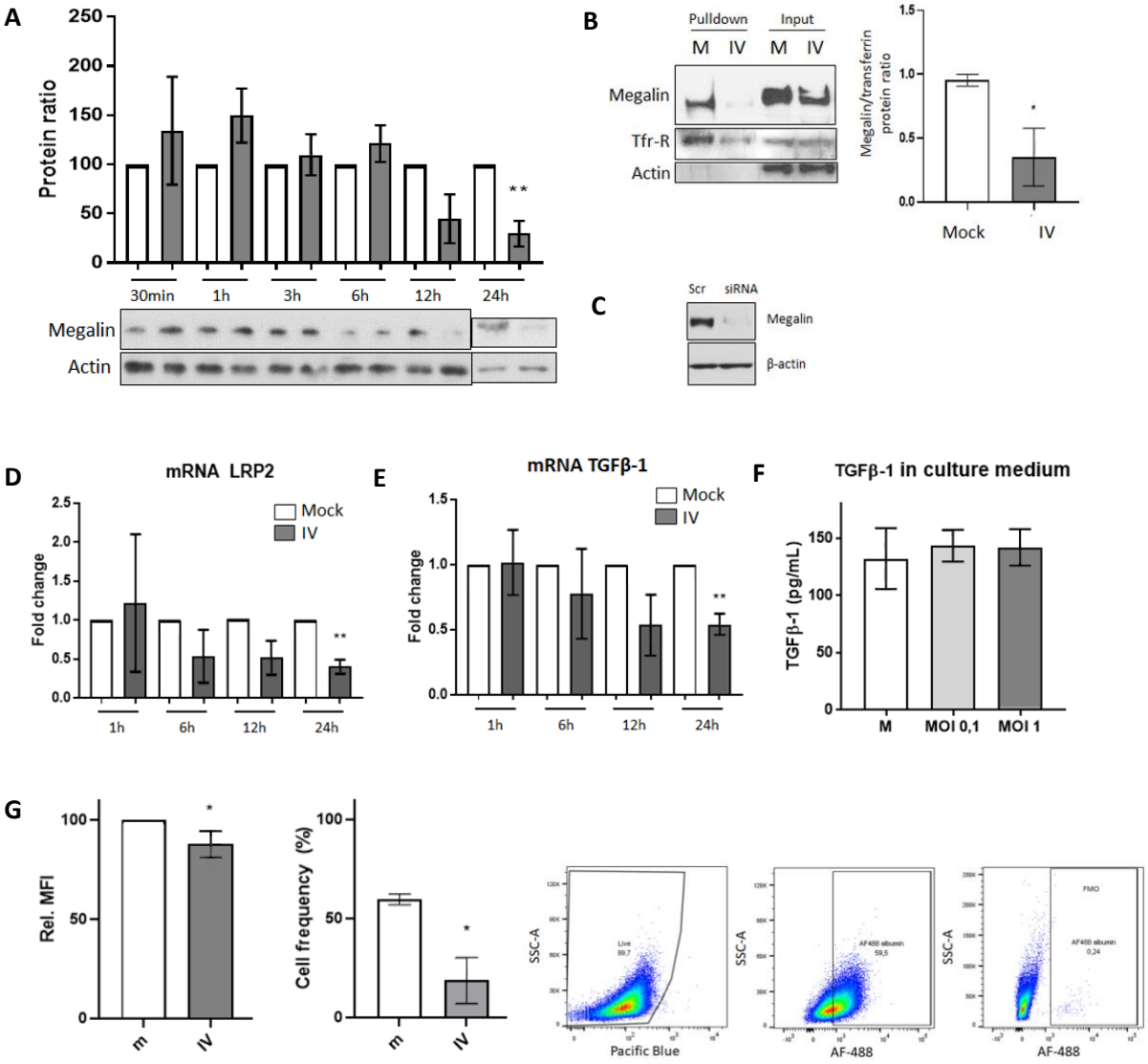

Figure 3.4 *Megalin and TGF-β1 expression are downregulated in IV-inoculated MLE-12 cells.* **A:** MLE-12 cells were inoculated with IV at MOI 1, incubated for 30min, 1h, 3h, 6h, 12h and 24h. The graph shows the western blot densitometry analysis megalin normalized to beta-actin and to each mock control. A representative blot for each time point is shown. **B:** Surface biotinylation assay was performed on MLE-12 cells inoculated with PR8 MOI1 incubated for 24h. Left: representative blot. Right: Densitometry analysis and quantification of megalin, normalized to transferrin. **C:** Antibody specificity characterization: megalin siRNA was transfected into to MLE-12 cells, and the megalin expression was analyzed by WB. Scr: scramble RNA (control). **D-E:** mRNA was isolated from mock and IV-treated cells, at 1, 6, 12 and 24h p.i.. LRP2 (**D**) and TGF-β1 (**E**) transcription levels were quantified by qPCR. **F:** ELISA results for active TGF-β1 levels measurement in MLE-12 culture medium 24h p.i. for mock (control), MOI 0,1 and MOI 1. **G:** Cells were inoculated with IV for 24h and incubated with AF488-albumin for 1h before being analyzed by FC. Image shows the relative median fluorescence intensity of AF488 (Rel. MFI, left), the percentages of cells that were positive for AF488 (Cell frequency, center) and the gating strategy for the experiment showing dead cells exclusion, AF488 detection and fluorescence minus one (FMO) control (right).

We also analyzed the AF488-albumin uptake levels in control and infected MLE-12 cells by FC (fig. 3.4 G). The results showed that after 24h of infection, there is a 15% decrease in albumin uptake in the infected cells compared to control as well as a reduction of the average percentage of cells that showed AF488 signal, from 59,6% to 18,7%.

Albumin uptake in precision-cut lung slices

Even when our results on infected MLE-12 cells showed differences in albumin uptake levels, we found no signs of activation of the TGF-β1/GSK3β axis. Cell monocultures do not accurately represent an infected lung's condition, where different cell types from lung tissue, circulatory system, and the immune system interact with each other. Also, cell cultures fail to faithfully recapitulate the morphologic, functional, molecular, proteomic, and lipidomic markers of the AT2 phenotype (L. G. Dobbs 1990; Beers and Moodley 2017). For this reason, we decided to set up a different, more physiological ex-vivo murine model: precision-cut lung slices (PCLS). In this model, mice lungs are cut in 200 μm slices that can be cultured, treated, and analyzed. First, we characterized the albumin uptake in PCLS by incubation with an AF488-albumin solution 100 μg/mL for different times or for one hour at four different concentrations, and albumin uptake of total live cells was analyzed by FC (fig. 3.5 A-C). Even more, by staining with antibodies against specific cell markers, we were able to quantify the levels of albumin uptake in alveolar epithelial cells at different albumin concentrations (fig. 3.5 D,E).

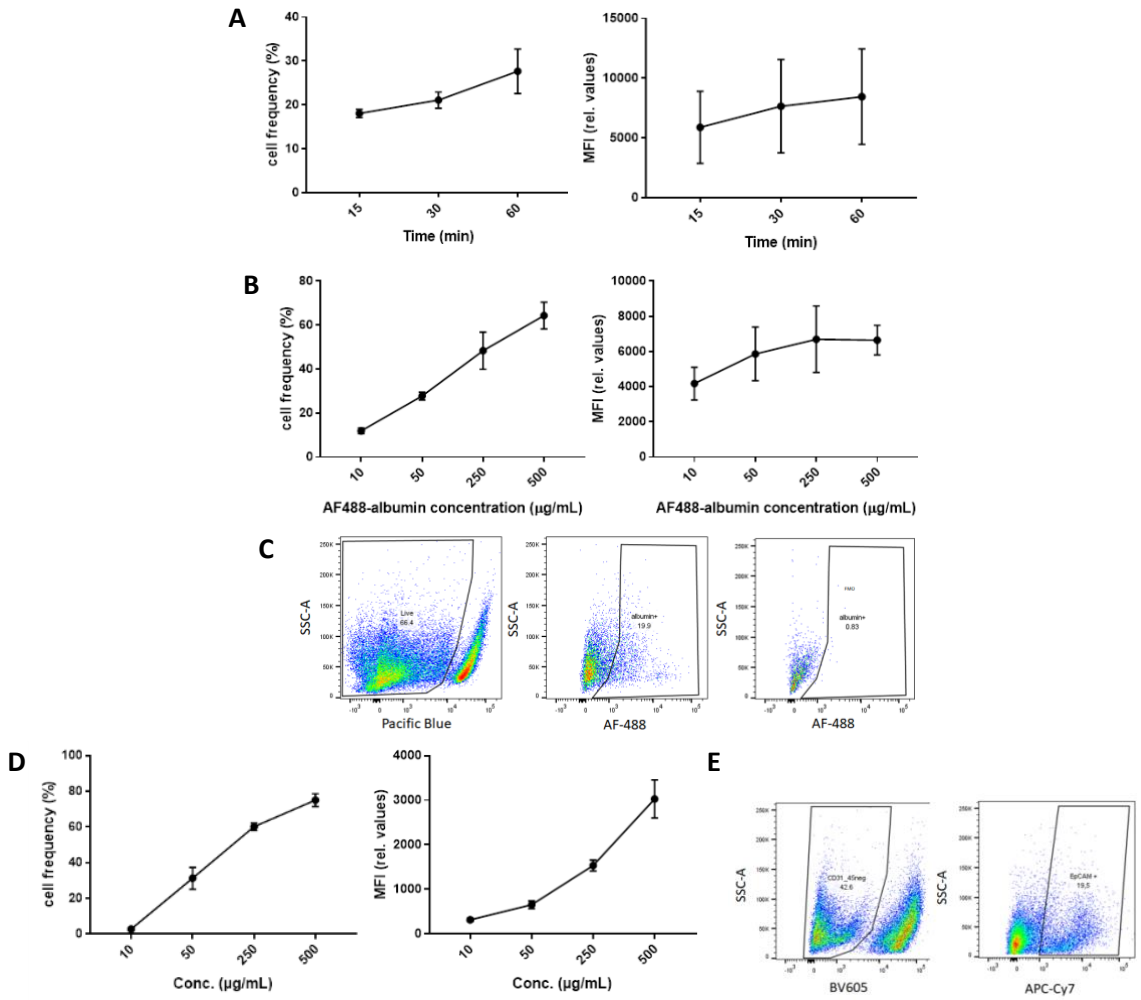

Figure 3.5 *Characterization of Albumin uptake in AEC from PCLS by flow cytometry.* **A:** PCLS were incubated in AF488-albumin 100µg/mL for 10, 30 or 60 min and albumin uptake was analyzed. Graphs show the frequency of total live AF488+ cells (as percentage) and the median fluorescence intensity (MFI) for each time point. **B:** PCLS were incubated for one hour in different concentrations of AF488-albumin solutions and albumin uptake was analyzed. Left panel: frequency of total live AF488+ cells (as percentage), right panel: median fluorescence intensity (MFI) for each concentration. **C:** Gating strategy for albumin uptake in total live cells. **D:** Albumin uptake levels in alveolar epithelial cells (AEC, CD31-, CD45-, EpCAM+) from PCLS shown in B. **E:** Gating strategy for AEC showing CD31 and CD45 cells exclusion, and selection of EpCAM+ cells.

Next, PCLS were incubated for one hour in a solution containing labeled albumin, dextran and transferrin, and analyzed by confocal microscopy. Stronger intensity signals were detected when PCLS were treated with albumin and transferrin, but not with dextran and the percentage of cells that internalized albumin and transferrin was significantly higher than dextran (fig. 3.6 A and B). Even more, when exposing the PCLS to AF488-albumin in the presence of 1000-fold molar concentration non-labeled albumin (competition assay), at 4°C, or in the presence of the dynamin GTPase activity inhibitor dynasore, which inhibits clathrin and caveola mediated endocytosis, the signal intensity of AF488 was dramatically reduced (fig. 3.6 C).

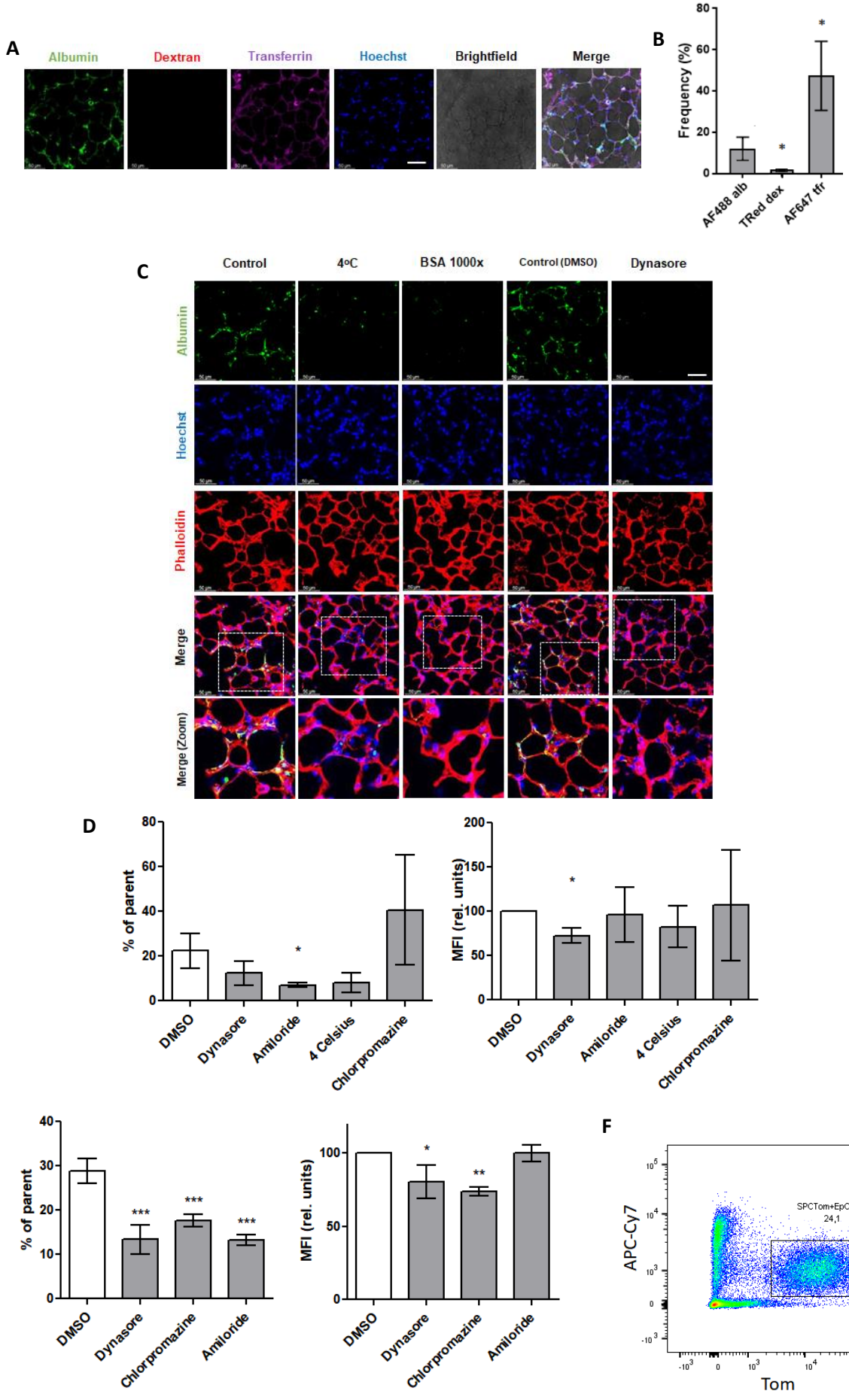
A
Albumin
Dextran
Transferrin
Hoechst
Brightfield
Merge
B
Frequency (%)
AF488 alb
TRed dex
AF647 tfr
C
Control
4°C
BSA 1000x
Control (DMSO)
Dynasore
Albumin
Hoechst
Phalloidin
Merge
Merge (Zoom)
D
% of parent
MFI (rel. units)
DMSO
Dynasore
Amiloride
4 Celsius
Chlorpromazine
E
% of parent
MFI (rel. units)
DMSO
Dynasore
Chlorpromazine
Amiloride
F
APC-Cy7
Tom
SPCTom+EpCAM+
24,1

Figure 3.6 *Albumin endocytosis in AEC from PCLS is an active process mediated by clathrin-dependent endocytosis.* **A – B:** PCLS were incubated 1h in a solution containing 250 µg/mL of AF488-albumin (green), AlexaFluor647-transferrin (purple) and lysine-fixable TexasRed-dextran (70,000 Da, red) **A:** Confocal microscope images. Scale bar 50 µm. Zoom 63X. **B:** Flow cytometry analysis showing frequency of cells with a positive signal for each fluorochrome (expressed as a percentage). **C.** Confocal images of PCLS incubated for 1h in AF488-albumin 250 µg/mL at 37°C (Control), at 4°C, in the presence of unlabeled albumin 100 mg/mL (BSA 1000x), DMSO 0.007% or Dynasore 100 µM. Scale bar 50 µm. Zoom 63X. **D – F:** PCLS were prepared from SftpcCreERT2/+; tdTomatoflox/flox mice, treated with tamoxifen for 24h and then incubated in AF488-albumin for 1 h in the presence of DMSO, Dynasore100 µM, Chlorpromazine 100 µM, Amiloride 1mM or at 4°C and analyzed by flow cytometry. Graphs show the FC analysis result with percentage of total live cells with a positive signal for AF488-albumin (left) and the median fluorescence intensity (MFI) for each sample (right). **(D)** total live cells and **(E)** SPC+ cells. **F:** Representative gating strategy showing dot plot for the analysis of SPC+ (x-axis), EpCAM+ (y-axis) cells (AT2). All bar graphs show mean ±SD of 3 independent experiments. Statistic comparisons are relative to mock controls.

We then quantified the albumin uptake levels in cells from PCLS by FC. By using SftpcCreERT2/+; tdTomato flox/flox mice, we characterized the albumin uptake in all cell types, as well as in AT2 cells only. At 4°C as well as in the presence of dynasore and clathrin-mediated endocytosis inhibitor chlorpromazine or the macropinocytosis inhibitor amiloride, the percentage of cells that assimilated labeled albumin was dramatically reduced either in the whole cell population or in AT2 cells only (fig. 3.6 D – F, and table 3.1). When analyzing the MFI, we were able to confirm a decrease in the uptake levels in the presence of the inhibitors chlorpromazine and dynasore, but not amiloride (fig. 3.6 E).

Table 3.1. Frequency of AF488 positive cells (%) and relative median fluorescence intensities (MFI) of total and AT2 cells from PCLS.

	DMSO	Dynasore	Amiloride	4 Celsius	Chlorpromazine
% Total live cells	22 ± 8	12 ± 5	7 ± 1	8 ± 4	41 ± 25
MFI Total live cells	100.0	73 ± 8	96 ± 31	83 ± 23	107 ± 63
% AT2 cells	28 ± 3	13 ± 3	13 ± 1	-	18 ± 1
MFI AT2 cells	100.0	80 ± 12	100 ± 6	-	74 ± 3

IV infection in PCLS

The next step was to characterize the viral infection in PCLS. To assess the infectious capability of the mouse-adapted PR8 IV strain in PCLS, we added to the culture medium $1x10^6$ p.f.u. per slice of tissue and incubated for 12, 24, or 48h before fixation, and staining with an influenza nucleoprotein (NP) specific antibody. The confocal microscopy imaging results showed the presence of NP in all three time points, with the highest expression after 24 and 48h of infection (fig. 3.7 A). By FC,

we were able to quantify the infection levels in AEC at times 1, 6, 12, 24, and 48h (fig. 3.7 B) and found that after 24 and 48h between 20 and 30% of the cells were infected. In order to minimize the chances of bacterial contamination of the cultured PCLS, we decided to incubate with the virus for 24h as timeframe for all PCLS experiments.

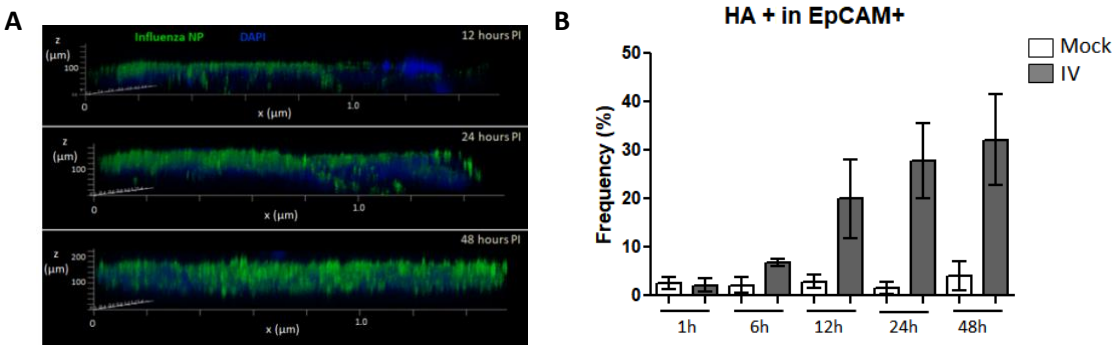

Figure 3.7 *Characterization of influenza infection in PCLS.* **A:** Confocal microscopy lateral view images showing the influenza NP signal (green) and DAPI staining (blue) in PCLS inoculated with PR8 $1x10^6$ p.f.u. per slice, and fixed in PFA 4% after 12h, 24h or 48h. **B:** FC analysis of influenza HA expression in cells obtained from PCLS homogenates, 1h, 6h, 12h 24h and 48h after inoculation. All bar graphs show mean ±SD of 5 to 6 independent experiments. Statistic comparisons are relative to mock controls.

In order to measure albumin uptake levels in AECs in this experimental model, we inoculated PCLS with $1x10^6$ pfu per slice for 24h and incubated them in AF488-albumin 250 µg/mL for 60 min. When observed by confocal microscopy, we were able to detect AF488-albumin signal co-localizing with RAGE and SPC, which suggests that albumin is being taken up by both AT1 and AT2 cell types. Moreover, the AF488 signal was dramatically reduced in the IV infected PCLS (fig. 3.8 A). When comparing the levels of albumin uptake in AEC from mock and inoculated PCLS by FC analysis (3.8 B-E), we found that the percentages of cells that internalize albumin did not vary significantly (fig. 3.8 C). However, when analyzing their relative MFI we found a significant decrease in the AF488-albumin signal in AEC from the inoculated samples after 24h and 48h post-inoculation (fig. 3.8 B, D). Even more, when analyzing the AEC from inoculated slices and discriminating between infected (HA+) and non-infected (HA-) we found that the decrease in albumin uptake levels measured as MFI persists in both infected and non-infected cells (fig 3.8 E).

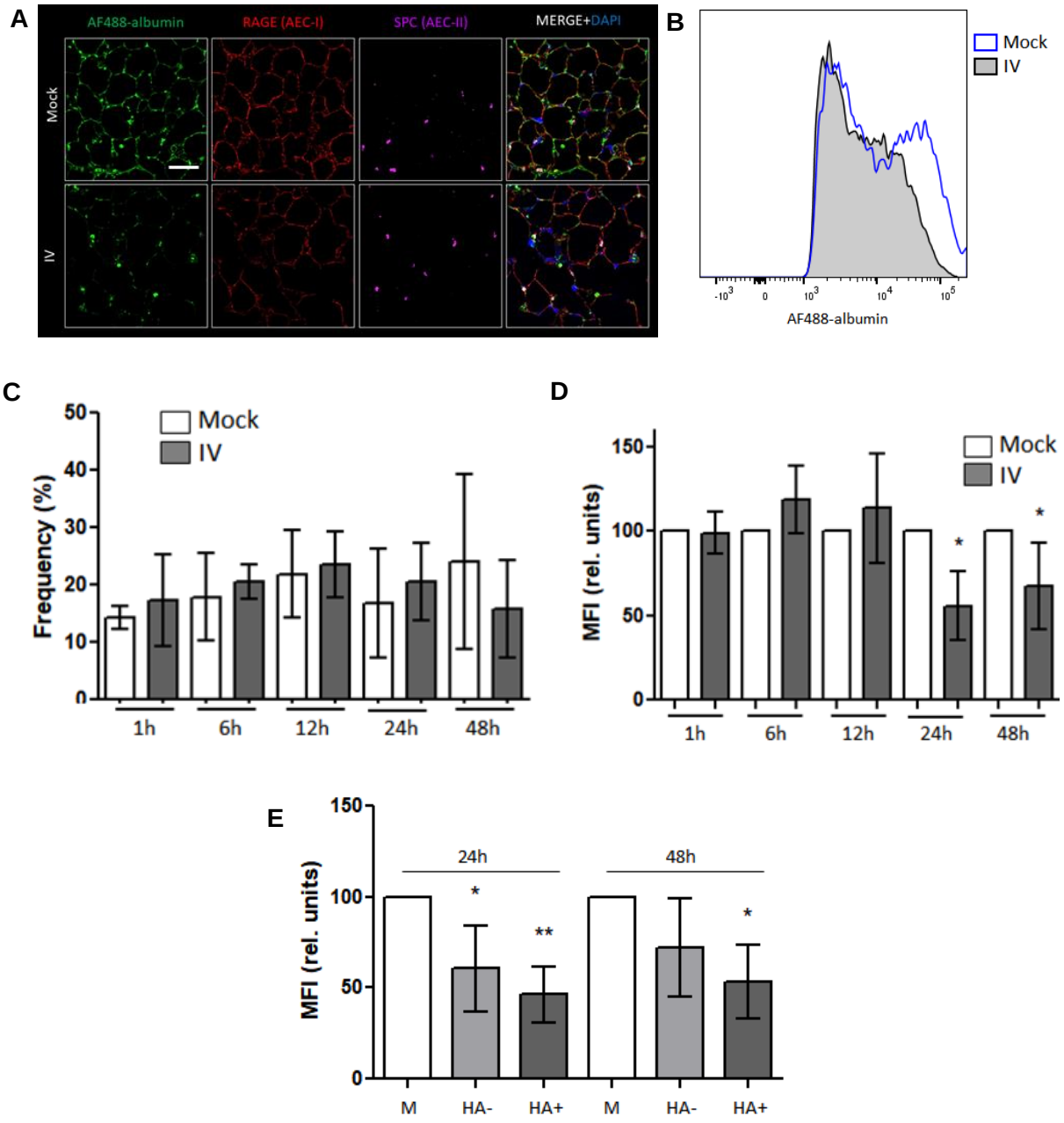

Figure 3.8 *Albumin endocytosis is impaired in IV-infected PCLS.* **A:** Confocal images of PCLS mock and IV inoculated with 1x10^6 pfu of PR8 virus (IV) for 24h and incubated in AF488-albumin (green) for 60 min and then fixed and stained with RAGE (red) and SPC (purple) antibodies. Scale bar 50 µm. Zoom 63X. **B-E.** PCLS were inoculated with PR8 for 1h, 6h, 12h, 24h and 48h and incubated in AF488-albumin for 60 min. Images show FC analysis of albumin uptake in EpCAM+ cells. **B:** Representative histograms for AF488-albumin fluorescence in AEC from mock and IV inoculated PCLS at 24h post inoculation. **C:** percentage of AF488-albumin+ cells. **D:** AF488 median fluorescence intensity (MFI) in the general AEC population from mock and PR8 inoculated PCLS. **E:** Graph showing the MFI analysis from AEC from mock PCLS (M), AEC from inoculated PCLS that did not express viral proteins (HA-) or AEC from inoculated PCLS that expressed viral proteins (HA+). All bar graphs show mean ±SD of 3 to 6 independent experiments. Statistic comparisons are relative to

Megalin expression in AEC from IV treated PCLS

We next set out to analyze megalin expression levels in AEC under IV infection conditions. By FC we measured megalin cell surface expression in AEC from mock

and PR8 inoculated PCLS after 24h and 48h (fig. 3.9 A-C). Cells were stained with a specific megalin antibody without prior permeabilization to ensure only cell surface megalin was detected. We found no significant differences in the percentage of cells expressing megalin (fig. 3.9 A) but a significant decrease in megalin MFI in AEC from inoculated samples (fig. 3.9 B), in both 24h and 48h, either expressing viral proteins (HA+) or not (HA-).

Moreover, a WB analysis of the total amount of megalin in PCLS homogenates revealed a substantial decrease in the full-length megalin abundance in the inoculated samples (fig. 3.9 D).

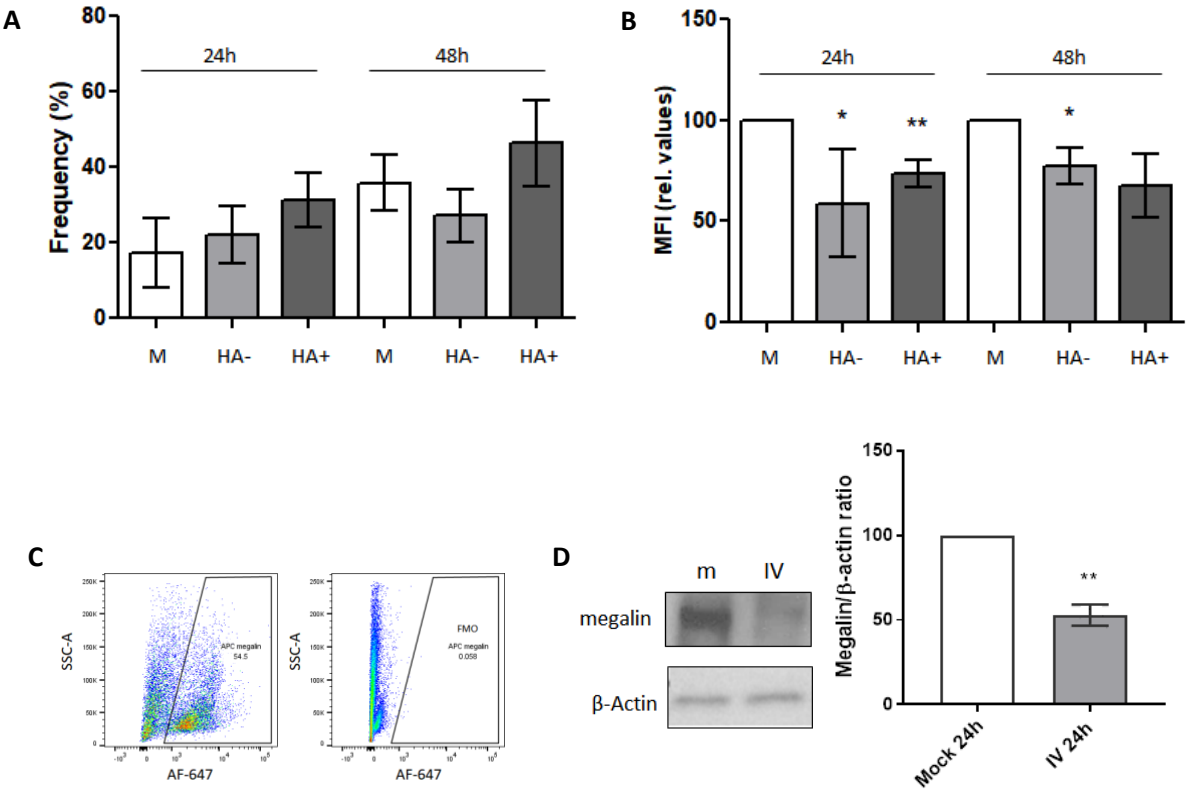

Figure 3.9 *Megalin cell surface expression is downregulated in AEC from IV inoculated PCLS.* **A-C.** PCLS were treated in mock or IV (PR8 inoculation) conditions, homogenized and live AEC were analyzed by FC. **A:** Percentages of cells expressing megalin on the surface at 24h and 48h post inoculation. EpCAM+ cells from mock PCLS (M) or from inoculated PCLS expressing viral proteins (HA+) and not expressing viral proteins (HA-) are shown. **B:** MFI of APC-megalin antibody on the cell surface. **C:** Dot plots showing the representative gating strategy for megalin and its FMO control. **D:** PCLS mock (m) and PR8 inoculated (IV) were incubated for 24h and extracted proteins were analyzed by WB. Left: Representative immunoblot for total cell megalin expression. Right: Densitometric quantification of WB megalin (600 kDa) expression, relative to actin and mock. All bar graphs show mean ±SD of 3 to 6 independent experiments. Statistic comparisons are relative to mock controls.

TGF-β1/GSK3β/ megalin axis in IV infection conditions in PCLS

Our next goal was to study whether or not the TGF-β1/GSK3β/ megalin axis plays a role in the downregulation of megalin expression in this *ex-vivo* model. We measured the concentration of active TGF-β1 in the media of mock and IV inoculated PCLS by ELISA, in a time-course analysis (fig. 3.10 A).

Although there were differences in the concentration of active TGF-β1 between time points 1h vs 6h and 1h vs 24h, both mock and infected, we found no significant differences between mock and infected samples of the same time point in all cases for our experimental setting (up to 48h after inoculation). When analyzing the phosphorylation levels of GSK3β from the treated PCLS by WB, we found no activation of this enzyme up to 24h post IV inoculation (fig. 3.10 B). We then treated the PCLS with the irreversible GSK3β inhibitor Tideglusib (TG) for 24h before the inoculation at two different concentrations 1.5 μM and 3.0 μM. We found that inhibition of GSK3β did not recover the whole-length megalin protein levels in the IV-inoculated PCLS (fig. 3.10 C-E). However, when we measured the AF488-albumin uptake levels in AEC from TG-treated IV-inoculated PCLS, our results showed no statistically significant differences between mock and IV in the TG-treated samples (fig. 3.10 F).

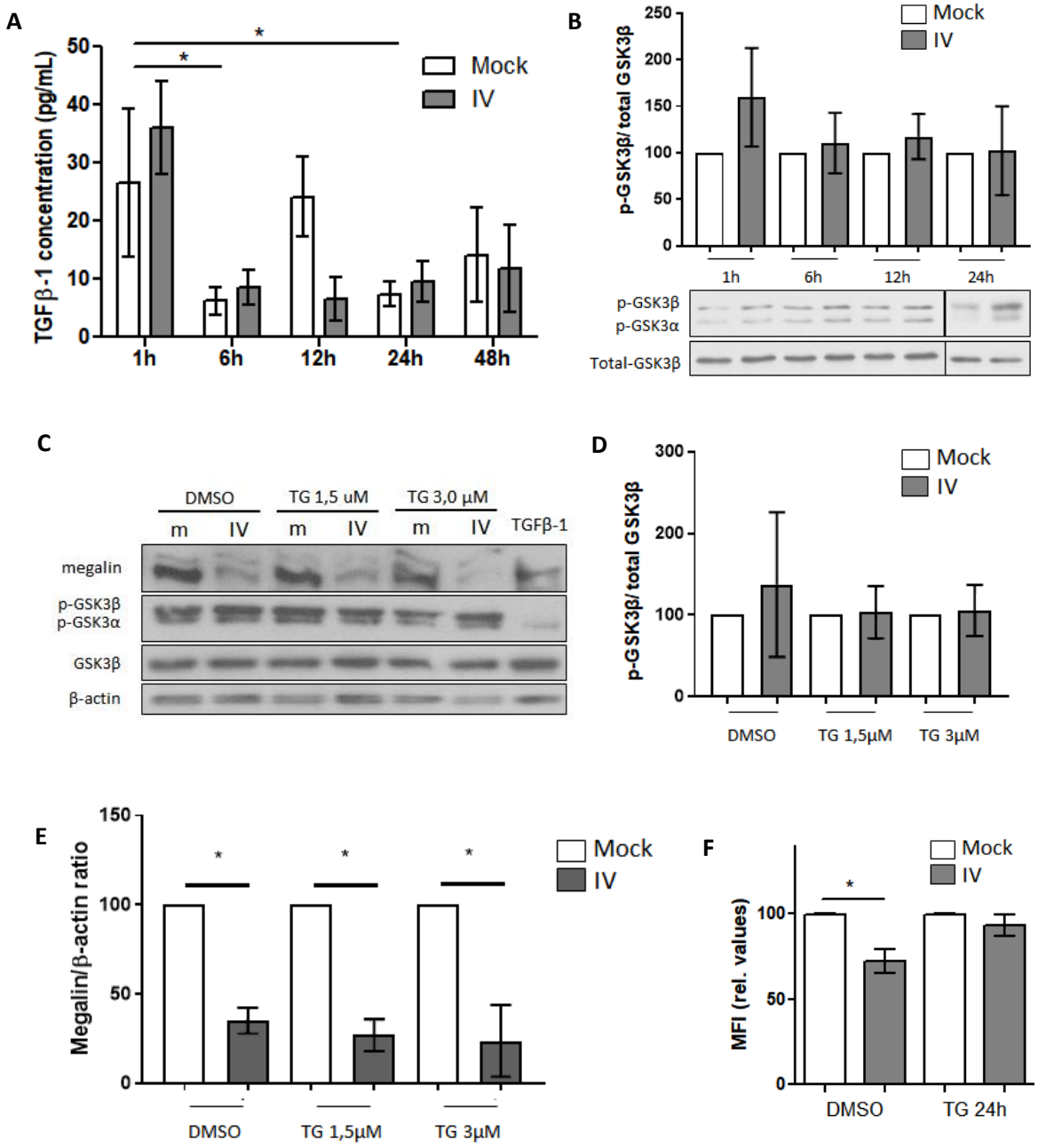

Figure 3.10. *Downregulation of megalin in IV infected PCLS is independent of GSK3β activation.* **A:** Quantification of active TGF-β1 in media from mock and PR8 inoculated PCLS incubated for 1h, 6h, 12h, 24h and 48h. **B:** Phosphorylation levels of GSK3β in PCLS homogenates, at 1h, 6h, 12h and 24h post PR8 inoculation. **C – E.** PCLS were treated with the irreversible GSK3β inhibitor Tideglusib (TG) at two different concentrations 1.5µM and 3µM or with vehicle (DMSO) for 24h prior to inoculation with PR8. Proteins were extracted and analyzed by WB. **C:** Representative immunoblots for megalin and phospho-GSK3β. TGF-β1 20 ng/mL was used as a TGF-β1 activity positive control. **D:** Densitometric quantification of phospho-GSK3β. **E:** Densitometric quantification of megalin in C. **F:** Median fluorescence intensity (MFI) of AF488 albumin from AEC from PCLS treated with IV for 24h and TG 3 µM for 24 h before IV inoculation (TG 24h). All graphs show mean ±SD of 3 to 6 independent experiments.

In vivo study

TGF-β1 is produced by many cells of the immune system and plays a crucial role in regulating immunity (M. O. Li et al. 2006). By using the *in-vitro* (cell culture) and *ex-vitro* (PCLS) models, we found no concluding evidence of direct activation of the TGF-β1/GSK3β/ megalin pathway during the experimental timeframe. However, these models are not able to represent accurately the entire immune system response during influenza infection.

For this reason, we decided to experiment in an infected live mice model where we could analyze TGF-β1 levels, study the changes in megalin expression and the GSK3β phosphorylation levels in the infected alveolar epithelium. In order to study the protein uptake process during influenza infection conditions, we inoculated mice with $3.5x10^2$ p.f.u. of IV PR8 or PBS alone (mock) and analyzed the lung tissues and bronchoalveolar lavages (BAL) 5 days after inoculation (Figure 3.11). By inoculating this amount of virus and setting this timepoint, we aimed to study the effects of IV in a condition where the integrity of the alveolar-capillary barrier would not be entirely compromised.

The analysis of the hematoxilin/eosine stainings of the alveolar region showed an increasing tendency on the average alveolar wall thickness of the infected mice (fig. 3.11 A-B). Importantly, we also found a significant increase on protein content in the BAL samples (fig. 3.11 C) which is an evidence of alveolar wall leakage. An FC analysis of the BAL cells showed that infected samples have significantly fewer resident alveolar macrophages (rAM) but increased percentages of polymorphonuclear leukocytes (PMN) and bone marrow-derived macrophages (BMM) (fig. 3.11 D).

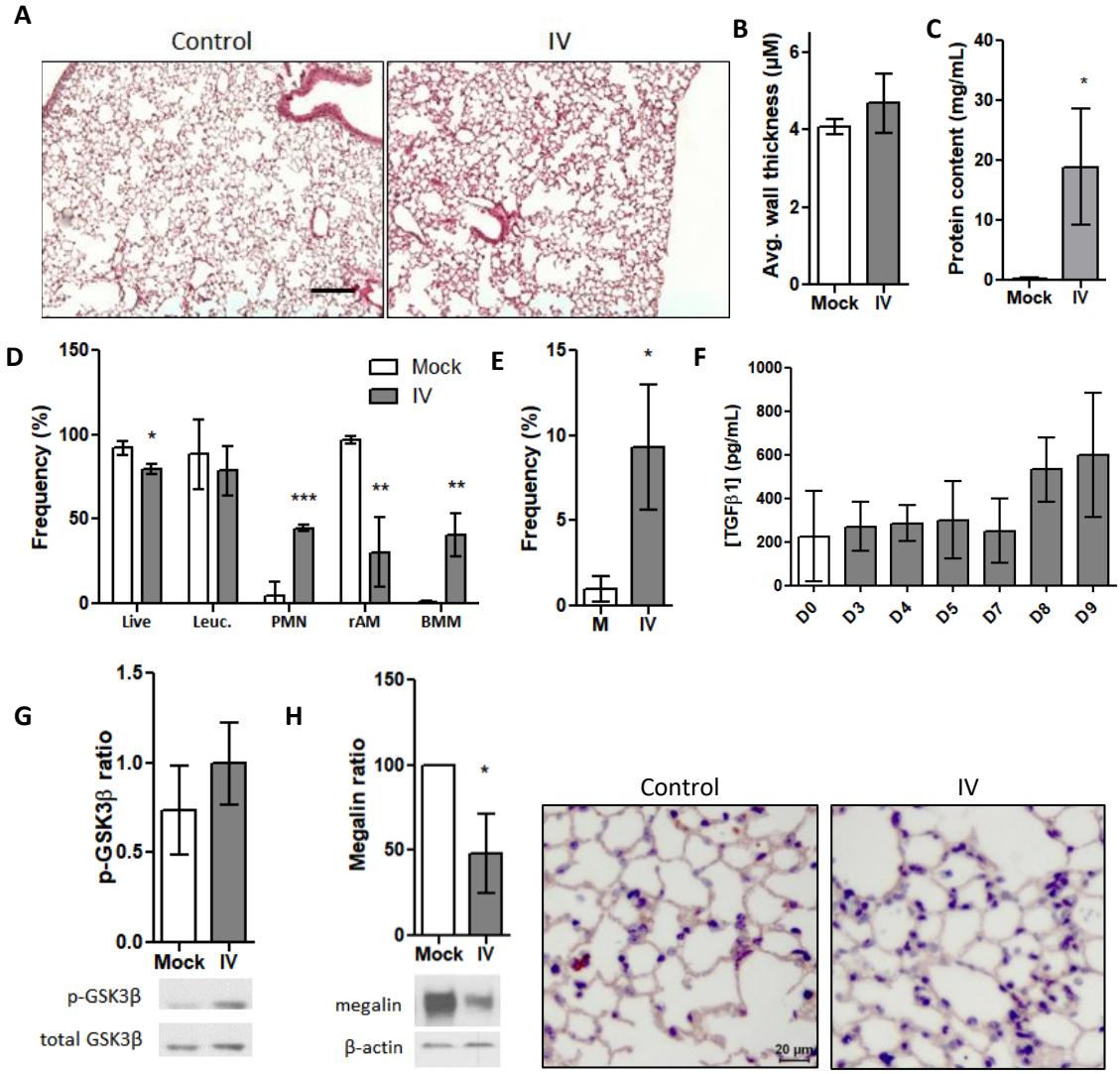

Figure 3.11. *Megalin is downregulated in AEC from IV of infected mice.* **A – G.** Lung samples were obtained from mice 5 days after intratrachaeal instillation of PR8 IV (n=5). **A:** Light micrograph showing a hematoxilin/eosin staining of lung cuts control and PR8 infected. Scale bar 100 µm. Zoom 10X. **B:** Average thickness from the alveolar-capillary wall in mock and infected (IV) samples. **C:** Protein contents from control (Mock) and infected (IV) mice BAL **D:** Cells from BAL were analyzed by FC. Graph shows the percentages of live cells (Live), total leucocytes (Leuc.), Polymorphonuclear cells (PMN), resident alveolar macrophages (rAM), and bone marrow macrophages (BMM). **E:** AEC from lung samples were analyzed by FC for viral surface proteins (HA). Graph shows percentages for HA^{pos} cells in mock (M) and infected (IV) samples. **F:** TGF-β1 levels were measured in BAL from mice control and IV infected for 3, 4, 5, 7, 8 and 9 days by ELISA. **G:** AEC were isolated and analyzed by western blot. Top: Densitometric quantification of p-GSK3β. Bottom: Representative blot. **H:** Total megalin levels were analyzed in AEC by WB (left) and Immunohistochemistry (right). Scale bar 20 µm. Zoom 63X.

We were also able to quantify the infection levels in AEC by FC, being the average percentage of infection approximately 10% (fig. 3.11 E). Interestingly, we measured active TGF-β1 concentrations by ELISA in samples of BAL from PR8 infected mice at day 0 (control), 3, 4, 5, 7, 8, and 9 post-infection. Although no statistically significant differences between samples were found, we can see an increasing tendency from

day 8 on (fig. 3.11 F). Additionally, analysis of the AEC protein extracts by WB showed no activation (dephosphorylation) of GSK3β (fig. 3.11 G) However, an evident decrease in the amount of total, whole length megalin was shown, which was also confirmed by megalin immunohistochemistry of fixed lung samples (fig. 3.11 H).

Furthermore, we analyzed the RNA expression profiles from AEC and BAL cells, by performing deep sequencing of all mRNA species (RNAseq) (fig. 3.12). We found that the majority of the differentially expressed genes (DEG) in AEC under influenza infection conditions are related to an innate immune response activation and anti-viral response genes (fig. 3.12 A). In infected and non-infected AEC samples the most expressed gene was surfactant protein C (*Sftpc*), which was expected since it is a known marker for AT2 cell, but its expression was not significantly affected by IV infection. We looked then for the expression of receptor molecules which have been described to bind albumin: megalin, secreted protein acidic and rich in cysteine (SPARC), the scavenger receptor CD36, and neonatal Fc receptor (Fcgrt) (Bern et al. 2015; Zhao et al. 2018) in AEC. *Megalin* and *Cd36* were the only ones significantly downregulated in the IV infected samples. *Megalin* mRNA counts decreased an average of more than 50% (fold change = 0.49) and *Cd36* an average 24% (fold change = 0.76).

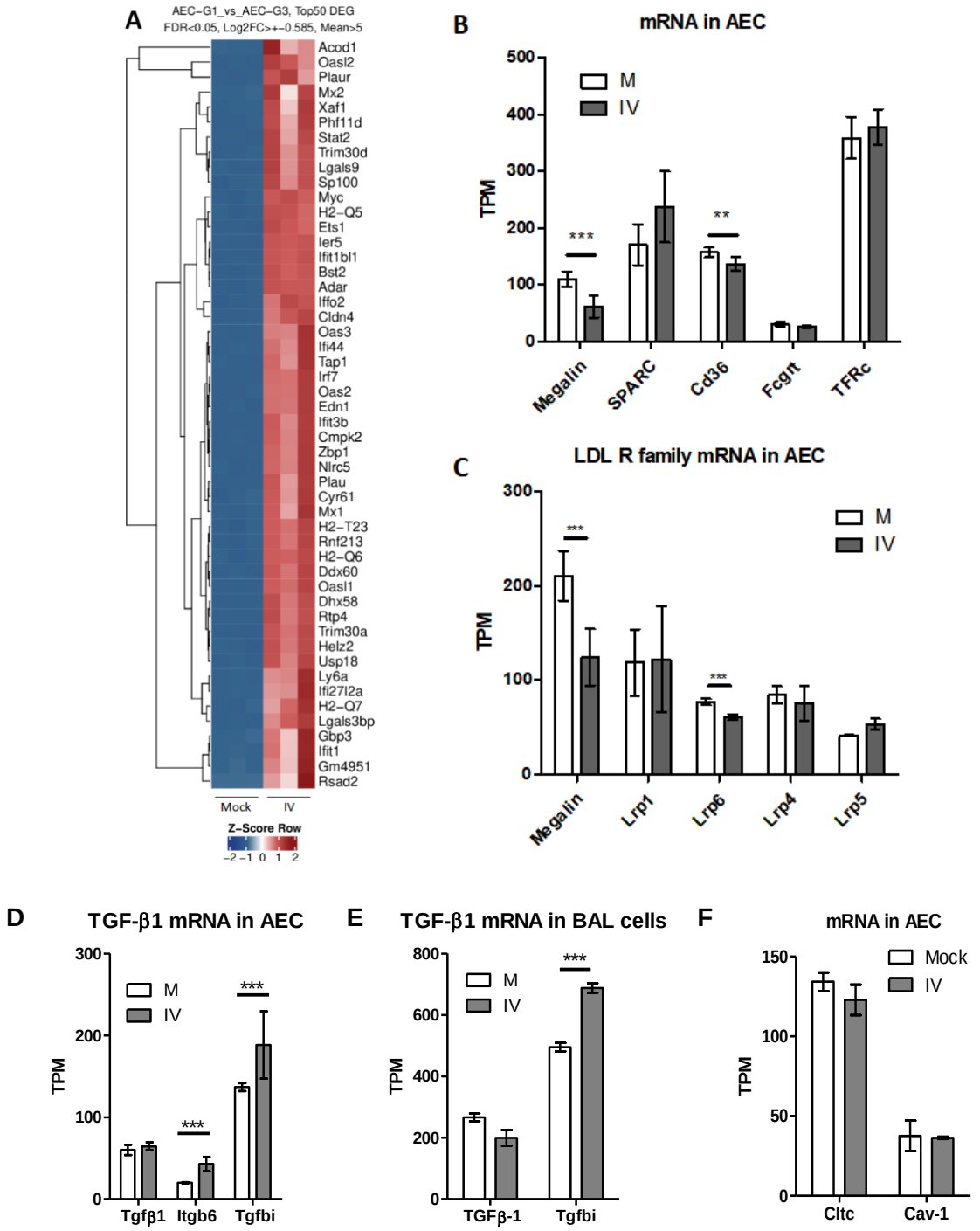

Figure 3.12. m*RNA expression in AEC and BAL cells from IV infected mice.* **A:** Top 50 differentially expressed genes (DEG) in AEC. **B:** mRNA expression levels in mock and infected (IV) AEC of the albumin receptors *megalin*, secreted protein acidic and rich in cysteine (*Sparc*), the scavenger receptor *Cd36*, and neonatal Fc receptor (*Fcgrt*). Expression levels or transferrin receptor (*TFr*) are shown for comparison. **C:** mRNA levels of the top 6 most expressed LDL receptor family members in AEC. **D – E:** *Tgfb1*, *Itgb6* and *Tgfbi* mRNA levels in AEC (**D**) and BAL (**E**). **F:** mRNA levels of clathrin (*Cltc*) and caveolin-1 (*Cav-1*) in AEC. Normalized RNAseq data, N=3. Bars represent mean ± SD. TPM: transcripts per million.

Members of the LDL receptor-related proteins (LRP) family have been described to undergo RIP receptor processor mechanism, in response to ligand binding which in

turn results in the receptor downregulation (Lal and Caplan 2011; Wygrecka et al. 2011). We then analyzed if IV treatment triggers downregulation not just in megalin but in other members of the LRP family as well. The data shows that in our experimental conditions, only megalin and Lrp6 showed a significant decrease under IV infection (figure 3.12 C). While the reduction in megalin mRNA expression was more than 50%, the reduction in Lrp6 mRNA counts was approximately 35%.

When we looked for TGF-β1 mRNA expression we found no signifigative differences either in AEC or BAL cells (figure 3.12 D). However, Tgfbi, a protein that is induced by the presence of active TGF-β1 in lung epithelial and other cell types (Skonier et al. 1992; Thapa, Lee, and Kim 2007), was upregulated with a fold change of 2.7 and 1.8 in AEC and BAL respectively. Moreover, integrin αvβ6 (Itgb6), a TGF-β inducible integrin that binds to and activates latent TGF-β (Snelgrove, Godlee, and Hussell 2011), was significantly upregulated.

Next we asked ourselves if the mRNA of proteins involved in the coating of vesicles in cellular endocytosis were differentially expressed in AEC. Not clathrin nor caveolin-1 showed significant variations in their mRNA expression levels (fig. 3.12 F).

MMPs expression and function in IV infection.

Since MMPs play a crucial role in RIP, we analyzed the differential expression of MMPs in AEC and BAL cells. In AEC from IV inoculated mice, MMP-19 was the only metalloprotease that showed a significant increment with a fold change of 4.2, while the expression of MMP-14 showed a moderate upregulation tendency (fig. 3.13 A). In BAL cells, MMP-14 expression was markedly upregulated in IV infected mice with a fold change of 56 compared to control, an increase of 5600%. At the same time expression levels of TIMP-2, the endogenous inhibitor of MT1-MMP (Hernandez-Barrantes et al. 2000), were not significantly changed (fig. 3.13 B). MMP-12 and -25 were both upregulated each with approximately a fold change of 5.

Next, we looked for MMPs protein expression in MLE-12 cells and PCLS in culture. Western blot analysis of protein expression in IV inoculated MLE-12 cells showed an upregulation of MMP-12. The expression of MMP-2, MMP-14 and MMP-19 were not significantly increased (figure 3.13 A). In IV inoculated PCLS the expression of

MMP-9 was downregulated, while the protein levels of MMP-2 and MMP-14 were unchanged.

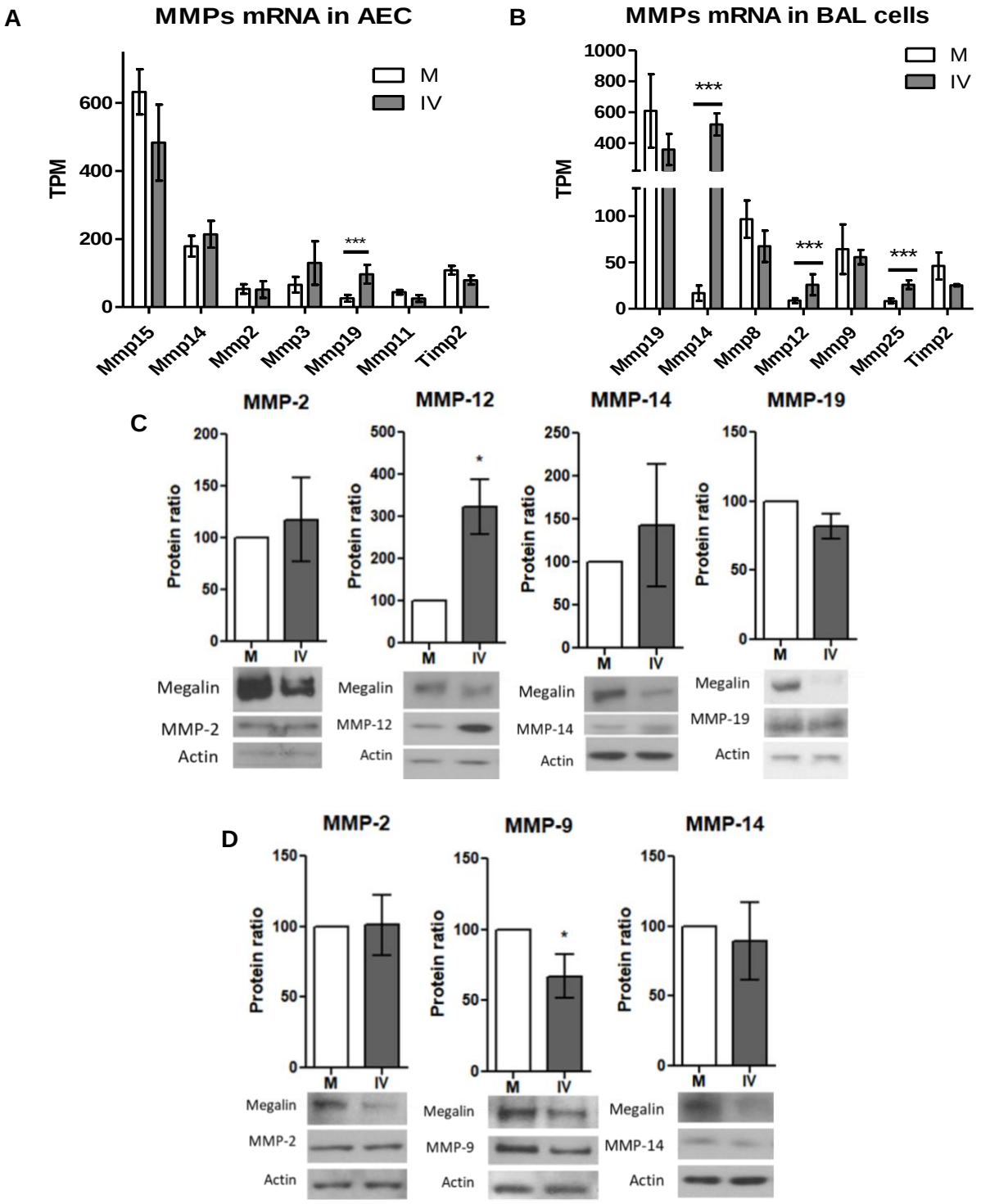

Figure 3.13. *Relative MMPs expression levels in influenza-inoculated AEC and BAL cells.* **A – B:** mRNA levels of the top 6 most expressed MMPs and *Timp2* in AEC (**A**) and BAL (**B**) from infected mice. Normalized RNAseq data, N=3. Bars represent mean ± SD. TPM: transcripts per million. **C – D:** MLE-12 cells (C) or PCLS (D) were inoculated with IV for 24h and the protein extracts analyzed by Western Blot. Representative blots and MMP/actin densitometry ratio graphs are shown. Values represent mean ± SD. N=3. **C:** In MLE-12 cells protein expression of MMP-12 was upregulated in IV conditions, while expression of MMP-2, MMP-14 and MMP-19 did not show significant differences. Representative megalin and actin WB bands are shown. **D:** In PCLS, protein expression of MMP-9 was downregulated, while no significant differences were found in MMP-2 and MMP-14 expression.

In our in vivo results, mRNA expression of MMP-14 was notably upregulated in BAL cells. Previous work from our group showed that MMP-14 interacts with megalin and suggested that it participates in the mechanism of megalin shedding from the plasma membrane (Mazzocchi et al. 2017). To analyze if the reduction in the plasma membrane abundance of megalin could be reverted by inhibition of MMP-14 we used the specific inhibitor NSC405020 in MLE-12 cells and PCLS cultures (figure 3.14). We found that MMP-14 inhibition partially recovered megalin expression in MLE-12 IV inoculated cells (fig. 3.14 A).

The albumin uptake levels of IV infected cells also showed a partial recovery (fig. 3.14 B). However, the number of cells that took albumin up in the IV treated condition was not improved, which shows that MMP-14 inhibition was not enough to reverse the effects of IV infection. In the PCLS model, we found a partial recovery on albumin uptake levels of the AEC of IV treated samples (fig. 3.14 D).

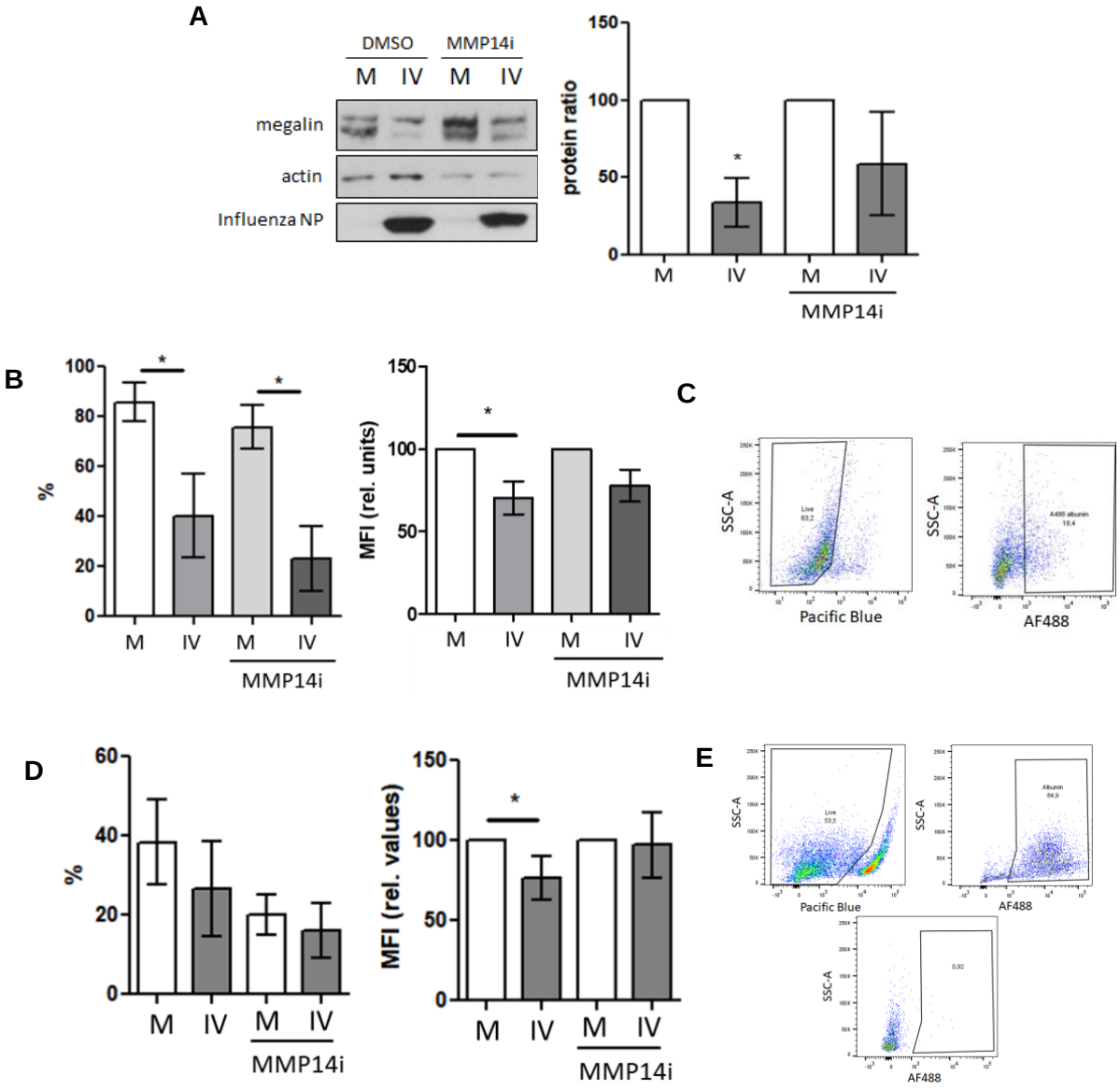

Figure 3.14. *Inhibition of MMP-14 partially recovers megalin abundance and albumin uptake in MLE-12 cells and PCLS.* **A:** MLE-12 cells were inoculated with IV (MOI 1) and incubated with the specific MMP14 inhibitor NSC405020 200µM (MMP14i) or vehicle (DMSO) for 24h. Total megalin was analyzed by western blot. Left: representative blot. Right: Densitometry quantification normalized to beta-actin. **B.** MLE-12 cells exposed to the same treatment as in A were incubated for one hour with AF488-albumin 50µM and analyzed by flow cytometry. Left: Cell frequency (%) of AF-488 albumin uptake in the AEC population Right: AF-488 median fluorescence intensity (MFI) of the cells. **C:** Gating strategy from B. **D:** PCLS were incubated in mock (M) or influenza virus (IV) conditions for 24h in the presence of MMP14 inhibitor NSC405020 (MMP14i) 200µM or vehicle (DMSO) and incubated with AF488-albumin for 1 h. Left: Flow cytometry data showing the median fluorescence intensity (MFI) of AF488 in AEC. Right: % of live cells per condition. N=3. **E:** Gating strategy and FMO control.

Discussion

ARDS accounts for more than 10% of all ICU admittances in the world and has an associated mortality of approximately 40%. Different pathologies can lead to this syndrome, with IV infection being one of the main causes. During ARDS the fluid and protein accumulation in the alveolar space -due to increased alveolar-capillary barrier permeability- impairs gas exchange in the alveoli. The concentration of protein in the alveoli is three times higher in non-survivors than in patients who recover from the disease (Bachofen and Weibel 1977). Hence, clearance of protein from the alveolar space is critical to improving the outcome of ARDS. However, as of today, no effective therapeutic approaches have been developed.

During ALI and ARDS the reparation of the alveolo-capillary barrier in combination with an effective fluid and protein removal are needed to restore the alveolar function. Several studies from our group have aimed to understand the underlying mechanisms and pathways that are involved in these processes (Buchäckert et al. 2012; Grzesik et al. 2013; Vohwinkel et al. 2017; Mazzocchi et al. 2017; Gwoździńska et al. 2017).

In the current study, we characterized the albumin uptake process in our study models: MLE-12 cells and PCLS. In MLE-12 cells we could establish that albumin uptake can be inhibited at 4°C and increased with the incubation time and albumin solution concentration (fig.3.1). Albumin clearance at 4 °C is attributable exclusively to passive transport processes because active processes are shut down at this temperature (Rutschman, Olivera, and Sznajder 1993). Dextran of the same MW as albumin (70 KDa), which was used as a micropinocytosis probe (L. Li et al. 2015), was taken up at much lower rates than albumin. When molecules are cleared faster than expected for their size is an indication that they are taken up by an active process (R. H. Hastings et al. 1995). Taken together, our results line up with previously described reports showing that albumin endocytosis in AEC is a receptor-mediated process (Buchäckert et al. 2012; Takano et al. 2015).

We were also able to show that inoculation with Influenza A/Puerto Rico/8/1934 H1N1 strain leads to productive infection in MLE-12 cells, and we optimized the infection protocol assessing infectivity levels at different time points and MOIs (fig.3.2).

Our group has previously described a TGF-β1/GSK3β-dependent mechanism for the downregulation of megalin, where the TGF-β1 mediated dephosphorylation and activation of GSK3β leads to the phosphorylation of the cytoplasmic tail of megalin, inducing its endocytosis (Buchäckert et al. 2012). We hypothesized that IV would induce this kinase's activation and that would lead to a decrease in cell surface megalin abundance. Contrary to our expectations, during our experimental time frame, we were not able to detect a decrease in GSK3β phosphorylation levels (fig. 3.3 B, C). The Receptor-regulated Smads or R-Smads are intracellular mediators that directly transduce extracellular TGF-β1 signals into the nucleus acting as transcription factors. They associate with type I cell surface TGF-β receptor and are phosphorylated on two serine residues at the C-terminal end (Weiss and Attisano 2013). Phosphorylation of SMAD2 and 3 can then be used as proof for the presence of active TGF-β on the cell surface. Moreover, megalin promoter contains two SMAD-binding elements, and the interaction between these and SMAD2 and 3 leads to a reduction in megalin expression (Cabezas, Farfán, and Marzolo 2019). Our results showed that the phosphorylation levels of SMAD2 were downregulated in the IV-treated samples during the first 3 hours post-infection and didn't show a significant difference compared to the control from 6h to 24h (fig. 3.3 B, C). Moreover, the downregulation in TGF-β1 mRNA levels (fig. 3.4 D) and the lack of an increase in active TGF-β1 presence in culture media (fig. 3.4 F), led us to infer that there is no increased TGF-β1 activity in the IV-treated MLE-12 cells at all the analyzed time points. However, when we compared cell surface and total megalin levels in mock and IV treated cells, we found a strong downregulation as early as 12h post infection (fig. 3.4 A, B). This was seen not only at the translational but also at the transcriptional levels, suggesting that IV is inducing megalin downregulation at both levels (fig. 3.4 D) even when neither TGF-β1 nor GSK3β activities were increased.

The binding and uptake assay (Yumoto et al. 2006; Buchäckert et al. 2012), showed a decreasing tendency in the FITC-albumin uptake levels of IV incubated cells over the experimental time frame, however, no statistically significant differences were found (fig. 3.3 A). This was reverted when the albumin uptake was assessed by FC, where we could see a clear decrease in the fluorescence intensity and in the percentages of cells that took albumin up in the IV-treated samples (fig. 3.4 G). This apparent discrepancy can be explained by the fact that FC provides a higher resolution in fluorescence measurements and excludes dead cells. This method also

allowed us to quantify a marked decrease in the percentage of live cells that endocytosed AF488-albumin. Interestingly, this albumin uptake downregulation was correlated by a decrease in the expression of megalin but not by the activation of GSK3β in all the considered time points. Put together, our results suggest that in IV inoculated MLE-12 cell cultures, downregulation of albumin uptake is independent of GSK3β activation.

During a viral infection, an organized host immune response is triggered to achieve viral clearance and recovery from infection. This response can be divided into a fast initiation phase and a resolution phase. During the initiation phase, there is an activation of the antiviral innate immunity involving the recognition of viral pathogen-associated molecular patterns, the recognition of damage-associated signals, and activation of the inflammasome and complement system. The resolution phase involves cellular immunity response and the production of antibodies (Yoo et al. 2013). In order to orchestrate these responses, the interaction of different cell types that participate in the inflammation process is needed. Also, TGFβ, a known modulator of the immune response, is produced by immune cells (M. O. Li et al. 2006; Worthington et al. 2012). On the other hand, culture of alveolar epithelial monolayers model only the AT2 cells, lacking components representing the endothelium and bronchial epithelium. Moreover, cell cultures are often transformed cells whose genome and metabolism have been altered (e.g. it has been proposed that cancer cells take albumin up at higher levels due to their metabolic rate (Merlot, Kalinowski, and Richardson 2014)). For these reasons, cell monocultures are a limited model for the study of the effects of IV infection in protein uptake of AEC. By utilizing a PCLS model we were able to study the AEC response in a more accurate lung environment where most lung cell types were represented including immune system lung-resident cells and lung parenchymal cells.

We were able to characterize the albumin uptake process in cultured mice PCLS by using FC and confocal microscopy. The time-course and albumin concentration curve experiments showed that protein uptake measures in AEC are reproducible and reliable (fig. 3.5). Similarly to MLE-12 cells, after one hour of incubation AF488-albumin was internalized by a higher percentage of cells than TR-dextran of the same molecular weight (fig. 3.6 B). In addition, the AF488-albumin uptake levels were strongly decreased at 4°C as well as in the presence of 1000-fold molar excess

of unlabeled albumin (fig. 3.6 C). Taken as a whole, our results are consistent with previous reports showing that albumin uptake in cell culture and isolated lungs is temperature-dependent and can be inhibited by competition, which are both indicators of a receptor-mediated and active process (Rummel 2007; Yumoto et al. 2012; Buchäckert et al. 2012; Takano et al. 2015).

Endocytosis inhibition studies allow determining the key routes and components of the albumin uptake process. Chlorpromazine is a cationic amphipathic drug that causes the assembly of clathrin and adaptor proteins on endosomal membranes thus preventing their assembly on the plasma membrane and blocking clathrin-dependent endocytosis. It was also shown to inhibit clathrin-independent endocytosis although it varies in specificity and efficacy depending on the cell type (Dutta and Donaldson 2012; Vercauteren et al. 2010).

Dynasore inhibits the GTPase activity of dynamin, which prevents the constriction and fission of endocytic vesicles from the membrane. It has been typically used to inhibit caveolar and clathrin-mediated endocytosis, however, it has been shown that it also can inhibit fluid-phase endocytosis and peripheral membrane ruffling (Preta, Cronin, and Sheldon 2015; Oh et al. 2012; R. J. Park et al. 2013).

Macropinocytosis is a process whereby a relatively large amount of the external fluid phase is engulfed by the cell, in respect to its volume. It has been shown to occur in AEC, where it can even internalize bigger particles like bacteria and viruses (García-Pérez et al. 2008; Torriani et al. 2019). It is defined as a highly coordinated process, with the participation of specific membrane components, that is triggered with distinct molecular regulators (Kumari, Mg, and Mayor 2010). The mechanisms of macropinosome scission from the plasma membrane haven't been fully described, however, there is evidence indicating that isoforms of dynamin are involved in this process in epithelial cells (Cao et al. 2007). Amiloride, a Na^+/H^+ exchanger inhibitor, is widely used as a macropinocytosis specific inhibitor (Koivusalo et al. 2010; Kumari, Mg, and Mayor 2010) although it has been shown to have alternate inhibitory effects on clathrin-mediated endocytosis of albumin in kidney epithelial and human carcinoma cells (Gekle, Freudinger, and Mildenberger 2001; Ivanov, Nusrat, and Parkos 2004).

In our results, incubation of PCLS with the inhibitors chlorpromazine, amiloride, and dynasore, showed a decrease in the percentage of total cells that assimilated

albumin, as well as the control at 4°C (fig. 3.6 D, left) suggesting that dynamin-mediated processes and possibly macropinocytosis play an important role in albumin endocytosis of lung cells, which may highlight the implication of macrophages in the albumin uptake process in the lung. However, when only AT2 cells were analyzed, the AF488 MFI decreased significantly with dynasore and chlorpromazine treatments, while the amiloride treatment did not affect the albumin uptake levels (fig. 3.6 E, right). Taken as a whole, these results suggest that endocytosis of albumin in alveolar epithelial cells from PCLS is mainly mediated by clathrin-mediated endocytosis. This lends support to previous findings in alveolar epithelial cell line models suggesting that the endocytosis of FITC-labeled albumin in cultured RLE-6TN cells, A549 cells, and in rat primary type II and type I-like cells is mainly clathrin-dependent, while the involvement of caveolae-mediated endocytosis of albumin played only a minor role (Yumoto et al. 2006; Ikehata et al. 2008; Yumoto et al. 2012; Buchäckert et al. 2012). One of the limitations of the use of fluorescently labeled albumin is that albumin movement across the alveolo-capillary barrier involves its degradation (Rummel 2007; Yumoto et al. 2006). FITC-labeled albumin degradation increases significantly the fluorescence intensity of the FITC molecules. If samples are not processed timely and kept at cold temperatures it may lead to inaccurate measurements of albumin uptake and hence special care should be taken to ensure accuracy and reproducibility. Future studies could benefit from the use of genetically modified mice expressing fluorescent reporters and/or knocking out genes of key components in order to determine their individual contribution to the protein transport mechanism from the alveolar space.

Despite intensive research, the precise mechanism by which proteins are cleared from the distal air spaces remains poorly understood. The pathophysiological relevance of active protein removal in the setting of acute lung injury is controversial and a topic of intense debate (Mazzocchi et al. 2017). In the review from Hastings et al. 2004, various reports referring to alveolar albumin transport were summarized. It was highlighted that two mechanisms of albumin transport may take place in the alveolar epithelium, each one acting in different settings. In albumin concentrations lower than 5 mg/mL, the transport of protein through the alveolar epithelium in whole lung models shows saturation kinetics, is dependent on the temperature and is sensitive to pharmacological agents which either stimulate or inhibit endocytosis. However, in concentrations of protein higher than 5 mg/mL, the rate of clearance is

not affected by pharmacological agents, doesn't show saturation kinetics, and is proportional to the concentration. Previous works from our group (Rummel 2007 and Buchäckert et al. 2012) where albumin concentrations lower than 1 mg/mL were used for most protein uptake experiments, suggested that the albumin transport occurring across the alveolar-capillary barrier is due to transcytosis, and is energy-dependent, which is in line with previous observations. During ARDS the protein concentrations in the alveolar edema can reach up to 95% of the plasma levels. In a recent medical study involving samples from 79 patients that received low tidal volume (lung-protective) ventilation at day 0 of ARDS, the interquartile range of the total protein concentration in BAL was 0.890–3.170 mg/mL with a median of 1.793 mg/mL (Hendrickson et al. 2017). These values further confirm that the process of transcytosis plays a relevant role in regulating the amount of protein in the alveolar environment in ARDS until edema resolution. Nevertheless, assessing the exact contribution of these active transport processes to the overall protein clearance in vivo in uninjured and injured lungs as well as in the setting of ARDS will require further research.

Infected AEC from PCLS showed an important decrease in albumin uptake levels. In contrast to what was observed in the inhibition studies where the endocytic processes were halted with chemical inhibitors of endocytosis, the frequency of the cells that internalized labeled albumin did not change significantly, however, the MFI was significantly reduced. This is consistent with the idea of a downregulation of the amounts of albumin receptor on the cell surface, which would not affect the percentage of cells that take up albumin but instead, reduces the amount of albumin being internalized (fig. 3.8) confirming a connection between protein uptake and the abundance of the receptor. Interestingly, in the cells from IV inoculated PCLS, albumin uptake levels were downregulated in both infected (HA^+) and non-infected (HA^-) cells as also was the cell surface expression of megalin (fig. 3.9). This suggests that the downregulation of the protein uptake and megalin abundance is independent of the infection status of the cells and that the presence of the virus in the medium is enough to induce the megalin negative regulation, either through a direct effect or through paracrine cell communication.

In the work of Vohwinkel et al. 2017, it was described that megalin expression on the cell surface can be downregulated by the phosphorylation of the PPPSP motif in

megalin's cytoplasmic domain by active GSK3β. We hypothesized that megalin downregulation under IV infection conditions is mediated by its phosphorylation through this kinase. However, similarly to what we saw in MLE-12 cells, we found no activation of GSK3β in PCLS at all the studied time points. In fact, when we used the specific GSK3β inhibitor Tideglusib, we found no recovery in megalin's expression under IV infection conditions (fig. 3.10). These data suggest that the activity of GSK3β is not needed to drive megalin's downregulation in our experimental setting. Interestingly, tideglusib treatment recovered partially the albumin uptake levels of infected samples, which implies that a secondary mechanism of albumin uptake that does not involve megalin can also be restored by GSK3β inhibition.

To further confirm our results, we performed an *in vivo* study, where we analyzed the effects of IV infection on the TGF-β1/GSK3β/megalin axis in mice lungs. We could document the morphometric and pathophysiological effects of a 5 days IV infection in mice lungs, like increased alveolar damage, evidence of protein leakage, and extravasation of leukocytes. Similarly to MLE-12 and PCLS models, we also found in the infected lungs decreased expression levels of megalin protein and RNA, as well as no signs of GSK3β activation (fig. 3.11 and fig. 3.12 B). Analysis of BALs from IV infected mice showed no significant increment in active TGF-β1 levels, however, an increasing tendency could be found from day 8 on. Since TGF-β1 has immunomodulatory and anti-inflammatory effects (Worthington et al. 2012) a raise in its levels is consistent with the start of the resolution phase, which in this mouse model occurs one week after infection. In our differential gene expression analysis we found no significant differences in TGF-β1 mRNA between mock and infected samples, however, the expressions of Tgfbi and Itgb6, two proteins that are induced by TGF-β1, were upregulated in AEC which suggests this cytokine is active under our IV experimental conditions.

The mRNA expression of membrane-related proteins that have been pointed out as potential albumin receptors showed that megalin (lrp2) is the receptor gene that undergoes the strongest downregulation in IV conditions. This is consistent with the results observed also in IV-inoculated MLE-12 cells.

CD36 is a membrane glycoprotein that acts as a scavenger receptor and is involved in transcytosis by its direct interaction with caveolin-1 and was singled out to be responsible for albumin transcytosis across dermal microvascular endothelium

(Raheel et al. 2019). It has also been implied in viral uptake in hepatic cells (Cheng et al. 2016). CD36 mRNA was highly expressed in control samples and significantly downregulated in infected samples. However, its contribution to albumin uptake processes in AEC has not been described so far and should be further investigated.

The SPARC protein is a secreted matricellular glycoprotein acting in the extracellular matrix environment that is expressed in many different cell types and is overexpressed in cancer cells. It is a protein that binds to albumin in the interstitium leading to the accumulation of albumin in the tumor periphery where it contributes to the enhanced permeation and retention effect observed in tumors (Merlot, Kalinowski, and Richardson 2014; C. R. Park et al. 2019). In our results, *Sparc* did not show differential expression between control and IV conditions which shows that a potential implication in albumin uptake in AEC is at least not regulated at a transcriptional level.

The human neonatal Fc receptor is expressed by the *Fcgrt* gene and mediates recycling and transcytosis of IgG and albumin in various cell types, with a role central to homeostatic regulation and conservation of albumin from intracellular catabolic degradation (Anderson et al. 2006). Similarly to *Sparc*, *Fcgrt* was not significantly downregulated in IV conditions and its mRNA expression levels were comparatively low. Nevertheless, SPARC and FCGRT proteins contribution to albumin uptake in the alveolar epithelium should be further investigated.

Other potential albumin receptors like the scavenger receptors gp60 (albondin), gp18, and gp30 could not be identified in our RNAseq analysis. Even when gp60 was one of the first specific albumin receptors described, the gene encoding albondin protein has to our knowledge not yet been mapped in animal or human genomes (Bern et al. 2015). Their contribution to albumin transport remains then to be further studied.

From the most expressed LRP gene family members, megalin (LRP2) has the highest expression levels in AEC. LRP1 is a multi-ligand receptor that binds and endocytoses a broad spectrum of over 40 ligands, including lipoproteins, extracellular matrix proteins, proteases, and protease/ inhibitor complexes and growth factors (L. Wujak, Markart, and Wygrecka 2016). It has also been reported to function as a receptor for TGFβ-1, mediating CHO cell growth inhibition upon its binding (Tseng, Huang, and Huang 2004). In ARDS conditions TNFα induces LRP1 MMP-14-

mediated shedding at the fibroblast surface which prevents the endocytosis and regulation of the activities of proteases like MMP-2 and MMP-9. MMPs exert both detrimental and beneficial effects during the repair of injured alveoli by further damaging the basement membrane and stimulating AT2 cells migration. Transient LRP1 inactivation promotes re-epithelialization and limits damage to the basement membrane. Conversely, prolonged LRP1 absence leads to imbalanced ECM deposition, excessive proteolysis, and pathological tissue remodeling, which may lead to pulmonary fibrosis (Wygrecka et al. 2011; L. Wujak, Markart, and Wygrecka 2016; Lukasz Wujak et al. 2018). In our study, the gene coding for lrp1 was also highly expressed in AECs although it did not show differential expression in IV conditions when compared to control. Most LRP1 function studies have focused on its capacity to internalize and regulate the activity of MMPs, however, due to its role as a multi-ligand receptor and its structural similarity to megalin, its contribution to alveolar protein clearance should be further studied.

LRP6 showed a significant downregulation as well in IV conditions. Although LRP6 belongs to the LDLR family, it has unique characteristics; for example, the cytoplasmic C-terminal domain of LRP6 contains at least one copy of a PPPSP motif instead of the NPxY common to all other LDLR family members. It is a Wnt co-receptor with essential functions in the Wnt/β-catenin pathway that controls embryonic development and adult homeostasis. Disruptions in *Lrp6* function have been linked to many complex human diseases, including metabolic syndrome, cancer, Alzheimer's disease, and osteoporosis (MacDonald, Tamai, and He 2009; Z. M. Wang et al. 2018). Some studies have shown that Wnt and its downstream typical signal transduction pathway have an important impact on ARDS resolution by regulating inflammatory responses and AT2 cell proliferation (Cai et al. 2015; H. F. Li and Liu 2019). Additional research is needed in order to further study if LRP6 also plays a role in the protein clearance process in the alveolar epithelium and to fully understand its contribution to ALI/ARDS resolution.

Furthermore, clathrin and caveolin-1 mRNA expression in AEC did not show differential expression in IV conditions, implying that their potential participation in albumin uptake downregulation in IV infection is at least, not regulated at a transcriptional level.

MMPs are a family of zinc-dependent endopeptidases that are involved in the degradation of various proteins in the ECM (Cui, Hu, and Khalil 2017). The contribution of MMPs to the pathology of ALI and ARDS has been studied for decades. Pro-inflammatory cytokines induce MMP over-expression and increase their activity thereby participating in airway and alveolar remodeling where MMPs play a role in both the destructive pathology and in the process of tissue repair. Chemical inhibition of MMPs in ALI has been shown to limit lung damage, presenting a potential therapeutic strategy for the treatment of this pathology (Davey, McAuley, and O'Kane 2011; Solun and Shoenfeld 2020).

Our data show that several MMPs mRNA were expressed in AEC and BAL cells of control and infected mice. Mmp19 expression was significantly upregulated in infected AEC samples. Also known as RASI-1, MMP-19 has been described to use components of the ECM as substrates, which implies a role in tissue remodeling (Davey, McAuley, and O'Kane 2011) and protection against the development of fibrosis after lung injury (Yu et al. 2012).

One striking observation was the 56-fold-change upregulation of MMP14 (also known as MT1-MMP) in BAL cells from infected mice. Known MMP-14 substrates in the ECM are collagen, gelatin, fibronectin, and laminin, but also non-ECM proteins like Pro-MMP-2 and -13, LRP1, and CD44 (Davey, McAuley, and O'Kane 2011; Rozanov et al. 2004; Wygrecka et al. 2011). MMP-14 is a membrane-tethered protease that has a mechanism of regulation in which the active enzyme undergoes a series of processing events, either autocatalytic or mediated by other proteases that result in the shedding of the catalytic domain. This shedding would shift the proteolytic activity from the plasma membrane to the pericellular environment (reviewed by Hernandez-Barrantes et al. 2002).

Upregulation of MMP-14 has previously been reported in ARDS (Wygrecka et al. 2011). These extremely elevated levels of MMP-14 mRNA expression were also found in the work of Talmi-Frank et al. 2016 with IV H1N1 infected mice, where most of the MMP-14-overexpressing cells after 5 days of infection were immune cells of myeloid origin. This report revealed important morphologic and compositional changes of the ECM in IV-infected lungs, which included the depletion of fibrillar collagens. These deleterious effects on the ECM were abolished when the mice were treated with an MMP-14 specific inhibitor antibody but not with the IV inhibitor

Oseltamivir, which indicates that the effect was due to the protease's activity. Additionally, in the same study, they also used a second mouse model of co-infection of IV with *Streptococcus pneumoniae* (Talmi-Frank et al. 2016) and showed that treatment with the specific MMP-14 inhibitor antibody significantly increased the survival of IV + bacteria-infected mice over the bacteria-only infected control. Mice that did not receive the inhibitor had bacteremia and dissemination of *S. pneumoniae* into the spleen and liver, while the infection of treated mice remained confined within the lungs. The results suggested that the ECM damage contribution to the lethal influenza infection is caused by infiltrating immune cells and their overexpression of MMP-14. This highlights the potential therapeutic strategy of a timely MMP-14 inhibition during IV infection.

Since we observed megalin protein downregulation in MLE-12 and PCLS IV infection models, we analyzed the protein levels of some MMPs by WB to see if they were upregulated in these models. The protein expression of MMP-14 in IV-treated MLE-12 and PCLS, however, was not significantly increased supporting that infiltrating monocytes and/or polymorphonuclear cells are the main source of this MMP during IV infection.

In MLE-12 cells, MMP-12 protein was significantly upregulated. Reports have shown strong overexpression of *Mmp-12* gene in AT2 cells during pulmonary inflammation triggered lung remodeling, linking it to tumorigenesis and chronic obstructive pulmonary disease (Lian et al. 2005; Qu et al. 2009). We were not able to test MMP-12 protein presence in lung samples, however, since many MMPs have overlapping roles it would be of interest to analyze the expression of this protein in vivo during IV and its potential role in megalin downregulation.

Lung stromal cells are also an important source of MMPs (Craig et al. 2015; L. Wujak, Markart, and Wygrecka 2016). In PCLS however, we did not observe an increase in the protein levels of the active forms of MMP-2, -9 or -14, three MMPs that have been shown to participate in megalin shedding from the cell surface (Mazzocchi et al. 2017). Nevertheless, in all experiments with IV-inoculated MLE-12 cells or PCLS, we detected a downregulation of megalin protein expression (cell surface and total). WB is a useful technique for the relative quantification of proteins. However, it is relevant to mention that MMPs can form inhibition complexes with TIMPs that will be dissociated during electrophoresis. Therefore, one limitation of this

technique is that even when changes in intensities of protein bands of MMPs active forms reflect changes in the protein synthesis by the cells, this may not represent accurately variations in their endogenous activities.

MMP-14 has been described to activate MMP-2 in response to bleomycin in AEC (Kunugi et al. 2001) and to mediate the proteolysis of the extracellular domain of LRP1 (Wygrecka et al. 2011). Previous work from our group showed that MMP-2 and MMP-14 can have direct physical interaction with megalin on the plasma membrane of AEC, which suggests that megalin could serve as a scaffold allowing the interaction of these metalloproteases and activation of the enzyme that later mediates the shedding of its own ectodomain (Mazzocchi et al. 2017). The small molecule NSC405020 specifically inhibits MMP-14 homodimerization via the MMP-14 PEX domain, a process that is required for proMMP-2 activation (Itoh et al. 2001; Zarrabi et al. 2011; Remacle et al. 2012). When we added this inhibitor in the culture medium of MLE-12 cells and PCLS the levels of expression of megalin and albumin uptake (MFI) in IV inoculated samples recovered partially, suggesting that MMP-14 may play a role in megalin shedding. Our data are in agreement with the published report of Mazzocchi et al. 2017, where it was shown that in TGF-β1 treated RLE-6tn cells, megalin's shedding was increased as well as MMP-14 expression and its distribution on the plasma membrane, while treatment with MMP-14 siRNA recovered the amounts of megalin protein expression as well as albumin binding and uptake levels. In our data, nevertheless, the percentage of cells that internalized albumin remained lower than for the mock condition, which suggests that MMP-14 is only partly responsible for albumin uptake downregulation in IV exposed AEC, and other players are participating in this process. Several nonspecific inhibitors of MMPs like tetracyclines and hydroxamates have been shown to limit lung damage, suggesting that these compounds could be used as a potential pharmacotherapeutic strategy for treating ALI/ARDS (Davey, McAuley, and O'Kane 2011).

In the work of Mazzocchi et al., it was suggested that TGF-β1 has a regulatory role in megalin shedding through the modulation of MMPs activities. The concentration of TGF-β1 used as a stimulus was at least two orders of magnitude higher than the ones we measured in our in vivo experiment. We did not find such an increase of active TGF-β1, nor increased SMAD2/3 phosphorylation, in our IV-infected samples.

The question of what is the stimulus that triggers megalin downregulation in AEC during IV infection remains open. Notably, it has been shown that several of the molecules that affect the expression of megalin at mRNA and protein levels are also its ligands (reviewed by Marzolo and Farfán 2011). For instance, vitamins A and D, which are endocytosed by megalin, increase megalin mRNA in different cell types (Liu et al. 1998). Another example is clusterin, a glycoprotein that binds to megalin and can act as an antiapoptotic agent in prostatic cells increases megalin mRNA and protein expression (Ammar and Closset 2008). The hormone angiotensin 2 exerts its signaling through binding the ATR1 receptor, but it can also be endocytosed by megalin and downregulate its expression (Hosojima et al. 2009) being an example of negative megalin regulation. It has also been shown that albumin concentrations higher than 10 mg/mL promote downregulation of megalin at both mRNA and protein levels and apoptosis after 24h of treatment in renal proximal tubule cells, an effect that seemed to be independent of TGF-β1 activity (Caruso-Neves et al. 2006).

The group of Biemesderfer et al. has shown that megalin undergoes Notch-like processing, where a signaling pathway is activated by ligand and the downstream effects of ligand binding may imply gene regulation (fig. 1.6). They showed that RIP of megalin in the kidneys can be activated by vitamin D-binding protein and may regulate vitamin D metabolism-related genes. However, they highlighted the need to address the question of whether all megalin ligands activate processing equally, and as a result, activate or repress the same genes (Biemesderfer 2006). In our study, we show a clear downregulation of megalin at a transcriptional and translational level upon IV infection. After post-translational modifications, megalin glycoprotein is heterogeneously glycosylated, where the most abundant glycans are SAα2,6Gal and SAα2,3Gal (Morelle et al. 2000). Since IV internalization depends on the interaction with its HA protein and cell surface receptors containing SA residues bound to galactose, megalin-mediated endocytosis is probably one of the viral entry mechanisms. It is tempting to speculate that the interaction between the virus itself and megalin could be triggering the receptor's downregulation.

To our knowledge, our study is the first that reports a strong downregulation of megalin expression in IV-inoculated MLE-12 cells, PCLS, and AEC from IV-infected C57BL/6 mice. We also show the effects of MMPs inhibition and discussed how a timely use of MMPs inhibitors could be a potential therapeutic target to increase

protein clearance during ALI/ARDS. However, the specific mechanisms that trigger megalin downregulation under IV infection and to which extent the implications of this event affect protein clearance in the lung under ALI/ARDS are not yet completely understood and would require further research.

Summary

Acute respiratory distress syndrome (ARDS) is a common complication of influenza virus (IV) infection. During ARDS, alveolar protein concentrations often reach 40-90% of plasma levels, causing severe impairment of gas exchange and promoting deleterious alveolar remodeling.

Protein clearance from the alveolar space is initiated by clathrin-mediated endocytosis, in part by the multi-ligand receptor megalin. Here, we aimed to investigate whether IV infection impairs alveolar protein clearance.

Infection with IV A/Puerto Rico/8/1934 H1N1 seasonal, mouse-adapted strain caused a marked downregulation of albumin uptake in MLE-12 cells and in alveolar epithelial cells (AEC) from PCLS, as assessed by flow cytometry and confocal microscopy, which was associated with decreased plasma membrane abundance, total protein levels and mRNA expression of megalin. Previous work from our group showed that megalin downregulation can be triggered by the binding of TGF-β1 to its receptor, which leads to the dephosphorylation and activation of glycogen synthase kinase -3β(GSK3β). The activity of this kinase phosphorylates the cytoplasmic domain of megalin, signal that internalizes the receptor and impairs protein uptake. Contrary to our expectations, we found no signs of activation of the TGF-β1/GSK3β/megalin axis in our in vitro models.

To further dissect the effects of IV infection on endocytic pathways, we infected mice with IV in vivo and subjected isolated AEC and cells obtained from bronchoalveolar lavage (BAL) to bulk RNA sequencing. Of note, downregulation of megalin and other endocytosis related receptors like the scavenger receptor *CD36* and *Lrp6* was evident in AEC. Moreover, we observed that downstream targets of TGF-β1, such as *Itgb6* and *Tgfbi* were markedly upregulated in AEC upon IV infection, suggesting the presence of the active form of the cytokine which is of relevance as our group had previously shown that activation of TGF-β1 is sufficient to reduce cell-surface abundance of megalin. We also identified a significant upregulation of MMP-14 in BAL cells. Moreover, the specific inhibition of this protease partially recovered the levels of total megalin and albumin uptake. This suggests that the previously described MMP-driven shedding mechanisms are potentially involved in downregulation of megalin and thus clearance of excess alveolar protein.

Importantly, it highlights the therapeutic potential of timely MMPs inhibition in the treatment of IV-induced ARDS.

As lower alveolar edema protein concentrations are associated with better outcomes in ARDS, identifying targetable mechanisms of impaired alveolar protein clearance after IV infection may hold a therapeutic promise.

Zusammenfassung

Das akute Atemnotsyndrom (ARDS) ist eine häufig vorkommende Komplikation einer Infektion mit einem Influenzavirus. Während des ARDS erreichen die alveolären Proteinkonzentrationen oft 40-90% der Plasmakonzentration, was zu einer schweren Beeinträchtigung des Gasaustauschs führt und einen schädlichen alveolären Umbau fördert.

Die Protein-Clearance aus dem Alveolarraum wird durch eine Clathrin-vermittelte Endozytose initiiert, zum Teil durch den Multiligandenrezeptor Megalin. Ziel der Untersuchung war, ob eine IV-Infektion die alveoläre Protein-Clearance beeinträchtigt.

Die Infektion mit dem saisonalen, mausadaptierten IV A/Puerto Rico/8/1934 H1N1-Stamm verursachte ein deutliches Herunterregulieren der Albuminaufnahme in MLE-12-Zellen und in alveolären Epithelzellen (AEC) aus PCLS, wie mittels Durchflusszytometrie und konfokaler Mikroskopie festgestellt wurde. Dies ging mit einer verringerten Plasmamembranabundanz, Gesamtproteinspiegeln und mRNA-Expression von Megalin einher. Frühere Arbeiten unserer Gruppe zeigten, dass das Herunterregulieren von Megalin durch die Bindung von TGF-β1 an seinen Rezeptor ausgelöst werden kann, was zur Dephosphorylierung und Aktivierung der Glykogensynthase-Kinase 3β (GSK3β) führt. Die Aktivität dieser Kinase phosphoryliert die zytoplasmatische Domäne von Megalin, ein Signal, das den Rezeptor internalisiert und die Proteinaufnahme beeinträchtigt. Entgegen unseren Erwartungen fanden wir in unseren in vitro-Modellen keine Anzeichen für eine Aktivierung der TGF-β1/GSK3β/Megalin-Achse.

Um die Auswirkungen der IV-Infektion auf endozytische Signalwege weiter zu untersuchen, infizierten wir Mäuse mit IV in vivo und unterzogen isolierte AEC und Zellen aus bronchoalveolärer Lavage (BAL) einer Massen-RNA-Sequenzierung. Auffällig war das Herrunterregulieren von Megalin und anderen mit der Endozytose verbundenen Rezeptoren wie dem Scavenger-Rezeptor *CD36* und *Lrp6* in AEC. Darüber hinaus beobachteten wir, dass Downstream-Targets von TGF-β1, wie *Itgb6* und *Tgfbi*, in AEC nach IV-Infektion deutlich hochreguliert wurden, was auf das Vorhandensein der aktiven Form des Zytokins hindeutet. Dies ist für uns von

Bedeutung, da unsere Gruppe zuvor gezeigt hatte, dass die Aktivierung von TGF-β1 ausreicht, um die Zelloberflächenhäufigkeit von Megalin zu reduzieren. Wir identifizierten auch ein signifikantes Hochregulieren von *MMP-14* in BAL-Zellen. Darüber hinaus erreichte die spezifische Hemmung dieser Protease teilweise die Werte des gesamten Megalins und der Albuminaufnahme, was darauf hindeutet, dass die zuvor beschriebenen MMP-getriebenen Shedding-Mechanismen möglicherweise am Herunterregulieren von Megalin und damit an der Clearance von überschüssigem Alveolarprotein beteiligt sind. Maßgeblich ist, dass es das therapeutische Potenzial einer rechtzeitigen MMP-Inhibition bei der Behandlung des IV-induzierten ARDS hervorhebt.

Da niedrigere alveoläre Ödemproteinkonzentrationen mit besseren Ergebnissen bei ARDS verknüpft sind, stellt die Identifizierung von zielgerichteten Mechanismen der beeinträchtigten alveolären Protein-Clearance nach IV-Infektion Hoffnung auf Therapiemöglichkeiten dar.

References

Agassandian, Marianna, and Rama K. Mallampalli. 2013. “Surfactant Phospholipid Metabolism.” *Biochimica et Biophysica Acta - Molecular and Cell Biology of Lipids* 1831 (3): 612–25. https://doi.org/10.1016/j.bbalip.2012.09.010.

Albertine, Kurt H. 2016. “Anatomy of the Lungs.” In *Murray and Nadel’s Textbook of Respiratory Medicine*, edited by V Courtney Broaddus, Robert J Mason, Joel D Ernst, Talmadge E King, Stephen C Lazarus, John F Murray, Jay A Nadel, Arthur S Slutsky, and Michael B B T - Murray and Nadel’s Textbook of Respiratory Medicine (Sixth Edition) Gotway, 3-21.e5. Philadelphia: Elsevier. https://doi.org/10.1016/B978-1-4557-3383-5.00001-4.

Ammar, Hayet, and Jean L. Closset. 2008. “Clusterin Activates Survival through the Phosphatidylinositol 3-Kinase/Akt Pathway.” *Journal of Biological Chemistry*. https://doi.org/10.1074/jbc.M800403200.

Anderson, Clark L., Chaity Chaudhury, Jonghan Kim, C. L. Bronson, Manzoor A. Wani, and Sudhasri Mohanty. 2006. “Perspective - FcRn Transports Albumin: Relevance to Immunology and Medicine.” *Trends in Immunology*. https://doi.org/10.1016/j.it.2006.05.004.

Apweiler, Rolf, Alex Bateman, Maria Jesus Martin, Claire O’Donovan, Michele Magrane, Yasmin Alam-Faruque, Emanuele Alpi, et al. 2014. “Activities at the Universal Protein Resource (UniProt).” *Nucleic Acids Research* 42 (D1): D191–98. https://doi.org/10.1093/nar/gkt1140.

Arnout, J., M. F. Hoylaerts, and H. R. Lijnen. 2006. “Haemostasis.” In *The Vascular Endothelium II*, edited by S. Moncada and A Higgs, 1–41. Springer Berlin Heidelberg. https://doi.org/10.1007/3-540-36028-X_1.

Ashbaugh, DavidG., D. Boyd Bigelow, ThomasL. Petty, and BernardE. Levine. 1967. “Acute Respiratory Distress in Adults.” *The Lancet* 290 (7511): 319–23. https://doi.org/10.1016/S0140-6736(67)90168-7.

Asten, Liselotte Van, Angie Luna Pinzon, Dylan W. De Lange, Evert De Jonge, Frederika Dijkstra, Sierk Marbus, Gé A. Donker, Wim Van Der Hoek, and Nicolette F. De Keizer. 2018. “Estimating Severity of Influenza Epidemics from Severe Acute Respiratory Infections (SARI) in Intensive Care Units.” *Critical Care*. https://doi.org/10.1186/s13054-018-2274-8.

Bachofen, Marianne, and Ewald R. Weibel. 1977. “Alterations of the Gas Exchange Apparatus in Adult Respiratory Insufficiency Associated with Septicemia 1, 2.” *American Review of Respiratory Disease* 116 (4): 589–615. https://doi.org/10.1164/arrd.1977.116.4.589.

Barkauskas, Christina E., Michael J. Cronce, Craig R. Rackley, Emily J. Bowie, Douglas R. Keene, Barry R. Stripp, Scott H. Randell, Paul W. Noble, and Brigid L.M. Hogan. 2013. “Type 2 Alveolar Cells Are Stem Cells in Adult Lung.” *Journal of Clinical Investigation*. https://doi.org/10.1172/JCI68782.

Bazzoni, Gianfranco, and Elisabetta Dejana. 2004. “Endothelial Cell-to-Cell Junctions: Molecular Organization and Role in Vascular Homeostasis.” *Physiological Reviews* 84 (3): 869–901.

https://doi.org/10.1152/physrev.00035.2003.

Beers, Michael F., and Yuben Moodley. 2017. “When Is an Alveolar Type 2 Cell an Alveolar Type 2 Cell?: A Conundrum for Lung Stem Cell Biology and Regenerative Medicine.” *American Journal of Respiratory Cell and Molecular Biology*. https://doi.org/10.1165/rcmb.2016-0426PS.

Bellani, Giacomo, John G. Laffey, Tài Pham, Eddy Fan, Laurent Brochard, Andres Esteban, Luciano Gattinoni, et al. 2016. “Epidemiology, Patterns of Care, and Mortality for Patients with Acute Respiratory Distress Syndrome in Intensive Care Units in 50 Countries.” *JAMA - Journal of the American Medical Association* 315 (8): 788–800. https://doi.org/10.1001/jama.2016.0291.

Bellinghausen, Carla, Gernot G.U. Rohde, Paul H.M. Savelkoul, Emiel F.M. Wouters, and Frank R.M. Stassen. 2016. “Viral-Bacterial Interactions in the Respiratory Tract.” *Journal of General Virology*. https://doi.org/10.1099/jgv.0.000627.

Bern, Malin, Kine Marita Knudsen Sand, Jeannette Nilsen, Inger Sandlie, and Jan Terje Andersen. 2015. “The Role of Albumin Receptors in Regulation of Albumin Homeostasis: Implications for Drug Delivery.” *Journal of Controlled Release* 211 (August): 144–62. https://doi.org/10.1016/j.jconrel.2015.06.006.

Bernard, G. R., A. Artigas, K. L. Brigham, J. Carlet, K. Falke, L. Hudson, M. Lamy, et al. 1994. “The American-European Consensus Conference on ARDS: Definitions, Mechanisms, Relevant Outcomes, and Clinical Trial Coordination.” In *American Journal of Respiratory and Critical Care Medicine*. https://doi.org/10.1164/ajrccm.149.3.7509706.

Berthiaume, Y., K. H. Albertine, M. Grady, G. Fick, and M. A. Matthay. 1989. “Protein Clearance from the Air Spaces and Lungs of Unanesthetized Sheep over 144 H.” *Journal of Applied Physiology*. https://doi.org/10.1152/jappl.1989.67.5.1887.

Biemesderfer, D. 2006. “Regulated Intramembrane Proteolysis of Megalin: Linking Urinary Protein and Gene Regulation in Proximal Tubule?” *Kidney International* 69 (10): 1717–21. https://doi.org/10.1038/sj.ki.5000298.

Blümel, Johannes, Reinhard Burger, Christian Drosten, Albrecht Gröner, Lutz Gürtler, Margarethe Heiden, Martin Hildebrandt, et al. 2009. “Influenza Virus.” *Transfusion Medicine and Hemotherapy* 36 (1): 32–39. https://doi.org/10.1159/000197314.

Bosch, Astrid A.T.M., Giske Biesbroek, Krzysztof Trzcinski, Elisabeth A.M. Sanders, and Debby Bogaert. 2013. “Viral and Bacterial Interactions in the Upper Respiratory Tract.” *PLoS Pathogens*. https://doi.org/10.1371/journal.ppat.1003057.

Bradley-Stewart, A., L. Jolly, W. Adamson, R. Gunson, C. Frew-Gillespie, K. Templeton, C. Aitken, W. Carman, S. Cameron, and C. McSharry. 2013. “Cytokine Responses in Patients with Mild or Severe Influenza A(H1N1)Pdm09.” *Journal of Clinical Virology* 58 (1): 100–107. https://doi.org/10.1016/j.jcv.2013.05.011.

Buchäckert, Yasmin, Sebastian Rummel, Christine U. Vohwinkel, Nieves M. Gabrielli, Benno A. Grzesik, Konstantin Mayer, Susanne Herold, Rory E. Morty, Werner Seeger, and István Vadász. 2012. “Megalin Mediates Transepithelial Albumin

Clearance from the Alveolar Space of Intact Rabbit Lungs." *The Journal of Physiology* 590 (20): 5167–81. https://doi.org/10.1113/jphysiol.2012.233403.

Budinger, G. R.Scott, Navdeep S. Chandel, Helen K. Donnelly, James Eisenbart, Monica Oberoi, and Manu Jain. 2005. "Active Transforming Growth Factor-B1 Activates the Procollagen I Promoter in Patients with Acute Lung Injury." *Intensive Care Medicine*. https://doi.org/10.1007/s00134-004-2503-2.

Busse, R., and I. Fleming. 2006. "Vascular Endothelium and Blood Flow." In *The Vascular Endothelium II*, 43–78. Springer Berlin Heidelberg. https://doi.org/10.1007/3-540-36028-X_2.

Cai, Shi Xia, Ai Ran Liu, Song Chen, Hong Li He, Qi Hong Chen, Jing Yuan Xu, Chun Pan, et al. 2015. "Activation of Wnt/β-Catenin Signalling Promotes Mesenchymal Stem Cells to Repair Injured Alveolar Epithelium Induced by Lipopolysaccharide in Mice." *Stem Cell Research and Therapy*. https://doi.org/10.1186/s13287-015-0060-y.

Caley, Matthew P., Vera L.C. Martins, and Edel A. O'Toole. 2015. "Metalloproteinases and Wound Healing." *Advances in Wound Care* 4 (4): 225–34. https://doi.org/10.1089/wound.2014.0581.

Cao, Hong, Jing Chen, Muyiwa Awoniyi, John R. Henley, and Mark A. McNiven. 2007. "Dynamin 2 Mediates Fluid-Phase Micropinocytosis in Epithelial Cells." *Journal of Cell Science*. https://doi.org/10.1242/jcs.010686.

Carlson, Christina M., Elizabeth A. Turpin, Lindsey A. Moser, Kevin B. O'Brien, Troy D. Cline, Jeremy C. Jones, Terrence M. Tumpey, et al. 2010. "Transforming Growth Factor-β: Activation by Neuraminidase and Role in Highly Pathogenic H5N1 Influenza Pathogenesis." *PLoS Pathogens*. https://doi.org/10.1371/journal.ppat.1001136.

Caruso-Neves, C., Ana Acacia S. Pinheiro, Hui Cai, Jackson Souza-Menezes, and William B. Guggino. 2006. "PKB and Megalin Determine the Survival or Death of Renal Proximal Tubule Cells." *Proceedings of the National Academy of Sciences* 103 (49): 18810–15. https://doi.org/10.1073/pnas.0605029103.

Cheng, Jun Jun, Jian Rui Li, Meng Hao Huang, Lin Lin Ma, Zhou Yi Wu, Chen Chen Jiang, Wen Jing Li, et al. 2016. "CD36 Is a Co-Receptor for Hepatitis C Virus E1 Protein Attachment." *Scientific Reports*. https://doi.org/10.1038/srep21808.

Christ, Annabel, Maike Marczenke, and Thomas E. Willnow. 2020. "LRP2 Controls Sonic Hedgehog-Dependent Differentiation of Cardiac Progenitor Cells during Outflow Tract Formation." *Human Molecular Genetics* 29 (19): 3183–96. https://doi.org/10.1093/hmg/ddaa200.

Christensen, Erik I., Henrik Birn, Tina Storm, Kathrin Weyer, and Rikke Nielsen. 2012. "Endocytic Receptors in the Renal Proximal Tubule." *Physiology* 27 (4): 223–36. https://doi.org/10.1152/physiol.00022.2012.

Clark, J. G., J. A. Milberg, K. P. Steinberg, and L. D. Hudson. 1995. "Type III Procollagen Peptide in the Adult Respiratory Distress Syndrome. Association of Increased Peptide Levels in Bronchoalveolar Lavage Fluid with Increased Risk for Death." *Annals of Internal Medicine*. https://doi.org/10.7326/0003-4819-122-1-199501010-00003.

Cochi, Shea E., Jordan A. Kempker, Srinadh Annangi, Michael R. Kramer, and Greg S. Martin. 2016. “Mortality Trends of Acute Respiratory Distress Syndrome in the United States from 1999 to 2013.” *Annals of the American Thoracic Society* 13 (10): 1742–51. https://doi.org/10.1513/AnnalsATS.201512-841OC.

Corbel, M., E. Boichot, and V. Lagente. 2000. “Role of Gelatinases MMP-2 and MMP-9 in Tissue Remodeling Following Acute Lung Injury.” *Brazilian Journal of Medical and Biological Research* 33 (7): 749–54. https://doi.org/10.1590/S0100-879X2000000700004.

Craig, Vanessa J., Li Zhang, James S. Hagood, and Caroline A. Owen. 2015. “Matrix Metalloproteinases as Therapeutic Targets for Idiopathic Pulmonary Fibrosis.” *American Journal of Respiratory Cell and Molecular Biology*. https://doi.org/10.1165/rcmb.2015-0020TR.

Crapo, J. D., B. E. Barry, P. Gehr, M. Bachofen, and E. R. Weibel. 1982. “Cell Number and Cell Characteristics of the Normal Human Lung.” *American Review of Respiratory Disease*. https://doi.org/10.1164/arrd.1982.126.2.332.

Cubillos-Rojas, Monica, Fabiola Amair-Pinedo, Irantzu Tato, Ramon Bartrons, Francesc Ventura, and Jose Luis Rosa. 2010. “Simultaneous Electrophoretic Analysis of Proteins of Very High and Low Molecular Mass Using Tris-Acetate Polyacrylamide Gels.” *Electrophoresis* 31 (8): 1318–21. https://doi.org/10.1002/elps.200900657.

Cui, Ning, Min Hu, and Raouf A. Khalil. 2017. “Biochemical and Biological Attributes of Matrix Metalloproteinases.” In *Progress in Molecular Biology and Translational Science*. https://doi.org/10.1016/bs.pmbts.2017.02.005.

Dahlin, Katherine, Edward M. Mager, Lennell Allen, Zachary Tigue, Lee Goodglick, Madhuri Wadehra, and Leland Dobbs. 2004. “Identification of Genes Differentially Expressed in Rat Alveolar Type I Cells.” *American Journal of Respiratory Cell and Molecular Biology*. https://doi.org/10.1165/rcmb.2003-0423OC.

Davey, A., D. F. McAuley, and C. M. O’Kane. 2011. “Matrix Metalloproteinases in Acute Lung Injury: Mediators of Injury and Drivers of Repair.” *European Respiratory Journal* 38 (4): 959–70. https://doi.org/10.1183/09031936.00032111.

Demling, Nina, Carsten Ehrhardt, Michael Kasper, Michael Laue, Lilla Knels, and Ernst Peter Rieber. 2006. “Promotion of Cell Adherence and Spreading: A Novel Function of RAGE, the Highly Selective Differentiation Marker of Human Alveolar Epithelial Type I Cells.” *Cell and Tissue Research* 323 (3): 475–88. https://doi.org/10.1007/s00441-005-0069-0.

Dhainaut, Jean François, Julien Charpentier, and Jean Daniel Chiche. 2003. “Transforming Growth Factor-β: A Mediator of Cell Regulation in Acute Respiratory Distress Syndrome.” In *Critical Care Medicine*. https://doi.org/10.1097/01.ccm.0000057901.92381.75.

Diem, Kathrin, Michael Fauler, Giorgio Fois, Andreas Hellmann, Natalie Winokurow, Stefan Schumacher, Christine Kranz, and Manfred Frick. 2020. “Mechanical Stretch Activates Piezo1 in Caveolae of Alveolar Type I Cells to Trigger ATP Release and Paracrine Stimulation of Surfactant Secretion from Alveolar Type II Cells.” *The FASEB Journal* 34 (9): 12785–804.

https://doi.org/10.1096/fj.202000613RRR.

Dobbs, L. G. 1990. “Isolation and Culture of Alveolar Type II Cells.” *American Journal of Physiology - Lung Cellular and Molecular Physiology*. https://doi.org/10.1152/ajplung.1990.258.4.l134.

Dobbs, Leland G., Robert Gonzalez, Michael A. Matthay, Ethan P. Carter, Lennell Allen, and A. S. Verkman. 1998. “Highly Water-Permeable Type I Alveolar Epithelial Cells Confer High Water Permeability between the Airspace and Vasculature in Rat Lung.” *Proceedings of the National Academy of Sciences of the United States of America*. https://doi.org/10.1073/pnas.95.6.2991.

Dubois, Julia, Olivier Terrier, and Manuel Rosa-Calatrava. 2014. “Influenza Viruses and MRNA Splicing: Doing More with Less.” *MBio* 5 (3): 1–13. https://doi.org/10.1128/mBio.00070-14.

Dutta, Dipannita, and Julie G. Donaldson. 2012. “Search for Inhibitors of Endocytosis.” *Cellular Logistics*. https://doi.org/10.4161/cl.23967.

Emonard, Hervé, and Etienne Marbaix. 2015. “Low-Density Lipoprotein Receptor-Related Protein in Metalloproteinase-Mediated Pathologies: Recent Insights.” *Metalloproteinases In Medicine* 2 (February): 9–18. https://doi.org/10.2147/MNM.S63616.

Evans, M. J., L. J. Cabral, R. J. Stephens, and G. Freeman. 1973. “Renewal of Alveolar Epithelium in the Rat Following Exposure to NO2.” *American Journal of Pathology*.

Evans, T. W. 2002. “Review Article: Albumin as a Drug - Biological Effects of Albumin Unrelated to Oncotic Pressure.” *Alimentary Pharmacology and Therapeutics, Supplement* 16 (5): 6–11. https://doi.org/10.1046/j.1365-2036.16.s5.2.x.

Fahy, Ruairi J., Frank Lichtenberger, Christine B. McKeegan, Gerard J. Nuovo, Clay B. Marsh, and Mark D. Wewers. 2003. “The Acute Respiratory Distress Syndrome: A Role for Transforming Growth Factor-B1.” *American Journal of Respiratory Cell and Molecular Biology* 28 (4): 499–503. https://doi.org/10.1165/rcmb.2002-0092OC.

Finkelstein, J. N., and D. L. Shapiro. 1982. “Isolation of Type II Alveolar Epithelial Cells Using Low Protease Concentrations.” *Lung*. https://doi.org/10.1007/BF02719276.

Folkesson, Hans G, Michael A Matthay, B. R. Westrom, Kwang J Kim, Biirje W Karlsson, and Randolph H Hastings. 1996. “Alveolar Epithelial Clearance of Protein.” *Journal of Applied Physiology* 80 (5): 1431–45. https://doi.org/10.1152/jappl.1996.80.5.1431.

García-Pérez, Blanca Estela, Juan Carlos Hernández-González, Samuel García-Nieto, and Julieta Luna-Herrera. 2008. “Internalization of a Non-Pathogenic Mycobacteria by Macropinocytosis in Human Alveolar Epithelial A549 Cells.” *Microbial Pathogenesis*. https://doi.org/10.1016/j.micpath.2008.01.009.

García-Sastre, Adolfo. 2010. “Influenza Virus Receptor Specificity.” *The American Journal of Pathology* 176 (4): 1584–85. https://doi.org/10.2353/ajpath.2010.100066.

Gekle, Michael, Ruth Freudinger, and Sigrid Mildenberger. 2001. “Inhibition of Na+-H+ Exchanger-3 Interferes with Apical Receptor-Mediated Endocytosis via Vesicle Fusion.” *Journal of Physiology*. https://doi.org/10.1111/j.1469-7793.2001.0619h.x.

Gil, J., D. A. Silage, and J. M. McNiff. 1981. “Distribution of Vesicles in Cells of Air-Blood Barrier in the Rabbit.” *Journal of Applied Physiology Respiratory Environmental and Exercise Physiology*. https://doi.org/10.1152/jappl.1981.50.2.334.

Goerke, Jon. 1998. “Pulmonary Surfactant: Functions and Molecular Composition.” *Biochimica et Biophysica Acta - Molecular Basis of Disease*. https://doi.org/10.1016/S0925-4439(98)00060-X.

Goodale, RL, B. Goetzman, and MB Visscher. 1970. “Hypoxia and Iodoacetic Acid and Alveolocapillary Barrier Permeability to Albumin.” *American Journal of Physiology-Legacy Content* 219 (5): 1226–30. https://doi.org/10.1152/ajplegacy.1970.219.5.1226.

Gorin, A. B., and P. A. Stewart. 1979. “Differential Permeability of Endothelial and Epithelial Barriers to Albumin Flux.” *Journal of Applied Physiology* 47 (6): 1315–24. https://doi.org/10.1152/jappl.1979.47.6.1315.

Gotts, Jeffrey E., Jason Abbott, and Michael A. Matthay. 2014. “Influenza Causes Prolonged Disruption of the Alveolar-Capillary Barrier in Mice Unresponsive to Mesenchymal Stem Cell Therapy.” *American Journal of Physiology-Lung Cellular and Molecular Physiology* 307 (5): L395–406. https://doi.org/10.1152/ajplung.00110.2014.

Gratama, Jan W., Jean-Luc D’hautcourt, Frank Mandy, Gregor Rothe, David Barnett, George Janossy, Stefano Papa, Gerd Schmitz, Rodica Lenkei, and The European Working Group on Clini. 1998. “Flow Cytometric Quantitation of Immunofluorescence Intensity: Problems and Perspectives.” *Cytometry* 33 (2): 166–78. https://doi.org/10.1002/(SICI)1097-0320(19981001)33:2<166::AID-CYTO11>3.0.CO;2-S.

Grzesik, Benno A., Christine U. Vohwinke, Rory E. Morty, Konstantin Mayer, Susanne Herold, Werner Seeger, and István Vadász. 2013. “Efficient Gene Delivery to Primary Alveolar Epithelial Cells by Nucleofection.” *American Journal of Physiology - Lung Cellular and Molecular Physiology* 305 (11): L786–94. https://doi.org/10.1152/ajplung.00191.2013.

Gwoździńska, Paulina, Benno A. Buchbinder, Konstantin Mayer, Susanne Herold, Rory E. Morty, Werner Seeger, and István Vadász. 2017. “Hypercapnia Impairs ENaC Cell Surface Stability by Promoting Phosphorylation, Polyubiquitination and Endocytosis of β-ENaC in a Human Alveolar Epithelial Cell Line.” *Frontiers in Immunology* 8 (MAY). https://doi.org/10.3389/fimmu.2017.00591.

Haies, D. M., J. Gil, and E. R. Weibel. 1981. “Morphometric Study of Rat Lung Cells. I. Numerical and Dimensional Characteristics of Parenchymal Cell Population.” *American Review of Respiratory Disease*. https://doi.org/10.1164/arrd.1981.123.5.533.

Hallman, M., B. L. Epstein, and L. Gluck. 1981. “Analysis of Labeling and Clearance of Lung Surfactant Phospholipids in Rabbit. Evidence of Bidirectional Surfactant

Flux between Lamellar Bodies and Alveolar Lavage." *Journal of Clinical Investigation*. https://doi.org/10.1172/JCI110310.

Hastings, R. H., H. G. Folkesson, V. Petersen, R. Ciriales, and M. A. Matthay. 1995. "Cellular Uptake of Albumin from Lungs of Anesthetized Rabbits." *American Journal of Physiology-Lung Cellular and Molecular Physiology* 269 (4): L453–62. https://doi.org/10.1152/ajplung.1995.269.4.L453.

Hastings, R. H., J. R. Wright, K. H. Albertine, R. Ciriales, and M. A. Matthay. 1994. "Effect of Endocytosis Inhibitors on Alveolar Clearance of Albumin, Immunoglobulin G, and SP-A in Rabbits." *American Journal of Physiology - Lung Cellular and Molecular Physiology*. https://doi.org/10.1152/ajplung.1994.266.5.l544.

Hastings, Randolph H, Hans G Folkesson, and Michael a Matthay. 2004. "Mechanisms of Alveolar Protein Clearance in the Intact Lung." *American Journal of Physiology-Lung Cellular and Molecular Physiology* 286 (4): L679–89. https://doi.org/10.1152/ajplung.00205.2003.

Hendrickson, Carolyn M., Jason Abbott, Hanjing Zhuo, Kathleen D. Liu, Carolyn S. Calfee, and Michael A. Matthay. 2017. "Higher Mini-BAL Total Protein Concentration in Early ARDS Predicts Faster Resolution of Lung Injury Measured by More Ventilator-Free Days." *American Journal of Physiology-Lung Cellular and Molecular Physiology* 312 (5): L579–85. https://doi.org/10.1152/ajplung.00381.2016.

Hernandez-Barrantes, Sonia, Margarida Bernardo, Marta Toth, and Rafael Fridman. 2002. "Regulation of Membrane Type-Matrix Metalloproteinases." *Seminars in Cancer Biology* 12 (2): 131–38. https://doi.org/10.1006/scbi.2001.0421.

Hernandez-Barrantes, Sonia, Marta Toth, M M Bernardo, Maria Yurkova, David C. Gervasi, Yuval Raz, QingXiang Amy Sang, and Rafael Fridman. 2000. "Binding of Active (57 KDa) Membrane Type 1-Matrix Metalloproteinase (MT1-MMP) to Tissue Inhibitor of Metalloproteinase (TIMP)-2 Regulates MT1-MMP Processing and pro-MMP-2 Activation." *The Journal of Biological Chemistry* 275 (16): 12080–89. https://doi.org/10.1074/jbc.275.16.12080.

Herold, Susanne, Christin Becker, Karen M. Ridge, and G. R.Scott Budinger. 2015. "Influenza Virus-Induced Lung Injury: Pathogenesis and Implications for Treatment." *European Respiratory Journal* 45 (5): 1463–78. https://doi.org/10.1183/09031936.00186214.

Hoffman, Olivia, Nana Burns, István Vadász, Holger K. Eltzschig, Michael G. Edwards, and Christine U. Vohwinkel. 2017. "Detrimental ELAVL-1/HuR-Dependent GSK3β MRNA Stabilization Impairs Resolution in Acute Respiratory Distress Syndrome." *PLoS ONE* 12 (2): 1–15. https://doi.org/10.1371/journal.pone.0172116.

Högner, Katrin, Thorsten Wolff, Stephan Pleschka, Stephanie Plog, Achim D. Gruber, Ulrich Kalinke, Hans Dieter Walmrath, et al. 2013. "Macrophage-Expressed IFN-β Contributes to Apoptotic Alveolar Epithelial Cell Injury in Severe Influenza Virus Pneumonia." *PLoS Pathogens* 9 (2). https://doi.org/10.1371/journal.ppat.1003188.

Hollenhorst, Monika I., Katrin Richter, and Martin Fronius. 2011. "Ion Transport by

Pulmonary Epithelia." *Journal of Biomedicine and Biotechnology* 2011: 1–16. https://doi.org/10.1155/2011/174306.

Hosojima, Michihiro, Hiroyoshi Sato, Keiko Yamamoto, Ryohei Kaseda, Taeko Soma, Asako Kobayashi, Akiyo Suzuki, et al. 2009. "Regulation of Megalin Expression in Cultured Proximal Tubule Cells by Angiotensin II Type 1A Receptor- And Insulin-Mediated Signaling Cross Talk." *Endocrinology*. https://doi.org/10.1210/en.2008-0886.

Huebers, H. A., and C. A. Finch. 1987. "The Physiology of Transferrin and Transferrin Receptors." *Physiological Reviews* 67 (2): 520–82. https://doi.org/10.1152/physrev.1987.67.2.520.

Ikehata, Mika, Ryoko Yumoto, Kosuke Nakamura, Junya Nagai, and Mikihisa Takano. 2008. "Comparison of Albumin Uptake in Rat Alveolar Type II and Type I-like Epithelial Cells in Primary Culture." *Pharmaceutical Research* 25 (4): 913–22. https://doi.org/10.1007/s11095-007-9426-x.

Itoh, Yoshifumi, Akiko Takamura, Noriko Ito, Yoshiro Maru, Hiroshi Sato, Naoko Suenaga, Takanori Aoki, and Motoharu Seiki. 2001. "Homophilic Complex Formation of MT1-MMP Facilitates ProMMP-2 Activation on the Cell Surface and Promotes Tumor Cell Invasion." *EMBO Journal*. https://doi.org/10.1093/emboj/20.17.4782.

Ivanov, Andrei I., Asma Nusrat, and Charles A. Parkos. 2004. "Endocytosis of Epithelial Apical Junctional Proteins by a Clathrin-Mediated Pathway into a Unique Storage Compartment." *Molecular Biology of the Cell*. https://doi.org/10.1091/mbc.E03-05-0319.

Jain, Rajan, Christina E. Barkauskas, Norifumi Takeda, Emily J. Bowie, Haig Aghajanian, Qiaohong Wang, Arun Padmanabhan, et al. 2015. "Plasticity of Hopx+ Type I Alveolar Cells to Regenerate Type II Cells in the Lung." *Nature Communications*. https://doi.org/10.1038/ncomms7727.

Jansing, Nicole L., Jazalle McClendon, Peter M. Henson, Rubin M. Tuder, Dallas M. Hyde, and Rachel L. Zemans. 2017. "Unbiased Quantitation of Alveolar Type II to Alveolar Type I Cell Transdifferentiation during Repair after Lung Injury in Mice." *American Journal of Respiratory Cell and Molecular Biology* 57 (5): 519–26. https://doi.org/10.1165/rcmb.2017-0037MA.

Jenkins, R. Gisli, Xiao Su, George Su, Christopher J. Scotton, Eric Camerer, Geoffrey J. Laurent, George E. Davis, Rachel C. Chambers, Michael A. Matthay, and Dean Sheppard. 2006. "Ligation of Protease-Activated Receptor 1 Enhances α Vβ6 Integrin-Dependent TGF-β Activation and Promotes Acute Lung Injury." *Journal of Clinical Investigation*. https://doi.org/10.1172/JCI27183.

Johanns, Manuel, Pascale Lemoine, Virginie Janssens, Giuseppina Grieco, Soren K. Moestrup, Rikke Nielsen, Erik I. Christensen, et al. 2017. "Cellular Uptake of ProMMP-2:TIMP-2 Complexes by the Endocytic Receptor Megalin/LRP-2." *Scientific Reports* 7 (1): 4328. https://doi.org/10.1038/s41598-017-04648-y.

John, Theresa A., Stephen M. Vogel, Richard D. Minshall, Karen Ridge, Chinnaswamy Tiruppathi, and Asrar B. Malik. 2001. "Evidence for the Role of Alveolar Epithelial Gp60 in Active Transalveolar Albumin Transport in the Rat Lung." *The Journal of Physiology* 533 (2): 547–59.

https://doi.org/10.1111/j.1469-7793.2001.0547a.x.

Kalil, Andre C., and Paul G. Thomas. 2019. “Influenza Virus-Related Critical Illness: Pathophysiology and Epidemiology.” *Critical Care* 23 (1): 258. https://doi.org/10.1186/s13054-019-2539-x.

Kalina, M., and R. Socher. 1990. “Internalization of Pulmonary Surfactant into Lamellar Bodies of Cultured Rat Pulmonary Type II Cells.” *Journal of Histochemistry and Cytochemistry*. https://doi.org/10.1177/38.4.2156921.

Karhadkar, Tejas R., Thomas D. Meek, and Richard H. Gomer. 2021. “Inhibiting Sialidase-Induced TGF- β 1 Activation Attenuates Pulmonary Fibrosis in Mice.” *Journal of Pharmacology and Experimental Therapeutics* 376 (1): 106–17. https://doi.org/10.1124/jpet.120.000258.

Kasper, M., T. Reimann, U. Hempel, K. W. Wenzel, A. Bierhaus, D. Schuh, V. Dimmer, G. Haroske, and M. Müller. 1997. “Loss of Caveolin Expression in Type I Pneumocytes as an Indicator of Subcellular Alterations during Lung Fibrogenesis.” *Histochemistry and Cell Biology*. https://doi.org/10.1007/s004180050200.

Kawami, Masashi, Tadashi Shimonakamura, Ryoko Yumoto, and Mikihisa Takano. 2018. “Transport of AOPP-Albumin into Human Alveolar Epithelial A549 Cell.” *Journal of Pharmacy & Pharmaceutical Sciences* 21 (1): 247–55. https://doi.org/10.18433/jpps29905.

Kerjaschki, D., and M. G. Farquhar. 1982. “The Pathogenic Antigen of Heymann Nephritis Is a Membrane Glycoprotein of the Renal Proximal Tubule Brush Border.” *Proceedings of the National Academy of Sciences of the United States of America*. https://doi.org/10.1073/pnas.79.18.5557.

Kim, Kwang Jin, and Asrar B. Malik. 2003. “Protein Transport across the Lung Epithelial Barrier.” *American Journal of Physiology - Lung Cellular and Molecular Physiology* 284 (2 28-2). https://doi.org/10.1152/ajplung.00235.2002.

Kinnard, W. V., R. Tuder, P. Papst, and J. H. Fisher. 1994. “Regulation of Alveolar Type II Cell Differentiation and Proliferation in Adult Rat Lung Explants.” *American Journal of Respiratory Cell and Molecular Biology* 11 (4): 416–25. https://doi.org/10.1165/ajrcmb.11.4.7917310.

Koivusalo, Mirkka, Christopher Welch, Hisayoshi Hayashi, Cameron C. Scott, Moshe Kim, Todd Alexander, Nicolas Touret, Klaus M. Hahn, and Sergio Grinstein. 2010. “Amiloride Inhibits Macropinocytosis by Lowering Submembranous PH and Preventing Rac1 and Cdc42 Signaling.” *Journal of Cell Biology* 188 (4): 547–63. https://doi.org/10.1083/jcb.200908086.

Kühnle, Nathalie, Verena Dederer, and Marius K. Lemberg. 2019. “Intramembrane Proteolysis at a Glance: From Signalling to Protein Degradation.” *Journal of Cell Science* 132 (16): jcs217745. https://doi.org/10.1242/jcs.217745.

Kumari, Sudha, Swetha Mg, and Satyajit Mayor. 2010. “Endocytosis Unplugged: Multiple Ways to Enter the Cell.” *Cell Research*. https://doi.org/10.1038/cr.2010.19.

Kunugi, Shinobu, Yuh Fukuda, Masamichi Ishizaki, and Nobuaki Yamanaka. 2001. “Role of MMP-2 in Alveolar Epithelial Cell Repair after Bleomycin Administration

in Rabbits.” *Laboratory Investigation*. https://doi.org/10.1038/labinvest.3780344.

Lal, Mark, and Michael Caplan. 2011. “Regulated Intramembrane Proteolysis: Signaling Pathways and Biological Functions.” *Physiology* 26 (1): 34–44. https://doi.org/10.1152/physiol.00028.2010.

Ley, K., and J. Reutershan. 2006. “Leucocyte-Endothelial Interactions in Health and Disease.” In *The Vascular Endothelium II. Handbook of Experimental Pharmacology*, 176:97–133. Springer Berlin Heidelberg. https://doi.org/10.1007/3-540-36028-X_4.

Li, H. F., and J. Y. Liu. 2019. “Effects of MiR-26a on Respiratory Distress Syndrome in Neonatal Rats via the Wnt/β-Catenin Signaling Pathway.” *European Review for Medical and Pharmacological Sciences*. https://doi.org/10.26355/eurrev_201903_17400.

Li, Lei, Tao Wan, Min Wan, Bei Liu, Ran Cheng, and Rongying Zhang. 2015. “The Effect of the Size of Fluorescent Dextran on Its Endocytic Pathway.” *Cell Biology International* 39 (5): 531–39. https://doi.org/10.1002/cbin.10424.

Li, Ming O., Yisong Y. Wan, Shomyseh Sanjabi, Anna-Karin L. Robertson, and Richard A. Flavell. 2006. “Transforming Growth Factor-Beta Regulation of Immune Responses.” *Annual Review of Immunology* 24 (1): 99–146. https://doi.org/10.1146/annurev.immunol.24.021605.090737.

Li, Yuanli, Rong Cong, and Daniel Biemesderfer. 2008. “The COOH Terminus of Megalin Regulates Gene Expression in Opossum Kidney Proximal Tubule Cells.” *American Journal of Physiology-Cell Physiology* 295 (2): C529–37. https://doi.org/10.1152/ajpcell.00037.2008.

Lian, Xuemei, Cong Yan, Yulin Qin, Lana Knox, Tingyu Li, and Hong Du. 2005. “Neutral Lipids and Peroxisome Proliterator-Activated Receptor-γ Control Pulmonary Gene Expression and Inflammation-Triggered Pathogenesis in Lysosomal Acid Lipase Knockout Mice.” *American Journal of Pathology*. https://doi.org/10.1016/S0002-9440(10)62053-6.

Liao, Yang, Gordon K. Smyth, and Wei Shi. 2014. “FeatureCounts: An Efficient General Purpose Program for Assigning Sequence Reads to Genomic Features.” *Bioinformatics* 30 (7): 923–30. https://doi.org/10.1093/bioinformatics/btt656.

Liu, W., W. R. Yu, T. Carling, C. Juhlin, J. Rastad, P. Ridefelt, G. Åkerström, and P. Hellman. 1998. “Regulation of Gp330/Megalin Expression by Vitamins A and D.” *European Journal of Clinical Investigation*. https://doi.org/10.1046/j.1365-2362.1998.00253.x.

Love, Michael I., Wolfgang Huber, and Simon Anders. 2014. “Moderated Estimation of Fold Change and Dispersion for RNA-Seq Data with DESeq2.” *Genome Biology* 15 (12): 550. https://doi.org/10.1186/s13059-014-0550-8.

Lozano, Rafael, Mohsen Naghavi, Kyle Foreman, Stephen Lim, Kenji Shibuya, Victor Aboyans, Jerry Abraham, et al. 2012. “Global and Regional Mortality from 235 Causes of Death for 20 Age Groups in 1990 and 2010: A Systematic Analysis for the Global Burden of Disease Study 2010.” *The Lancet*. https://doi.org/10.1016/S0140-6736(12)61728-0.

MacDonald, Bryan T., Keiko Tamai, and Xi He. 2009. “Wnt/β-Catenin Signaling: Components, Mechanisms, and Diseases.” *Developmental Cell*. https://doi.org/10.1016/j.devcel.2009.06.016.

Marzolo, María-paz, and Pamela Farfán. 2011. “New Insights into the Roles of Megalin/LRP2 and the Regulation of Its Functional Expression.” *Biological Research* 44 (1): 89–105. https://doi.org/10.4067/S0716-97602011000100012.

Massagué, Joan. 1992. “Receptors for the TGF-β Family.” *Cell* 69 (7): 1067–70. https://doi.org/10.1016/0092-8674(92)90627-O.

Mathers, Colin, Gretchen Stevens, Dan Hogan, Wahyu Retno Mahanani, and Jessica Ho. 2017. “Global and Regional Causes of Death: Patterns and Trends, 2000–15.” In *Disease Control Priorities, Third Edition (Volume 9): Improving Health and Reducing Poverty*. https://doi.org/10.1596/978-1-4648-0527-1_ch4.

Matthay, M. A., Y. Berthiaume, and N. C. Staub. 1985. “Long-Term Clearance of Liquid and Protein from the Lungs of Unanesthetized Sheep.” *Journal of Applied Physiology*. https://doi.org/10.1152/jappl.1985.59.3.928.

Matthay, M. A., C. C. Landolt, and N. C. Staub. 1982. “Differential Liquid and Protein Clearance from the Alveoli of Anesthetized Sheep.” *Journal of Applied Physiology Respiratory Environmental and Exercise Physiology*. https://doi.org/10.1152/jappl.1982.53.1.96.

Matthay, Michael A., Roy G. Brower, Shannon Carson, Ivor S. Douglas, Mark Eisner, Duncan Hite, Steven Holets, et al. 2011. “Randomized, Placebo-Controlled Clinical Trial of an Aerosolized β 2 -Agonist for Treatment of Acute Lung Injury.” *American Journal of Respiratory and Critical Care Medicine* 184 (5): 561–68. https://doi.org/10.1164/rccm.201012-2090OC.

Matthay, Michael A., Rachel L. Zemans, Guy A. Zimmerman, Yaseen M. Arabi, Jeremy R. Beitler, Alain Mercat, Margaret Herridge, Adrienne G. Randolph, and Carolyn S. Calfee. 2019. “Acute Respiratory Distress Syndrome.” *Nature Reviews Disease Primers* 5 (1): 18. https://doi.org/10.1038/s41572-019-0069-0.

Mazzocchi, Luciana C., Christine U. Vohwinkel, Konstantin Mayer, Susanne Herold, Rory E. Morty, Werner Seeger, and István Vadász. 2017. “TGF-β Inhibits Alveolar Protein Transport by Promoting Shedding, Regulated Intramembrane Proteolysis, and Transcriptional Downregulation of Megalin.” *American Journal of Physiology-Lung Cellular and Molecular Physiology* 313 (5): L807–24. https://doi.org/10.1152/ajplung.00569.2016.

Merlot, Angelica M., Danuta S. Kalinowski, and Des R. Richardson. 2014. “Unraveling the Mysteries of Serum Albumin-More than Just a Serum Protein.” *Frontiers in Physiology* 5 AUG (August): 1–7. https://doi.org/10.3389/fphys.2014.00299.

Millar, Fraser R., Charlotte Summers, Mark J. Griffiths, Mark R. Toshner, and Alastair G. Proudfoot. 2016. “The Pulmonary Endothelium in Acute Respiratory Distress Syndrome: Insights and Therapeutic Opportunities.” *Thorax* 71 (5): 462–73. https://doi.org/10.1136/thoraxjnl-2015-207461.

Morelle, Willy, Stuart M. Haslam, Martin Ziak, Jürgen Roth, Howard R. Morris, and Anne Dell. 2000. “Characterization of the N-Linked Oligosaccharides of Megalin

(Gp330) from Rat Kidney." *Glycobiology* 10 (3): 295–304. https://doi.org/10.1093/glycob/10.3.295.

Morikawa, Masato, Rik Derynck, and Kohei Miyazono. 2016. "TGF- β and the TGF-β Family: Context-Dependent Roles in Cell and Tissue Physiology." *Cold Spring Harbor Perspectives in Biology* 8 (5). https://doi.org/10.1101/cshperspect.a021873.

Morty, Rory E., Oliver Eickelberg, and Werner Seeger. 2007. "Alveolar Fluid Clearance in Acute Lung Injury: What Have We Learned from Animal Models and Clinical Studies?" *Intensive Care Medicine*. https://doi.org/10.1007/s00134-007-0662-7.

Moss, Marc, David T. Huang, Roy G. Brower, Niall D. Ferguson, Adit A. Ginde, M. N. Gong, Colin K. Grissom, et al. 2019. "Early Neuromuscular Blockade in the Acute Respiratory Distress Syndrome." *New England Journal of Medicine*. https://doi.org/10.1056/NEJMoa1901686.

Murphy, Gillian, and Hideaki Nagase. 2011. "Localizing Matrix Metalloproteinase Activities in the Pericellular Environment." *FEBS Journal* 278 (1): 2–15. https://doi.org/10.1111/j.1742-4658.2010.07918.x.

Newman, Geoff R., Lee Campbell, Chris von Ruhland, Bharat Jasani, and Mark Gumbleton. 1999. "Caveolin and Its Cellular and Subcellular Immunolocalisation in Lung Alveolar Epithelium: Implications for Alveolar Epithelial Type I Cell Function." *Cell and Tissue Research* 295 (1): 111–20. https://doi.org/10.1007/s004410051217.

Nguyen, Christopher, Shawn Kaku, Dominic Tutera, Ware G. Kuschner, and Juliana Barr. 2016. "Viral Respiratory Infections of Adults in the Intensive Care Unit." *Journal of Intensive Care Medicine* 31 (7): 427–41. https://doi.org/10.1177/0885066615585944.

Oh, Phil, Thierry Horner, Halina Witkiewicz, and Jan E. Schnitzer. 2012. "Endothelin Induces Rapid, Dynamin-Mediated Budding of Endothelial Caveolae Rich in ET-B." *Journal of Biological Chemistry*. https://doi.org/10.1074/jbc.M111.338897.

Page-McCaw, Andrea, Andrew J. Ewald, and Zena Werb. 2007. "Matrix Metalloproteinases and the Regulation of Tissue Remodelling." *Nature Reviews Molecular Cell Biology* 8 (3): 221–33. https://doi.org/10.1038/nrm2125.

Palmer, R. M. J., A. G. Ferrige, and S. Moncada. 1987. "Nitric Oxide Release Accounts for the Biological Activity of Endothelium-Derived Relaxing Factor." *Nature* 327 (6122): 524–26. https://doi.org/10.1038/327524a0.

Park, Cho Rong, Jung Hwan Jo, Myung Geun Song, Ji Yong Park, Young Hwa Kim, Hyewon Youn, Sun Ha Paek, et al. 2019. "Secreted Protein Acidic and Rich in Cysteine Mediates Active Targeting of Human Serum Albumin in U87MG Xenograft Mouse Models." *Theranostics*. https://doi.org/10.7150/thno.34883.

Park, Ryan J., Hongying Shen, L. Liu, Xinran Liu, Shawn M. Ferguson, and P. De Camilli. 2013. "Dynamin Triple Knockout Cells Reveal off Target Effects of Commonly Used Dynamin Inhibitors." *Journal of Cell Science* 126 (22): 5305–12. https://doi.org/10.1242/jcs.138578.

Patton, John S. 1996. "Mechanisms of Macromolecule Absorption by the Lungs."

Advanced Drug Delivery Reviews 19 (1): 3–36. https://doi.org/10.1016/0169-409X(95)00113-L.

Peck, Tyler J., and Kathryn A. Hibbert. 2019. “Recent Advances in the Understanding and Management of Ards [Version 1; Peer Review: 2 Approved].” *F1000Research*. https://doi.org/10.12688/f1000research.20411.1.

Peters, Dorothea M., I. Vadasz, L. Wujak, Małgorzata Wygrecka, Andrea Olschewski, Christin Becker, Susanne Herold, et al. 2014. “TGF- Directs Trafficking of the Epithelial Sodium Channel ENaC Which Has Implications for Ion and Fluid Transport in Acute Lung Injury.” *Proceedings of the National Academy of Sciences* 111 (3): E374–83. https://doi.org/10.1073/pnas.1306798111.

Pober, Jordan S., and Ramzi S. Cotran. 1990. “The Role of Endothelial Cells in Inflammation.” *Transplantation*. https://doi.org/10.1097/00007890-199010000-00001.

Pober, Jordan S., and William C. Sessa. 2007. “Evolving Functions of Endothelial Cells in Inflammation.” *Nature Reviews. Immunology* 7 (10): 803–15. https://doi.org/10.1038/nri2171.

Predescu, Sanda A., Dan N. Predescu, and Asrar B. Malik. 2007. “Molecular Determinants of Endothelial Transcytosis and Their Role in Endothelial Permeability.” *American Journal of Physiology-Lung Cellular and Molecular Physiology* 293 (4): L823–42. https://doi.org/10.1152/ajplung.00436.2006.

Preta, Giulio, James G. Cronin, and I. Martin Sheldon. 2015. “Dynasore - Not Just a Dynamin Inhibitor.” *Cell Communication and Signaling*. https://doi.org/10.1186/s12964-015-0102-1.

Qu, Peng, Hong Du, Xi Wang, and Cong Yan. 2009. “Matrix Metalloproteinase 12 Overexpression in Lung Epithelial Cells Plays a Key Role in Emphysema to Lung Bronchioalveolar Adenocarcinoma Transition.” *Cancer Research*. https://doi.org/10.1158/0008-5472.CAN-09-0577.

Quintero-Fabián, Saray, Rodrigo Arreola, Enrique Becerril-Villanueva, Julio César Torres-Romero, Victor Arana-Argáez, Julio Lara-Riegos, Mario Alberto Ramírez-Camacho, and María Elizbeth Alvarez-Sánchez. 2019. “Role of Matrix Metalloproteinases in Angiogenesis and Cancer.” *Frontiers in Oncology* 9 (December). https://doi.org/10.3389/fonc.2019.01370.

Raheel, Hira, Siavash Ghaffari, Negar Khosraviani, Victoria Mintsopoulos, Derek Auyeung, Changsen Wang, Yun Hye Kim, et al. 2019. “CD36 Mediates Albumin Transcytosis by Dermal but Not Lung Microvascular Endothelial Cells: Role in Fatty Acid Delivery.” *American Journal of Physiology-Lung Cellular and Molecular Physiology* 316 (5): L740–50. https://doi.org/10.1152/ajplung.00127.2018.

Ranieri, V. Marco, Gordon D. Rubenfeld, B. Taylor Thompson, Niall D. Ferguson, Ellen Caldwell, Eddy Fan, Luigi Camporota, and Arthur S. Slutsky. 2012. “Acute Respiratory Distress Syndrome.” *JAMA* 307 (23). https://doi.org/10.1001/jama.2012.5669.

Remacle, A. G., V. S. Golubkov, S. A. Shiryaev, R. Dahl, J. L. Stebbins, A. V. Chernov, A. V. Cheltsov, M. Pellecchia, and A. Y. Strongin. 2012. “Novel MT1-

MMP Small-Molecule Inhibitors Based on Insights into Hemopexin Domain Function in Tumor Growth." *Cancer Research* 72 (9): 2339–49. https://doi.org/10.1158/0008-5472.CAN-11-4149.

Riel, Debby Van, Vincent J. Munster, Emmie De Wit, Guus F. Rimmelzwaan, Ron A.M. Fouchier, Ab D.M.E. Osterhaus, and Thijs Kuiken. 2006. "H5N1 Virus Attachment to Lower Respiratory Tract." *Science* 312 (5772): 399. https://doi.org/10.1126/science.1125548.

Riel, Debby Van, Vincent J. Munster, Emmie De Wit, Guus F. Rimmelzwaan, Ron A.M. Fouchier, Albert D.M.E. Osterhaus, and Thijs Kuiken. 2007. "Human and Avian Influenza Viruses Target Different Cells in the Lower Respiratory Tract of Humans and Other Mammals." *American Journal of Pathology* 171 (4): 1215–23. https://doi.org/10.2353/ajpath.2007.070248.

Riviello, Elisabeth D., Willy Kiviri, Theogene Twagirumugabe, Ariel Mueller, Valerie M. Banner-Goodspeed, Laurent Officer, Victor Novack, Marguerite Mutumwinka, Daniel S. Talmor, and Robert A. Fowler. 2016. "Hospital Incidence and Outcomes of the Acute Respiratory Distress Syndrome Using the Kigali Modification of the Berlin Definition." *American Journal of Respiratory and Critical Care Medicine* 193 (1): 52–59. https://doi.org/10.1164/rccm.201503-0584OC.

Rogers, Gary N., and James C. Paulson. 1983. "Receptor Determinants of Human and Animal Influenza Virus Isolates: Differences in Receptor Specificity of the H3 Hemagglutinin Based on Species of Origin." *Virology* 127 (2): 361–73. https://doi.org/10.1016/0042-6822(83)90150-2.

Rojas-Quintero, Joselyn, Xiaoyun Wang, Jennifer Tipper, Patrick R. Burkett, Joaquin Zuñiga, Amit R. Ashtekar, Francesca Polverino, et al. 2018. "Matrix Metalloproteinase-9 Deficiency Protects Mice from Severe Influenza A Viral Infection." *JCI Insight* 3 (24). https://doi.org/10.1172/jci.insight.99022.

Rossman, Jeremy S., and Robert A. Lamb. 2011. "Influenza Virus Assembly and Budding." *Virology* 411 (2): 229–36. https://doi.org/10.1016/j.virol.2010.12.003.

Rozanov, Dmitri V., Elizabeth Hahn-Dantona, Dudley K. Strickland, and Alex Y. Strongin. 2004. "The Low Density Lipoprotein Receptor-Related Protein LRP Is Regulated by Membrane Type-1 Matrix Metalloproteinase (MT1-MMP) Proteolysis in Malignant Cells." *Journal of Biological Chemistry*. https://doi.org/10.1074/jbc.M311569200.

Rummel, Sebastian. 2007. "Mechanisms of Alveolar Protein Clearance in Isolated Rabbit Lungs: Role of Clathrin- and Caveolae-Mediated Endocytosis of Albumin by the Alveolar Epithelium." Justus-Liebig-Universität Giessen.

Rutschman, D. H., W. Olivera, and J. I. Sznajder. 1993. "Active Transport and Passive Liquid Movement in Isolated Perfused Rat Lungs." *Journal of Applied Physiology*. https://doi.org/10.1152/jappl.1993.75.4.1574.

Sanders, Catherine J., Peter Vogel, Jennifer L. McClaren, Resha Bajracharya, Peter C. Doherty, and Paul G. Thomas. 2013. "Compromised Respiratory Function in Lethal Influenza Infection Is Characterized by the Depletion of Type I Alveolar Epithelial Cells beyond Threshold Levels." *American Journal of Physiology-Lung Cellular and Molecular Physiology* 304 (7): L481–88.

https://doi.org/10.1152/ajplung.00343.2012.

Sanderson, Michael J. 2011. “Exploring Lung Physiology in Health and Disease with Lung Slices.” *Pulmonary Pharmacology and Therapeutics*. https://doi.org/10.1016/j.pupt.2011.05.001.

Schroeter, E. H., J. A. Kisslinger, and R. Kopan. 1998. “Notch-1 Signalling Requires Ligand-Induced Proteolytic Release of Intracellular Domain.” *Nature* 393 (6683): 382–86. https://doi.org/10.1038/30756.

Schultz-Cherry, S, and V S Hinshaw. 1996. “Influenza Virus Neuraminidase Activates Latent Transforming Growth Factor Beta.” *Journal of Virology* 70 (12): 8624–29. https://doi.org/10.1128/JVI.70.12.8624-8629.1996.

Shah, Raj D, and Richard G Wunderink. 2017. “Viral Pneumonia and Acute Respiratory Distress Syndrome.” *Clinics in Chest Medicine* 38 (1): 113–25. https://doi.org/10.1016/j.ccm.2016.11.013.

Shi, Minlong, Jianghai Zhu, Rui Wang, Xing Chen, Lizhi Mi, Thomas Walz, and Timothy A. Springer. 2011. “Latent TGF-β Structure and Activation.” *Nature*. https://doi.org/10.1038/nature10152.

Shinya, Kyoko, Masahito Ebina, Shinya Yamada, Masao Ono, Noriyuki Kasai, and Yoshihiro Kawaoka. 2006. “Influenza Virus Receptors in the Human Airway.” *Nature* 440 (7083): 435–36. https://doi.org/10.1038/440435a.

Short, Kirsty R., Thijs Kuiken, and Debby Van Riel. 2019. “Role of Endothelial Cells in the Pathogenesis of Influenza in Humans.” *Journal of Infectious Diseases*. https://doi.org/10.1093/infdis/jiz349.

Skonier, J, M Neubauer, L Madisen, K Bennett, G D Plowman, and A F Purchio. 1992. “CDNA Cloning and Sequence Analysis of Beta Ig-H3, a Novel Gene Induced in a Human Adenocarcinoma Cell Line after Treatment with Transforming Growth Factor-Beta.” *DNA and Cell Biology* 11 (7): 511–22. https://doi.org/10.1089/dna.1992.11.511.

Snelgrove, Robert J., Alexandra Godlee, and Tracy Hussell. 2011. “Airway Immune Homeostasis and Implications for Influenza-Induced Inflammation.” *Trends in Immunology*. https://doi.org/10.1016/j.it.2011.04.006.

Solun, B., and Y. Shoenfeld. 2020. “Inhibition of Metalloproteinases in Therapy for Severe Lung Injury Due to COVID-19.” *Medicine in Drug Discovery*. https://doi.org/10.1016/j.medidd.2020.100052.

Spuch, Carlos, Saida Ortolano, and Carmen Navarro. 2012. “LRP-1 and LRP-2 Receptors Function in the Membrane Neuron. Trafficking Mechanisms and Proteolytic Processing in Alzheimer’s Disease.” *Frontiers in Physiology* 3. https://doi.org/10.3389/fphys.2012.00269.

Steinberg, Kenneth P., Leonard D. Hudson, Richard B. Goodman, Catherine Lee Hough, Paul N. Lanken, Robert Hyzy, B. Taylor Thompson, and Marek Ancukiewicz. 2006. “Efficacy and Safety of Corticosteroids for Persistent Acute Respiratory Distress Syndrome.” *New England Journal of Medicine*. https://doi.org/10.1056/NEJMoa051693.

Subbarao, Kanta, and Tomy Joseph. 2007. “Scientific Barriers to Developing

Vaccines against Avian Influenza Viruses." *Nature Reviews Immunology* 7 (4): 267–78. https://doi.org/10.1038/nri2054.

Tagawa, Maki, Ryoko Yumoto, Keisuke Oda, Junyo Nagai, and Mikihisa Takano. 2008. "Low-Affinity Transport of FITC-Albumin in Alveolar Type II Epithelial Cell Line RLE-6TN." *Drug Metabolism and Pharmacokinetics*. https://doi.org/10.2133/dmpk.23.318.

Takano, Mikihisa, Masashi Kawami, Ayako Aoki, and Ryoko Yumoto. 2015. "Receptor-Mediated Endocytosis of Macromolecules and Strategy to Enhance Their Transport in Alveolar Epithelial Cells." *Expert Opinion on Drug Delivery* 12 (5): 813–25. https://doi.org/10.1517/17425247.2015.992778.

Talmi-Frank, Dalit, Zeev Altboum, Inna Solomonov, Yael Udi, Diego Adhemar Jaitin, Mordehay Klepfish, Eyal David, et al. 2016. "Extracellular Matrix Proteolysis by MT1-MMP Contributes to Influenza-Related Tissue Damage and Mortality." *Cell Host & Microbe* 20 (4): 458–70. https://doi.org/10.1016/j.chom.2016.09.005.

Teijaro, John R., Kevin B. Walsh, Stuart Cahalan, Daniel M. Fremgen, Edward Roberts, Fiona Scott, Esther Martinborough, Robert Peach, Michael B.A. Oldstone, and Hugh Rosen. 2011. "Endothelial Cells Are Central Orchestrators of Cytokine Amplification during Influenza Virus Infection." *Cell* 146 (6): 980–91. https://doi.org/10.1016/j.cell.2011.08.015.

Thapa, Narendra, Byung Heon Lee, and In San Kim. 2007. "TGFBIp/Big-H3 Protein: A Versatile Matrix Molecule Induced by TGF-β." *International Journal of Biochemistry and Cell Biology*. https://doi.org/10.1016/j.biocel.2007.06.004.

Tomashefski, Joseph F., and Carol F. Farver. 2008. "Anatomy and Histology of the Lung." In *Dail and Hammar's Pulmonary Pathology*, 20–48. New York, NY: Springer New York. https://doi.org/10.1007/978-0-387-68792-6_2.

Torii, Keizo, K Iida, Yutaka Miyazaki, Shinsuke Saga, Yasuhiro Kondoh, Hiroyuki Taniguchi, Fumio Taki, Kenzo Takagi, Mutsushi Matsuyama, and Ryujiro Suzuki. 1997. "Higher Concentrations of Matrix Metalloproteinases in Bronchoalveolar Lavage Fluid of Patients with Adult Respiratory Distress Syndrome." *American Journal of Respiratory and Critical Care Medicine* 155 (1): 43–46. https://doi.org/10.1164/ajrccm.155.1.9001287.

Torriani, Giulia, Jennifer Mayor, Gert Zimmer, Stefan Kunz, Sylvia Rothenberger, and Olivier Engler. 2019. "Macropinocytosis Contributes to Hantavirus Entry into Human Airway Epithelial Cells." *Virology*. https://doi.org/10.1016/j.virol.2019.02.013.

Tseng, Wen Fang, Shuan Shian Huang, and Jung San Huang. 2004. "LRP-1/TβR-V Mediates TGF-B1-Induced Growth Inhibition in CHO Cells." *FEBS Letters*. https://doi.org/10.1016/S0014-5793(04)00185-1.

Vadász, István, and Jacob I. Sznajder. 2006. "Hypoxia-Induced Alveolar Epithelial Dysfunction." *Journal of Organ Dysfunction* 2 (4): 244–49. https://doi.org/10.1080/17471060600763377.

Veldhuizen, Edwin J.A., and Henk P. Haagsman. 2000. "Role of Pulmonary Surfactant Components in Surface Film Formation and Dynamics." *Biochimica et Biophysica Acta - Biomembranes*. https://doi.org/10.1016/S0005-

2736(00)00256-X.

Vercauteren, Dries, Roosmarijn E. Vandenbroucke, Arwyn T. Jones, Joanna Rejman, Joseph Demeester, Stefaan C. De Smedt, Niek N. Sanders, and Kevin Braeckmans. 2010. “The Use of Inhibitors to Study Endocytic Pathways of Gene Carriers: Optimization and Pitfalls.” *Molecular Therapy*. https://doi.org/10.1038/mt.2009.281.

Visse, Robert, and Hideaki Nagase. 2003. “Matrix Metalloproteinases and Tissue Inhibitors of Metalloproteinases: Structure, Function, and Biochemistry.” *Circulation Research*. https://doi.org/10.1161/01.RES.0000070112.80711.3D.

Vohwinkel, Christine U., Yasmin Buchäckert, Hamza M. Al-Tamari, Luciana C. Mazzocchi, Holger K. Eltzschig, Konstantin Mayer, Rory E. Morty, et al. 2017. “Restoration of Megalin-Mediated Clearance of Alveolar Protein as a Novel Therapeutic Approach for Acute Lung Injury.” *American Journal of Respiratory Cell and Molecular Biology* 57 (5): 589–602. https://doi.org/10.1165/rcmb.2016-0358OC.

Vries, Alfons C J de, AndréW. Schram, Joseph M Tager, Joseph J Batenburg, and Lambert M G van Golde. 1985. “A Specific Acid α-Glucosidase in Lamellar Bodies of the Human Lung.” *Biochimica et Biophysica Acta (BBA) - Lipids and Lipid Metabolism* 837 (3): 230–38. https://doi.org/https://doi.org/10.1016/0005-2760(85)90046-3.

Wagner, Günter P., Koryu Kin, and Vincent J. Lynch. 2012. “Measurement of MRNA Abundance Using RNA-Seq Data: RPKM Measure Is Inconsistent among Samples.” *Theory in Biosciences* 131 (4): 281–85. https://doi.org/10.1007/s12064-012-0162-3.

Wang, Yanjie, Zan Tang, Huanwei Huang, Jiao Li, Zheng Wang, Yuanyuan Yu, Chengwei Zhang, et al. 2018. “Pulmonary Alveolar Type I Cell Population Consists of Two Distinct Subtypes That Differ in Cell Fate.” *Proceedings of the National Academy of Sciences* 115 (10): 2407–12. https://doi.org/10.1073/pnas.1719474115.

Wang, Z. M., J. Q. Luo, L. Y. Xu, H. H. Zhou, and W. Zhang. 2018. “Harnessing Low-Density Lipoprotein Receptor Protein 6 (LRP6) Genetic Variation and Wnt Signaling for Innovative Diagnostics in Complex Diseases.” *Pharmacogenomics Journal*. https://doi.org/10.1038/tpj.2017.28.

Weibel, Ewald R. 2015. “On the Tricks Alveolar Epithelial Cells Play to Make a Good Lung.” *American Journal of Respiratory and Critical Care Medicine*. https://doi.org/10.1164/rccm.201409-1663OE.

Weiss, Alexander, and Liliana Attisano. 2013. “The TGFbeta Superfamily Signaling Pathway.” *Wiley Interdisciplinary Reviews: Developmental Biology* 2 (1): 47–63. https://doi.org/10.1002/wdev.86.

Willnow, Thomas E., Jan Hilpert, Scott A. Armstrong, Astrid Rohlmann, Robert E. Hammer, Dennis K. Burns, and Joachim Herz. 1996. “Defective Forebrain Development in Mice Lacking Gp330/Megalin.” *Proceedings of the National Academy of Sciences of the United States of America* 93 (16): 8460–64. https://doi.org/10.1073/pnas.93.16.8460.

Willnow, Thomas E., Anders Nykjaer, and Joachim Herz. 1999. “Lipoprotein Receptors: New Roles for Ancient Proteins.” *Nature Cell Biology* 1 (6): E157–62. https://doi.org/10.1038/14109.

Willnow, Thomas E, Annette Hammes, and Suzanne Eaton. 2007. “Lipoproteins and Their Receptors in Embryonic Development : More than Cholesterol Clearance” 3249: 3239–49. https://doi.org/10.1242/dev.004408.

Willson, Douglas F., Jonathon D. Truwit, Mark R. Conaway, Christine S. Traul, and Edmund E. Egan. 2015. “The Adult Calfactant in Acute Respiratory Distress Syndrome Trial.” *Chest*. https://doi.org/10.1378/chest.14-1139.

Worthington, John J., Thomas M. Fenton, Beata I. Czajkowska, Joanna E. Klementowicz, and Mark A. Travis. 2012. “Regulation of TGFβ in the Immune System: An Emerging Role for Integrins and Dendritic Cells.” *Immunobiology* 217 (12): 1259–65. https://doi.org/10.1016/j.imbio.2012.06.009.

Wu, Xinhui, Eline M. van Dijk, I. Sophie T. Bos, Loes E.M. Kistemaker, and Reinoud Gosens. 2019. “Mouse Lung Tissue Slice Culture.” In *Methods in Molecular Biology*. https://doi.org/10.1007/978-1-4939-9086-3_21.

Wujak, L., P. Markart, and Malgorzata Wygrecka. 2016. “The Low Density Lipoprotein Receptor-Related Protein (LRP) 1 and Its Function in Lung Diseases.” *Histology and Histopathology* 31 (7): 733–45. https://doi.org/10.14670/HH-11-746.

Wujak, Lukasz, Jennifer Schnieder, Liliana Schaefer, and Malgorzata Wygrecka. 2018. “LRP1: A Chameleon Receptor of Lung Inflammation and Repair.” *Matrix Biology*. https://doi.org/10.1016/j.matbio.2017.12.007.

Wygrecka, Malgorzata, Jochen Wilhelm, Ewa Jablonska, Dariusz Zakrzewicz, Klaus T. Preissner, Werner Seeger, Andreas Guenther, and Philipp Markart. 2011. “Shedding of Low-Density Lipoprotein Receptor–Related Protein-1 in Acute Respiratory Distress Syndrome.” *American Journal of Respiratory and Critical Care Medicine* 184 (4): 438–48. https://doi.org/10.1164/rccm.201009-1422OC.

Yoo, Jae Kwang, Taeg S. Kim, Matthew M. Hufford, and Thomas J. Braciale. 2013. “Viral Infection of the Lung: Host Response and Sequelae.” *Journal of Allergy and Clinical Immunology*. https://doi.org/10.1016/j.jaci.2013.06.006.

Yu, Guoying, Elisabetha Kovkarova-Naumovski, Paul Jara, Anil Parwani, Daniel Kass, Victor Ruiz, Carlos Lopez-Otiń, et al. 2012. “Matrix Metalloproteinase-19 Is a Key Regulator of Lung Fibrosis in Mice and Humans.” *American Journal of Respiratory and Critical Care Medicine*. https://doi.org/10.1164/rccm.201202-0302OC.

Yumoto, Ryoko, Hiromi Nishikawa, Miho Okamoto, Hirokazu Katayama, Junya Nagai, and Mikihisa Takano. 2006. “Clathrin-Mediated Endocytosis of FITC-Albumin in Alveolar Type II Epithelial Cell Line RLE-6TN.” *American Journal of Physiology-Lung Cellular and Molecular Physiology* 290 (5): L946–55. https://doi.org/10.1152/ajplung.00173.2005.

Yumoto, Ryoko, Sayuri Suzuka, Keisuke Oda, Junya Nagai, and Mikihisa Takano. 2012. “Endocytic Uptake of FITC-Albumin by Human Alveolar Epithelial Cell Line A549.” *Drug Metabolism and Pharmacokinetics* 27 (3): 336–43.

https://doi.org/10.2133/dmpk.DMPK-11-RG-127.

Zarrabi, Kevin, Antoine Dufour, Jian Li, Cem Kuscu, Ashleigh Pulkoski-Gross, Jizu Zhi, Youjun Hu, Nicole S. Sampson, Stanley Zucker, and Jian Cao. 2011. “Inhibition of Matrix Metalloproteinase 14 (MMP-14)-Mediated Cancer Cell Migration.” *Journal of Biological Chemistry*. https://doi.org/10.1074/jbc.M111.256644.

Zhao, Pengfei, Yonghui Wang, Aihua Wu, Yuefeng Rao, and Yongzhuo Huang. 2018. “Roles of Albumin-Binding Proteins in Cancer Progression and Biomimetic Targeted Drug Delivery.” *ChemBioChem*. https://doi.org/10.1002/cbic.201800201.

Zheng, G., D. R. Bachinsky, I. Stamenkovic, D. K. Strickland, D. Brown, G. Andres, and R. T. McCluskey. 1994. “Organ Distribution in Rats of Two Members of the Low-Density Lipoprotein Receptor Gene Family, Gp330 and LRP/Alpha 2MR, and the Receptor-Associated Protein (RAP).” *Journal of Histochemistry & Cytochemistry* 42 (4): 531–42. https://doi.org/10.1177/42.4.7510321.

Zhou, Fei, Hui Li, Li Gu, Meng Liu, Chun xue Xue, Bin Cao, and Chen Wang. 2018. “Risk Factors for Nosocomial Infection among Hospitalised Severe Influenza A(H1N1)Pdm09 Patients.” *Respiratory Medicine*. https://doi.org/10.1016/j.rmed.2017.11.017.

Zou, Zhiying, Brian Chung, Thao Nguyen, Sueann Mentone, Brent Thomson, and Daniel Biemesderfer. 2004. “Linking Receptor-Mediated Endocytosis and Cell Signaling: Evidence for Regulated Intramembrane Proteolysis of Megalin in Proximal Tubule.” *The Journal of Biological Chemistry* 279 (33): 34302–10. https://doi.org/10.1074/jbc.M405608200.

Acknowledgments

I would like to express my gratitude to Prof. Dr. Werner Seeger for his supervision of my doctoral studies. I would also like to specially thank my advisor Dr. Istvan Vadasz, Ph.D. for giving me the opportunity of doing this doctorate, his supervision of my work and his support. I also want to thank Luciana Mazzocchi, Ph.D. for sharing her knowledge and expertise, Paulina Gwozdzinska, Ph.D., Dr. Vitalii Kryvenko, Ph.D. and Miriam Wessendorf for their support with laboratory experiments and for their valuable comments.

I am also grateful to Prof. Dr. Christos Samakovlis for his advice and the access to his laboratory facilities and equipment. Also, thanks to Dr. Athanasios Fysikopoulos, Maroua Ghoul, Stefan Hadzic, Ph.D. and Dr. Janine Koepke for their advice and support with the experiments.

I would also like to thank Prof. Dr. Susanne Herold for her support and the access to the biosafety 2 facilities. I would specially like to thank Dr. Christina Malainou and Christin Peteranderl, Ph.D., Larissa Hamann, Stefanie Jarmer and Margarida Barroso for their technical support, their valuable insights, and for always creating a great work environment.

I am grateful to the MBML team, Dr. Rory Morty, Elie El Agha, Ph.D., Dr. Janine Koepke and Ivonne Vázquez Armendariz, Ph.D. for their support and tutoring in the program. Also, a big thank you to all my classmates for making this experience even better.

I also want to thank Shawn Mlynek, for reviewing the English grammar and Mathias Burk for his help with translations.

Finally, I would like to thank my family and friends, scattered around the world, for their continuous support during all these years.